THE DEVELOPMENT OF A GAS LASER SYSTEM FOR THE MEASUREMENT OF ATOMIC PARAMETERS AND ITS APPLICATION TO SOME ENERGY LEVELS IN NEON

A DISSERTATION SUBMITTED TO THE GRADUATE DIVISION OF THE UNIVERSITY OF HAWAII IN PARTIAL FULFILLMENT OF THE REQUIREMENTS FOR THE DEGREE OF

DOCTOR OF PHILOSOPHY

IN PHYSICS

JUNE 1968

By

Roger Alan Lilly

Dissertation Committee:

John R. Holmes, Chairman
John T. Jefferies
Howard McAllister
Vincent Z. Peterson
William Pong

ABSTRACT

The development of gas lasers has provided the experimental atomic physicist with a new tool for the selective probing of atomic energy levels. This dissertation describes the development of a gas laser system for the measurement of atomic parameters. The system has been applied to the measurement of transition probabilities and collision excitation cross sections in neon.

The experimental technique utilizes a helium-neon laser oscillating at 3.39 microns -- $3s_2$-$3p_4$ (Paschen notation) -- to perturb the population density of the $3s_2$ level in a neon discharge. This perturbation is coupled to the $3s_3$ neon level through non-radiative collision induced transitions.

The perturbations of the excited state population densities are followed by observing the intensity changes in spontaneous emission from the $3s_2$ and $3s_3$ levels. By analyzing the intensity changes from these two levels as a function of pressure, we have been able to determine the product of the lifetime of the $3s_3$ level and the cross section for collision induced transitions between the $3s_2$ and $3s_3$ levels. This product is $\tau_3 q_{23} = (9.93 \pm .80) \times 10^{-23}$ sec-cm^2. The same measurements yield the ratio of the transition probability for the $3s_2$-$2p_4$ and the $3s_3$-$2p_5$ transitions. The measured ratio is $7.10 \pm .57$.

In order to be able to vary the pressure, the atoms to be investigated are contained within a gas discharge cell placed within the laser cavity. A phase sensitive detection system is employed. Relative transition probabilities for ten other visible lines originating on the $3s_2$ and $3s_3$ levels have also been determined. These relative transition probabilities are placed on an absolute scale using a recently measured value for the $3s_2$-$2p_4$ transition.

The experimental values are compared to theoretically calculated transition probabilities for which a j-ℓ coupling model was used. This comparison points out the rather large departure of these levels from j-ℓ coupling. Suggestions are made concerning the improvement of the system and its application to other problems.

TABLE OF CONTENTS

ABSTRACT iii

LIST OF TABLES vi

LIST OF FIGURES vii

CHAPTER I. STATEMENT OF THE PROBLEM
Introduction 1
Lasers 4
Previous Measurement Techniques 9
The Problem 16
References 20

CHAPTER II. THEORETICAL ANALYSIS
Excited State Population Densities and Relaxation Rates in Neon 22
Excitation Transfer Collisions 31
References 40

CHAPTER III. EXPERIMENTAL APPARATUS AND PROCEDURE
Vacuum System 43
Construction of the Laser 47
Description of the Laser and Laser Cavity 51
Alignment of the Laser Cavity 61
Monochromator 71
Intensity Calibration 74
Differential Intensity Measurement . . . 78
References 86

CHAPTER IV. EXPERIMENTAL RESULTS
Preliminary Results 88
Relative Intensities 97
Differential Intensity 97
Errors 108
References 117

CHAPTER V. DISCUSSION OF RESULTS
Comparison With Previous Experimental Work 118
Comparison with Theory 121
Summary 123
References 126

BIBLIOGRAPHY 127

LIST OF TABLES

TABLE		PAGE
I.	Neon Energy Levels	17
II.	Relative Photon Response	90
III.	Relative Transition Probabilities	98
IV.	Relative Transition Probabilities	99
V.	Final Results	116
VI.	Relative Transition Probabilities for $3s_2$ - 2p Transitions	119
VII.	Absolute Transition Probabilities	120
VIII.	Comparison of Theoretical Transition Probabilities with Experimentally Determined Transition Probabilities	122

LIST OF FIGURES

FIGURE		PAGE
1.	Helium and Neon Energy-Level Diagram	23
2.	Hypothetical Energy-Level Diagram	32
3.	Schematic Diagram of the Experimental Apparatus	42
4.	Vacuum System	44
5.	Experimental Setup	55
6.	Boyd-Kogelnik Stability Diagram	56
7.	Littrow Prism Reflector	60
8.	Laser Mounting	62
9.	Mirror Mount	66
10.	Discharge Tube Mount	67
11.	Prism Reflector Mount	70
12.	Grating Ghost	72
13.	Photomultiplier Voltage Divider	76
14.	Lock-in Amplifier Block Diagram	81
15.	Reference Signal Circuit	83
16.	Relative Intensity Response	89
17.	ΔI_3 vs. ΔI_2	92
18.	Zeeman Transitions Between Laser Levels	94
19.	Optical Arrangement	96
20.	$\Delta I_{(6328)}/\Delta I_{(6313)}$ vs. the Reciprocal of the Pressure	102
21.	$\Delta I_{(6351)}/\Delta I_{(6313)}$ vs. the Reciprocal of the Pressure	103

FIGURE PAGE

22. $\Delta I_{(6328)}/\Delta I_{(6313)}$ vs. the Reciprocal of the Pressure. Discharge Current 8ma 104

23. $\Delta I_{(6313)}/\Delta I_{(6328)}$ vs. the Pressure 105

24. $\Delta I_{(6313)}/\Delta I_{(6351)}$ vs. the Pressure 106

25. $\Delta I_{(6313)}/\Delta I_{(6328)}$ vs. the Pressure. Discharge Current 8ma 107

26. $\Delta I_3/\Delta I_2$ As a Function of Current 110

CHAPTER I

STATEMENT OF THE PROBLEM

Introduction

It has long been realized that the light emitted or absorbed by atoms carries information concerning their structure and internal motions. The regularities observed in spectra emitted by monatomic gases were among the most important data which led physicists in the early years of this century to an understanding of the structure of atoms and to the discovery of the principles which govern the behavior of matter on the atomic scale.

The fundamental relation between the spectra of an atom and its structure was first recognized by Bohr. In 1913 Bohr started the modern theory of atomic structure and the theory of the interpretation of optical spectra with his interpretation of the spectrum of the hydrogen atom. Although much effort had previously been applied to the investigation of atomic spectra and many spectral series had been discovered, Bohr's theory gave for the first time a convincing quantitative account of the structure of any spectrum.

The investigations which followed this success soon revealed details, however, which indicated that Bohr's theory had only limited applications.

Sommerfeld extended Bohr's theory by considering elliptic as well as circular orbits in an attempt to resolve some

of the difficulties encountered by the Bohr theory. In 1925, Uhlenbeck and Goudsmit further extended Bohr's theory when they pointed out that certain features of atomic spectra could be explained if it were assumed that the electron spins about an axis through its center of mass and that it has both angular momentum and a magnetic moment.

Bohr's theory of the hydrogen atom did not provide a detailed description of the radiation process in which the electron makes a transition from one permitted energy level to another, the energy difference being accounted for by the emission or absorption of a quantum of radiation. It was quickly realized that not all possible transitions between energy levels actually took place and selection rules were introduced which specify certain permitted transitions. Before the discovery of quantum mechanics, the only theoretical basis upon which selection and intensity rules could be understood was the correspondence principle. This asserts that for large quantum numbers the intensity of the spectral lines must be determined by classical electromagnetic theory.

With the introduction of quantum mechanics, as formulated by Schrödinger and Heisenberg and later extended to the relativistic case by Dirac, many of the finer details of atomic spectra could be accounted for satisfactorily. The fundamental result of quantum theory of radiation is that the probability of a single quantum electric dipole spontaneous

transition from a state i to a state j of an atom is proportional to the square of a matrix element x_{ij} which is calculable by an integral of the type

$$x_{ij} = \int \psi_i^* ex \psi_j d\tau \qquad (1)$$

It is evident that in order to be able to calculate a transition probability it is necessary to know the function ψ; that is, to have a knowledge of the wave function of the atom for both the state i and state j. Although transition probabilities are calculable in principle, in many cases of interest an adequate knowledge of the wave function is lacking. Hence, experimental methods are necessary to determine transition probabilities.

An analogous situation is that of the calculation of collision cross sections between atoms. In recent years interest has grown concerning knowledge of cross sections for collisions of the second kind. A collision of the second kind includes all collision processes in which the following conditions are fulfilled:

(1) One of the colliding particles is either an excited atom (metastable or otherwise) or an ion.

(2) The other colliding particle is either an electron, a normal atom, or a normal molecule.

(3) During the collision either all or a part of the excitation of particle (1) is transferred to particle (2).

The discovery of the laser in 1960[1] has provided the experimental atomic physicist with a new tool for the investigation of atomic collisions and for selectively probing atomic energy levels in order to obtain information about transition probabilities and other atomic parameters.

Lasers

The generation of coherent light by stimulated emission is a subject involving aspects of both pure physics and radio-frequency engineering. In this section we will not attempt to give an exhaustive review of laser theory, but to present only an introduction to laser theory and the properties of the output beam which are necessary for an understanding of the experimental methods used in this thesis.

The first appearance of the notion of stimulated emission was in 1917 when Einstein showed that in order to describe adequately the interaction of radiation with matter, the process must be included whereby an atom in the excited state is stimulated to decay to a lower state by the presence of radiation.[2] The process is generally discussed by reference to two levels of a quantized atomic system. In particular, if we exclude the case of degeneracy in two atomic levels E_2 and E_1 ($E_2 > E_1$) so that there exists only one electronic configuration per energy level, then we can state that a photon of energy $h\nu_{12} = E_2 - E_1$ is as likely to stimulate emission in an encounter with an upper state E_2 as it is to

be absorbed in an encounter with a lower state E_1. Thus if there are more atoms in the upper state E_2 than atoms in the lower state E_1, an incident stream of photons will be increased in number as long as this condition persists, provided that there is no prevalence of competitive processes which absorb or scatter the frequency ν_{12}.

Since the population density of the lower state under equilibrium conditions is always greater than that of the upper state, the laser condition is described as a population inversion; that is, if lasing action is to take place the population of the upper state must be greater than the population of the lower state. The attainment of such a steady state nonthermodynamical equilibrium situation is the basic necessity for obtaining continuous laser oscillation.

The methods used for obtaining such an inverted population are varied. In the case of solid systems, the remarkably simple method of exposing the material to an intense light source is found to work in many cases. For gas systems rather greater subtlety is required. An electronically excited discharge is generally used. The general theory of lasers can be found in a paper by Lamb.[3] Threshold conditions for obtaining oscillation are given by many authors.[4]

Since a gas laser was built and used in this experiment, we will limit our discussion in the following to gas lasers.

Although many of the properties discussed will pertain to gas lasers in general, we will specifically direct our attention to the helium-neon laser.[5]

The relevant energy levels of the helium-neon laser system, the first gas laser to be operated in the optical region, are shown in figure 1. The broader features of the operation of the system on the 3.39 micron line are as follows: the 2^1S level of helium has no optically allowed downward transitions since the only lower states in the spectrum are the 2^3S excited state and the 1^1S ground state. In light elements such as helium, intercombination lines have a vanishingly small transition probability. Thus radiative relaxation between the 2^1S state and the 2^3S state will not occur. Likewise radiative relaxation of the 2^1S level to the 1^1S ground state is forbidden by the parity selection rule $\Delta\ell = \pm 1$. Thus atoms in the 2^1S state will remain there until de-excited by any non-radiative process which may occur. In low pressure discharges with no other gas present, the main loss of such metastables will be collisions with the wall.

From figure 1, we see that the energy of the 3s levels of neon lies close to that of the 2^1S state of helium. For reasons which will be discussed in chapter II, we may expect a high probability of energy transfer from the helium metastables to neon atoms in the 3s levels. From the 3s group of

levels the neon atoms may decay radiatively to the ground state or to the group of ten 3p and ten 2p levels.

The selective excitation of the 3s levels of neon in a discharge containing a mixture of helium and neon is the mechanism responsible for the population inversion necessary to maintain continuous laser oscillation.

The transition probability between the $3s_2$ and the $3p_4$ states of neon is extremely large. This very large transition probability makes the gain of the laser on this transition very high. The gain is so large that the amplifying medium, that is, the helium-neon discharge, saturates (this is explained in some detail in chapter III). The laser constructed and operated in this experiment utilized the saturation feature of this laser transition.

Because of the low gain per unit length of the amplifying medium for most laser transitions, it is necessary to make many passes through the discharge tube to have a gain greater than unity. This necessitates the use of a reflecting cavity. Mirrors are placed at both ends of the discharge tube in order that the radiation may be reflected back and forth through the tube for a large number of times before escaping from the system. Since these mirrors have to be highly reflecting (reflectivities greater than 98%), the radiation intensity outside the cavity is about two orders of magnitude less than that inside. In order to be able to

do inter-cavity work, as well as ease in aligning laser mirrors, the Brewster angle window laser was developed.[6]

Such a laser is used in this experiment. The discharge tube is sealed with windows which are set at Brewster's angle to the axis of the tube. Thus experimental work may be placed within the cavity between the end of the discharge tube and the mirror. This is possible only if the insertion of experimental apparatus within the cavity does not introduce large losses into the system.

The nature of the output of the laser is changed due to the Brewster angle windows. The output radiation is linearly polarized in the plane of the axis of the tube and the normal to the Brewster angle windows. This polarization has a potentially harmful effect upon the experiment. This will be discussed in detail in chapter IV.

Another feature of the output from a laser, important in this experiment, is the dramatic narrowing of the line width of the laser output. Although it is not immediately clear what temperature may be ascribed to the gas under laser discharge conditions, which are necessarily not equilibrium conditions, a mean gas temperature of about 400 degrees K has been experimentally observed.[7] The associated Doppler width is therefore approximately 5×10^9 sec^{-1}. The theoretical line width of laser radiation is less than one hertz.[8] In practice it is impossible to obtain such a degree of

spectral purity because of mechanical variations, thermal drift, etc. It is certain, however, that the actual width will be somewhere between 10^3 and 10^6 times smaller than the Doppler width.

Now the separation between frequencies of axial cavity modes is given by c/2L, where c is the velocity of light in an amplifying medium and L the length of the cavity. For a one meter cavity, this amounts to 1.5×10^8 sec^{-1}. Thus there will be several cavity modes lying within the Doppler width of the neon transition. If the laser is operated in such a manner that only one cavity mode is oscillating, it is evident that if this radiation interacts with the atoms in a gas discharge only certain of the excited atoms in the discharge will be able to interact with this radiation. Specifically, only those atoms whose velocity component in the direction of propagation of the laser radiation places them on the proper point on the Doppler shift curve will be able to absorb this radiation. The possible consequences of this feature of laser radiation on this experiment will be discussed in more detail in chapter IV.

Previous Measurement Techniques

Most transition probability measurements can be classified by moderately well-defined experimental methods. It is our purpose here to illustrate the main methods in current use, in order to be able to point out the advantages of the

system developed for this thesis.

Few reviews or books deal at all comprehensively with measurement techniques. Perhaps the most general references are the book of Mitchell and Zemansky,[9] the report of Korff and Breit,[10] the book OPTICAL TRANSITION PROBABILITIES[11] which consists of translations of Russian articles of the period 1924-60, and the review by E. W. Foster.[12]

Perhaps the most obvious approach to the measurement of oscillator strengths or transition probabilities is the measurement of line intensities. However the upper level is always an excited state for which the occupation density can be determined only with limited accuracy. Furthermore, self-absorption has to be considered, particularly if the lower level is the ground state and in many cases even if the lower level is an excited state. Taking all this into account, the highest accuracy is possible only for the determination of relative probabilities of spontaneous transitions from a common level. One has then for the ratio of the transition probabilities

$$\frac{A_{ij}}{A_{ik}} = \frac{I_{ij}}{I_{ik}} \frac{\nu_{ik}}{\nu_{ij}} \qquad (2)$$

Therefore the measurement is reduced to determining the ratio of intensities by a calibrated detector.

Arc sources have been used for the quantitative measurement of transition probabilities.[13] In ordinary atmospheric

pressure arcs, the processes which usually dominate in populating and de-populating the excited states do not involve the absorption and emission of radiation. If the principal populating and de-populating mechanism is atomic collisions, the excited state populations in an arc are almost the same as if thermal equilibrium existed at some temperature T. With the aid of the Saha and Boltzmann equations, one can then determine the relative populations of the excited levels. A large number of transition probabilities have been measured using arc sources. The basic shortcoming in emission techniques of measuring transition probabilities is in determining the excited state populations.

Another direct method of determining transition probabilities or oscillator strength consists of absorption measurements. If radiation from a continuum source passes through a layer of thickness Δx containing a known number N_j of absorbing atoms, the intensity I suffers a relative reduction

$$\frac{\Delta I}{I} = - \frac{\pi e^2}{m_e c} N_j \, f_{ji} \, \Delta x \qquad (3)$$

This relationship presumes that stimulated emission from the level i can be ignored. The assumption is practically always justified if absorption from the ground level is observed in the absence of other excitation. The number N_j of absorbing atoms, if one is making an observation of an absorption from

the ground level, can be found from the ideal gas law.

The assumption of ignoring stimulated emission is not justified in the measurement of absorption and the determination of oscillator values from excited levels. The effect of stimulated emission, although often negligible, enters equation (3) as indicated in equation (4).

$$\frac{\Delta I}{I} = - \frac{\pi e^2}{m_e c} N_j f_{ji} \left(1 - \frac{g_j N_i}{g_i N_j}\right) \Delta x \qquad (4)$$

In any event, the population density of the excited level now appears in the equation. It is possible that this density can be related to the normal atom concentration through the Boltzmann factor, if an effective temperature can be determined by some means. As evidenced by the mere existence of the laser, however, such an effective temperature can not necessarily be defined for all levels. These difficulties do not exist, of course, if one is content with relative values. In the intensity ratios of lines starting from the same level (if stimulated emission is negligible), the population density cancels out.

Anomalous dispersion measurement is another widely used technique for obtaining oscillator strengths. This technique depends upon the more or less sharp variation of the magnitude and slope of the index of refraction of a material near regions of resonance. The resonance regions of a medium are characterized by their absorption. Thus it is not unexpected,

that anomalous dispersion is a direct measure of the corresponding oscillator strengths. In particular, in the case of low absorber densities, such as gases in the neighborhood of an isolated line ν_{ji},

$$n-1 = \frac{N_j e^2}{2\pi m_e} \frac{f_{ji}}{(\nu_{ji}^2 - \nu^2)} \left(1 - \frac{g_j}{g_i} \frac{N_i}{N_j}\right) \qquad (5)$$

Although the effect at low concentrations is small, it is nevertheless possible to measure the dispersion quite accurately by interferometric means as a variation of optical path length. The use of the dispersion method for f value determinations has certain advantages over absorption measurement. The restriction to optically thin layers is not necessary. Moreover, the method is more easily extended to excited media, so that oscillator values from levels other than the ground state can be determined. Ladenburg[14] did extensive work with this approach and many Russian workers[15] have also used this technique.

As with the absorption technique, the difficulties of determining the occupation numbers of the levels, do not exist if one is content with relative values. However, this technique, along with that of absorption, has difficulty in measuring even relative oscillator strengths or transition probabilities for highly excited levels. The difficulty is in obtaining sufficient atoms in the excited state which is to be studied. Unless a source of radiation is very intense,

the population of the level to be studied must be a fairly sizeable percentage of the total gas population. This is something which is not always easily achieved for highly excited levels.

The major uncertainty in most methods of measuring transition probabilities is inadequate knowledge of the number of radiating particles. It is possible to combine lifetime measurements with relative transition probabilities to obtain absolute values. The direct methods of lifetime measurement measure basically the time interval τ between the excitation of atoms to a given energy level and the radiation decay of the excited population to 1/e. Excitation is possible by a variety of energy sources, but the most important are those of light and electron collision. The former involve fluorescence. Fluorescence has the practical advantage that levels can be excited selectively since intense monochromatic sources with matching photon energy are usually available. However, they are usually limited to levels which can be excited by resonance radiation. Selective excitation is more difficult to achieve by electron impact. However, electron pulses can be produced with shorter duration and better definition than those of light. The lack of the selective excitation generally leads to radiative cascade from higher lying levels into the level of interest thus tending to confuse the measurements.

The quenching of resonance radiation by foreign gases was one of the first instances of experimental observation of collisions of the second kind. It was first noticed by Wood[16] that the introduction of a small amount of air into a mercury resonance lamp reduced the intensity of the emitted resonance radiation.

Further experiments on mercury, sodium, and cadmium resonance radiation indicated that this was a very general phenomenon that takes place whenever the foreign gas atoms or molecules are capable of receiving some or all of the excitation energy of the excited atoms in the resonance lamp. The general features of collisions of the second kind will be discussed in more detail in chapter II.

In order to study such collisions, it is of course necessary to populate, in some manner, the energy level which is under consideration. In general, this means either electron excitation or radiation excitation. For studies of collisions, these types of excitation suffer from the same deficiencies as brought out in the discussion on transition probability measurements. In the case of levels which are not connected to the ground state, it is difficult to obtain excitation radiation of sufficient intensity and electron excitation suffers from the inability to excite states selectively.

The Problem

The problem of determining atomic transition probabilities and excited state lifetimes is an old one in physics, although it has received relatively little experimental attention in recent years. The advent of the laser, as well as advances in photoelectric recording and optical techniques, makes many early methods well worth reviewing and revising. The development of the laser, and in particular the gas laser, has provided a source with which selective excitation is possible for those levels between which a laser transition takes place. This should allow the use, with these levels, of those techniques which hitherto have been limited to levels which could be reached with resonance radiation.

The levels which can be investigated in this manner are limited to those between which a laser transition takes place. This is not as severe a limitation as one might expect, as may be seen by an examination of table I. Here is listed all the neon levels up to an energy of twenty volts above the ground state. All those levels which serve either as an upper or lower laser level are designated with an asterisk. Neon is one of the best explored laser mediums and has perhaps an unusually large number of lasing transitions. However, the total number of gas laser transitions discovered so far is almost staggering considering the first gas laser was discovered less than eight years ago and thus table I does not present an extremely over-optimistic example.

TABLE I. NEON ENERGY LEVELS[a]

Neon level - Paschen Notation[b]

$1s_5$	$3d_6$	$*3p_3$
$1s_4$	$3d_5$	$*3p_5$
$1s_3$	$*3d'_4$	$*3p_4$
$*1s_2$	$*3d_4$	$*3p_2$
$*2p_{10}$	$*3d_3$	$*3p_1$
$2p_9$	$*3d_2$	$*3s_5$
$*2p_8$	$*3d''_1$	$*3s_4$
$*2p_7$	$*3d'_1$	$*3s_3$
$*2p_6$	$*3s''''_1$	$*3s_2$
$*2p_3$	$*3s'''_1$	$4d_6$
$*2p_5$	$*3s''_1$	$*4d_5$
$*2p_4$	$3s'_1$	$4d'_4$
$*2p_2$	$*3p_{10}$	$*4d_4$
$*2p_1$	$3p_9$	$*4d_3$
$*2s_5$	$*3p_8$	$*4d_2$
$*2s_4$	$*3p_7$	$*4d''_1$
$*2s_3$	$*3p_6$	$*4d'_1$
$*2s_2$		

[a]Charlotte E. Moore, Atomic Energy Levels, Vol. I, Circular of the National Bureau of Standards 467.

[b]Levels designated with an asterisk indicate that the level has been observed as either the upper or lower level of a laser transition.

Transition probabilities are important for many fields of investigation. However, in many instances they are not at all well known. For example, although neon is frequently employed in investigations of high temperature gaseous phenomena and is an element of astrophysical interest, definitive values for the transition probabilities of the common spectral lines of the neutral atom have not been available.[17]

Theoretical calculations of transition probabilities in many instances yield, at best, order of magnitude results. Even with the use of intermediate coupling calculations, theoretical and experimental results can differ by a factor of two or three.[18] There is thus obviously a need for further experimental measurements of transition probabilities and lifetimes.

Therefore it was taken as the purpose of this dissertation research to develop a gas laser system which could be applied to the study of atomic parameters, such as transition probabilities and collision cross sections and to demonstrate the system's feasibility by applying it to particular cases.

As pointed out in the previous section, the major uncertainty in both absorption and emission techniques for measuring transition probabilities is the inadequate knowledge of the number of radiating particles. This uncertainty

extends even to the relative populations of different atomic levels. It will be shown in chapter II that for levels which lie close to a laser level, the approach to a partial thermalization of these two levels due to collisions of the second kind can be studied. This approach to partial thermalization allows one to measure transition probabilities and to study collisions of the second kind.

Since at the time this dissertation research was started, the best understood and perhaps most easily constructed laser was the helium-neon system, it was deemed desirable to concentrate the initial effort on this system.

REFERENCES

[1]Theodore H. Mainman, "Stimulated Radiation in Ruby," Nature, 187 (1960), 493.

[2]Albert Einstein, Physikalische Zeitschrift, 18 (1917), 121.

[3]Willis E. Lamb, Jr., "Theory of an Optical Maser," The Physical Review, 134 (1964), A1429.

[4]For example: George Birnbaum, Optical Masers, (New York, 1964), pp. 6, et seq. Max Garbuny, Optical Physics, (New York, 1965), pp. 327, et seq.

[5]Ali Javan, William R. Bennett, Jr., Donald R. Herriot, "Population Inversion and Continuous Optical Maser Oscillation in a Gas Discharge Containing a He-Ne Mixture," Physical Review Letters, 6 (1961), 106.

[6]W. W. Rigrod, H. Kogelnik, D. Brangaccio, D. R. Herriot, "Gaseous Optical Maser with External Concave Mirrors," Journal of Applied Physics, 33 (1962), 743.

[7]O. S. Heavens, Optical Masers, (London, 1964), p. 76.

[8]Ibid.

[9]Alan Mitchell and Mark Zemansky, Resonance Radiation and Excited Atoms, (London, 1934).

[10]S. A. Korf and G. Breit, "Optical Dispersion," Reviews of Modern Physics, 5 (1933), 471-503.

[11]Optical Transition Probabilities, Israel Program for Scientific Translation, (Jerusalem, 1962).

[12]E. W. Foster, "The Measurement of Oscillator Strengths in Atomic Spectra," Reports on Progress in Physics, 27 (1964), 470-551.

[13]Ibid., p. 485.

[14]Rudolf Ladenburg, "Dispersion in Electrically Excited Gases," Reviews of Modern Physics, 5 (1933), 243-256.

[15]Optical Transition Probabilities, op. cit.

[16]R. W. Wood, Physikalische Zeitschrift, 13 (1912), 353.

REFERENCES (cont.)

[17]B. M. Glennon and W. L. Wiese, "Bibliography on Atomic Transition Probabilities," National Bureau of Standards Miscellaneous Publication 278, (Washington D. C., 1964), pp. 64-65.

[18]David W. Koopman, "Line Strengths for Neutral and Singly Ionized Gases," Journal of the Optical Society of America, 54 (1964), 1354.

CHAPTER II

THEORETICAL ANALYSIS

It is the purpose of this chapter to outline and develop the necessary theoretical background for an understanding of the problem.[1] In the first section the equations governing the excited state population densities and relaxation rates of excited neon levels in the presence of a modulated laser radiation field are developed. Two types of relaxation from excited states are considered. The first is the usual radiative relaxation and the second is collisional excitation transfer relaxation. In the second section of this chapter, excitation transfer collisions of the type studied in this experiment are discussed in some detail and a very important relationship between excitation transfer cross sections, which was used in the first section of this chapter, is derived.

Excited State Population Densities and Relaxation Rates in Neon

In the experiment described in this thesis, we have utilized a laser to study collisional excitation transfer between two of the four excited states of the $(2p)^5 5s$ configuration of neon.[2] See figure 1. These are designated in Paschen notation[3] as the $3s_2$ and the $3s_3$ levels. The $3s_2$ level is the upper state of the well known 6328A laser

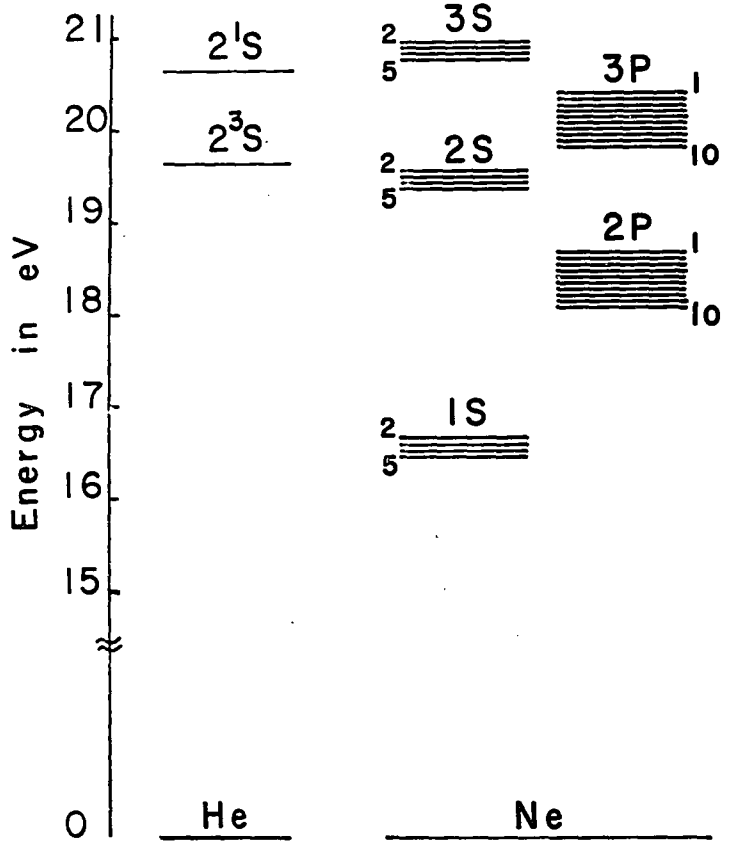

Simplified energy-level diagram of Helium and Neon

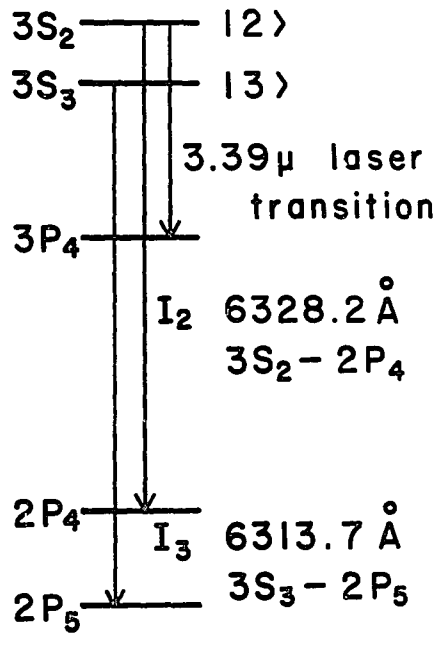

The Neon energy-levels and transitions directly involved in this experiment (Paschen notation)

FIGURE 1. HELIUM AND NEON ENERGY-LEVEL DIAGRAM

transition. It is also the upper state of 3.39 micron laser transition. It will be shown in this section, that measurements which follow the approach to thermalization between these two levels, directly yield the product of the lifetime of the $3s_3$ level and the collision cross section for non-radiative transfer of excitation between these levels and also the ratio of the Einstein A coefficients for transitions originating from these two levels.

Consider the experimental situation in which the output of a helium-neon laser oscillating on the 3.39 micron transition of neon is passed through a gas discharge cell containing excited neon atoms. This radiation interacts with the $3s_2$ level by inducing rapid transitions between the $3s_2$ and the lower laser level which is one of the ten levels of the $(2p)^5 4p$ neon configuration and is designated as $3p_4$ in Paschen notation. If the discharge cell contains only neon, the population density of the $3p_4$ level will be greater than that of the $3s_2$. As a result, when the laser radiation field is switched on, the population of the $3s_2$ level will increase sizeably. Since the $3s_3$ level lies only 50 cm^{-1} below the $3s_2$ level[4], they are strongly coupled by atomic collision. Thus when the laser field is on, the population of the $3s_3$ level will also increase. It is important to note that these levels are not radiatively coupled to each other.

In the following discussion, levels $3s_2$ and $3s_3$ are denoted by $|2\rangle$ and $|3\rangle$ respectively. The intensity of the applied laser field enters our discussion only through its influence on the population of level $|2\rangle$. Consider the rate equation for the steady state population of $|3\rangle$.

$$\frac{dn_3}{dt} = -\frac{n_3}{\tau_3} + \frac{n_2}{\theta_{23}} - \frac{n_3}{\theta_{32}} + R_3 = 0 \qquad (1)$$

Here, n_3 is the population of level $|3\rangle$, n_2 is the population of level $|2\rangle$ which is the upper laser level, τ_3 is the radiative lifetime[5] of level $|3\rangle$, θ_{23} is the collision relaxation time for a process involving a non-radiative transition from $|2\rangle$ to $|3\rangle$, θ_{32} is the relaxation time for the inverse process and R_3 is the net rate of excitation of $|3\rangle$ by all remaining processes, e.g., electron excitation, radiative cascade, etc.

The relaxation times θ_{32} and θ_{23} are functions of the gas pressure and in this experiment we study this pressure dependence in order to obtain information about the collision cross sections for non-radiative transitions between levels $|2\rangle$ and $|3\rangle$ and the ratio of transition probabilities for transitions originating from these two levels. However, the rate R_3, in general, will be a complicated function of the gas pressure and discharge current.[6] Therefore it is necessary to separate the effect of R_3 on the population n_3

to determine accurately the pressure variation of θ_{23} and θ_{32}.

Consider the rate equation for level $|3\rangle$ when the laser field is applied.

$$\frac{dn_3'}{dt} = -\frac{n_3'}{\tau_3} + \frac{n_2'}{\theta_{23}} - \frac{n_3'}{\theta_{32}} + R_3 = 0 \qquad (2)$$

Since all other conditions are assumed to be the same, the rate R_3 in equation (2) remains essentially unchanged from the R_3 in equation (1). However, the population of level $|2\rangle$ changes sizeably through its direct interaction with the laser field. Also the population of level $|3\rangle$ changes since it is coupled to level $|2\rangle$ via atomic collision. Therefore these population densities are primed; the other symbols in equation (2) retain the same meaning as that in equation (1). Subtracting equation (1) from equation (2), we obtain in the steady state

$$-\frac{\Delta n_3}{\tau_3} + \frac{\Delta n_2}{\theta_{23}} - \frac{\Delta n_3}{\theta_{32}} = 0 \qquad (3)$$

$$\Delta n_3 = n_3' - n_3 \qquad \Delta n_2 = n_2' - n_2$$

Δn_3 and Δn_2 are the changes induced in the population of levels $|2\rangle$ and $|3\rangle$ as the laser field is switched on and off. Notice that in equation (3) the rate R_3 has been eliminated. The changes in the population of these levels

as the laser field is switched on and off, may be determined by observing the changes in spontaneous emission originating from levels $|2\rangle$ and $|3\rangle$. The transitions used in this experiment are noted in figure 1b.

The non-radiative transitions expressed by the relaxation times θ_{32} and θ_{23} are produced by collisions involving atoms in the states $|2\rangle$ and $|3\rangle$ with atoms in the ground state. The collision rate $1/\theta_{32}$ due to collisions involving ground state atoms having a density n_o atoms per unit volume, may be written as

$$\frac{1}{\theta_{32}} = n_o \, v_r \, \sigma_{32} \tag{4}$$

where v_r is the mean relative thermal speed between colliding atoms and σ_{32} the collision cross section. As explained in the second section of this chapter, the product $v_r\sigma_{32}$ in equation (4) is to be interpreted as an average over the velocity distribution of the colliding atoms.

We re-write equation (3) in the following manner

$$\frac{\Delta n_3}{\Delta n_2} = \left[\frac{1}{\tau_3} + \frac{1}{\theta_{32}}\right]^{-1} \frac{1}{\theta_{23}} \tag{5}$$

In the limit of low pressure where the probability for radiative relaxation of level $|3\rangle$ is much greater than that for collisional relaxation to level $|2\rangle$, that is $\theta_{32} >> \tau_3$, equation (5) reduces to

$$\frac{\Delta n_3}{\Delta n_2} = \frac{\tau_3}{\theta_{23}} = n_o \, v_r \, \tau_3 \, \sigma_{23} \tag{6}$$

For high pressures where $\theta_{32} << \tau_3$, we obtain from equation (5)

$$\frac{\Delta n_3}{\Delta n_2} = \frac{\theta_{32}}{\theta_{23}} = \frac{\sigma_{23}}{\sigma_{32}} = \frac{g_3}{g_2} \exp[(E_2 - E_3)/kT] \tag{7}$$

Here g_2 and g_3 are the statistical weights of levels $|2\rangle$ and $|3\rangle$ respectively. The equality

$$\frac{\theta_{32}}{\theta_{23}} = \frac{g_3}{g_2} \exp[(E_2 - E_3)/kT] \tag{8}$$

is proven in the second section of this chapter.

It should be pointed out that although $\Delta n_3/\Delta n_2$ is given by a Boltzmann factor when $\theta_{32} << \tau_3$, this does not necessarily imply a thermalization of the ratio n_3/n_2. For this to occur, atom-atom collisions must also dominate the process described by R_3 which for gas discharges is primarily due to electron-atom collisions.[7]

The rate equation describing levels $|3\rangle$ and $|2\rangle$, simplifies because we have assumed the $3s_2$ and $3s_3$ levels to be isolated. By that we mean there are no other nearby levels which contribute significantly to changes in the population of levels $|3\rangle$ and $|2\rangle$ by collision induced transitions. That this assumption is not necessarily valid can be

seen by examination of figure 1. Thus we can see that in the rate equation for $|3\rangle$, we have ignored the contribution of transfer from the $3s_4$ and $3s_5$ levels as well as that from the 4d and 4d' levels. This amounts to neglecting second order changes in the population of $|3\rangle$ via changes in the $3s_4$, $3s_5$ and 4d levels.

To see just how great the second order changes might be, we consider again, the rate equation for $|3\rangle$. However this time we will include a third level, which we designate $|4\rangle$ in the rate equation. Thus we write

$$\frac{dn_3}{dt} = -\frac{n_3}{\tau_3} + \frac{n_2}{\theta_{23}} - \frac{n_3}{\theta_{32}} + \frac{n_4}{\theta_{43}} - \frac{n_3}{\theta_{34}} + R_3 = 0 \qquad (9)$$

Using the same procedure by which equation (3) was obtained, we can then write

$$-\frac{\Delta n_3}{\tau_3} + \frac{\Delta n_2}{\theta_{23}} - \frac{\Delta n_3}{\theta_{32}} + \frac{\Delta n_4}{\theta_{43}} - \frac{\Delta n_3}{\theta_{34}} = 0 \qquad (10)$$

Re-writing equation (10), we obtain

$$\frac{\Delta n_3}{\Delta n_2} = \left[\frac{1}{\tau_3} + \frac{1}{\theta_{32}} + \frac{1}{\theta_{34}}\right]^{-1}\left(\frac{1}{\theta_{23}} + \frac{\Delta n_4}{\Delta n_2}\frac{1}{\theta_{43}}\right) \qquad (11)$$

In the low pressure region where θ_{32} and θ_{34} are much greater than τ_3, equation (11) gives

$$\frac{\Delta n_3}{\Delta n_2} = \frac{\tau_3}{\theta_{23}} + \frac{\Delta n_4}{\Delta n_2}\frac{\tau_3}{\theta_{43}} \qquad (12)$$

Now in first order, the ratio $\Delta n_4/\Delta n_2$ in the low pressure region is given by

$$\frac{\Delta n_4}{\Delta n_2} = n_o \, v_r \, \tau_4 \, \sigma_{24} \tag{13}$$

Using this expression in equation (12), we obtain the following

$$\frac{\Delta n_3}{\Delta n_2} = n_o \, v_r \, \tau_3 \, \sigma_{23} + (n_o \, v_r)^2 \, \tau_3 \, \tau_4 \, \sigma_{24} \, \sigma_{43} \tag{14}$$

Thus there is a second order correction term essentially proportional to the cross section squared and therefore negligible in the low pressure region. In the high pressure region, equation (11) can be written as follows

$$\frac{\Delta n_3}{\Delta n_2} = \frac{\theta_{32}}{\theta_{23}} \left(1 + \frac{\theta_{32}}{\theta_{34}}\right)^{-1} + \frac{\Delta n_4}{\Delta n_2} \frac{\theta_{32}}{\theta_{43}} \left(1 + \frac{\theta_{32}}{\theta_{34}}\right)^{-1} \tag{15}$$

Using the first order value for $\Delta n_4/\Delta n_2$ in the high pressure region, we can then write the ratio $\Delta n_3/\Delta n_2$ in the high pressure region as

$$\frac{\Delta n_3}{\Delta n_2} = \frac{\sigma_{23}}{\sigma_{32}} \left(1 + \frac{\sigma_{34}}{\sigma_{32}}\right)^{-1} + \frac{\sigma_{24}}{\sigma_{42}} \frac{\sigma_{43}}{\sigma_{32}} \left(1 + \frac{\sigma_{34}}{\sigma_{32}}\right)^{-1} \tag{16}$$

Thus for the high pressure region, there is not only a second order correction term, but also a correction of the first order value. The extent of the first order correction

depends on the ratio of the cross section σ_{34}/σ_{32}. As will be discussed in the following section of this chapter, the cross section for this sort of event is a sharply peaked function of the energy discrepancy (ΔE). Thus one expects σ_{32} to be substantially larger than σ_{34} and thus the correction term to be very close to one.

Excitation Transfer Collisions

To begin with, we consider an atom which has two relatively isolated atomic states which we designate by $|1\rangle$ and $|2\rangle$ with energies E_1 and E_2 respectively. We take E_2 to be greater than E_1. This situation is shown in figure 2. By relatively isolated, we mean the energy spacing between these two levels and any other nearby level is very much greater than the thermal kinetic energy of the atoms.

In a gas discharge, there will be many processes which will be exciting levels $|1\rangle$ and $|2\rangle$. We wish to consider, explicitly, excitation and de-excitation of the following type. We consider collisions in which an atom in excited state $|2\rangle$ collides with an atom of the same species in the ground state. During such a process there can be excitation transfer[8] with one atom ending in state $|1\rangle$. The loss of internal energy is balanced by a gain in the relative kinetic energy of the atoms after collision. The inverse process where an atom in excited state $|1\rangle$ collides with an atom in the ground state and yields an atom in the excited

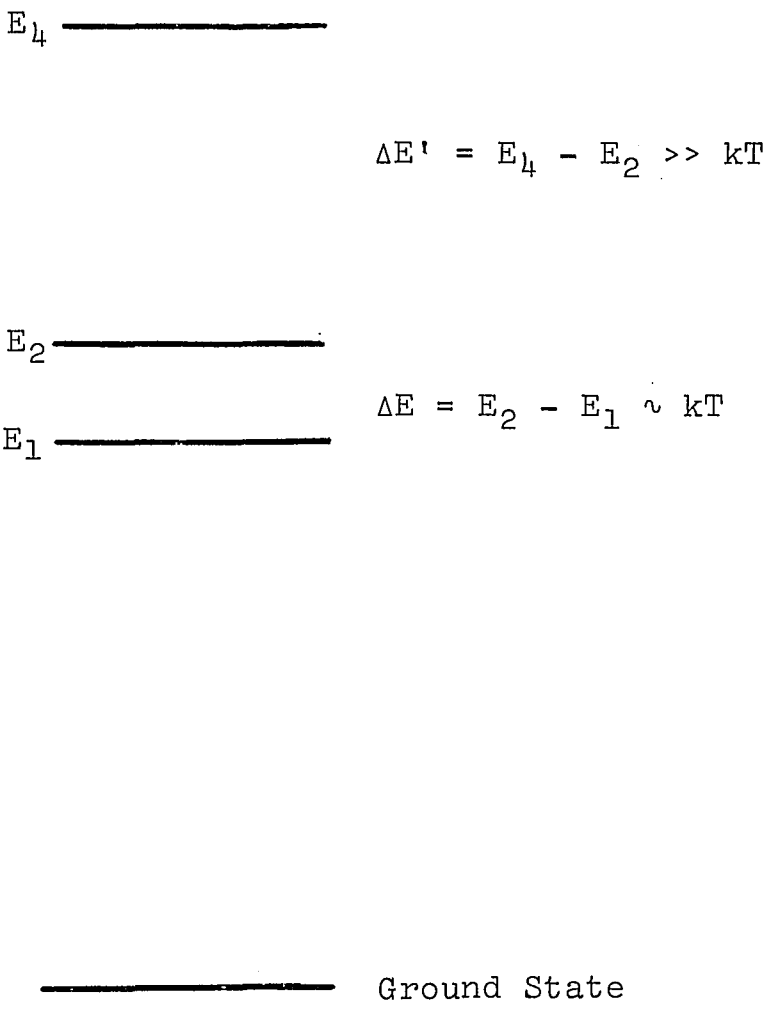

FIGURE 2. HYPOTHETICAL ENERGY-LEVEL DIAGRAM

state $|2\rangle$ can occur only if the relative kinetic energy before collision is greater than the energy difference $\Delta E = E_2 - E_1$ between states $|2\rangle$ and $|1\rangle$. Thus we can write for the rate of collisional excitation of level $|2\rangle$ from level $|1\rangle$, where the internal energy is increased by ΔE, as

$$\frac{n_1}{\theta_{12}} = \iiint dv_o^3 \iiint dv_1^3 n_1(v_1) n_o(v_o) v_r \sigma_{12}(v_r) \qquad (17)$$
$$(\tfrac{1}{2} m^* v_r^2 > \Delta E)$$

Here $n_1(v_1)dv_1^3$ is the number of atoms per unit volume in state $|1\rangle$ with velocity in the range $\vec{v}_1$ and $\vec{v}_1 + dv_1^3$, the quantity $n_o(v_o)dv_o^3$ is the number of atoms per unit volume in the ground state with velocity in the range $\vec{v}_o$ and $\vec{v}_o + dv_o^3$, v_r is the relative velocity $|\vec{v}_r| = |\vec{v}_o - \vec{v}_1|$ of the colliding atoms. m^* is the reduced mass of the colliding atoms and $\sigma_{12}(v_r)$ is the velocity dependent cross section for excitation transfer between states $|1\rangle$ and $|2\rangle$. θ_{12} is the relaxation time for the excitation transfer process. The integration is taken over that portion of phase space which corresponds to a relative kinetic energy larger than ΔE. For the reverse process where there are no restrictions on the relative kinetic energy of the colliding atoms, one can write

$$\frac{n_2}{\theta_{21}} = \iiint dv_o^3 \iiint dv_2^3 n_2(v_2) n_o(v_o) v_r \sigma_{21}(v_r) \qquad (18)$$

With the assumption that the velocity distribution of the atoms in state $|1\rangle$, state $|2\rangle$ and the ground state is Maxwellian at some temperature T, we can show by means of a transformation of the variables of the above two integrals and an application of the principle of detailed balancing that θ_{21} is related to θ_{12} by

$$\frac{\theta_{12}}{\theta_{21}} = \frac{g_1}{g_2} \exp(\Delta E/kT) \qquad (19)$$

Here g_1 and g_2 are the statistical weights of states $|1\rangle$ and $|2\rangle$ respectively, and k is the Boltzmann constant. This relation holds regardless of the details of the dependence of σ on the relative velocity v_r.

The relationship expressed by equation (19) will now be proved. Since we have assumed that the velocity of the atoms in $|1\rangle$, $|2\rangle$ and the ground state are Maxwellian at the same temperature T we can write

$$n_i(v_i) = n_i\left(\frac{m}{2\pi kt}\right)^{3/2} \exp(-\, mv_i^2/2kT)$$

We make the following transformation of variables

$$\vec{v}_r = \vec{v}_o - \vec{v}_1 \qquad \vec{v}_c = \frac{\vec{v}_o + \vec{v}_1}{2}$$

in rectangular components

$$v_{r_x} = v_{o_x} - v_{1_x} \qquad v_{c_x} = \frac{1}{2}(v_{o_x} + v_{1_x})$$

Now

$$dv_{o_x}\ dv_{1_x} = |J(v_{r_x}, v_{c_x})|\, dv_{r_x}\ dv_{c_x}$$

Where $J(v_{r_x}, v_{c_x})$ is the Jacobian of the transformation and is given by

$$J(v_{r_x}, v_{c_x}) = \begin{vmatrix} \frac{\partial v_{r_x}}{\partial v_{o_x}} & \frac{\partial v_{c_x}}{\partial v_{o_x}} \\ \frac{\partial v_{r_x}}{\partial v_{1_x}} & \frac{\partial v_{c_x}}{\partial v_{1_x}} \end{vmatrix} = 1$$

Thus

$$dv_{o_x}\ dv_{1_x} = dv_{r_x}\ dv_{1_x}$$

We then transform from rectangular coordinates in the phase space of v_r and v_c to spherical coordinates in the phase space of v_r and v_c. Thus we write

$$dv_r^3\ dv_c^3 = v_r^2\ v_c^2\ \sin\theta_r\ \sin\theta_c\ d\phi_r d\phi_c d\theta_r d\theta_c dv_r dv_c$$

After transforming variables in equation (17) and (18) and integrating over angles, we obtain

$$\frac{1}{\theta_{12}} = n_o\left(\frac{m}{2\pi kT}\right)^3 \int_o^\infty v_c \exp\left(-\frac{mv_c^2}{kt}\right) dv_c \left\{ \int_{v'}^\infty v_r^3 \sigma_{12}(v_r) e^{-\frac{m^* v_r^2}{2kT}} dv_c \right\} \tag{20}$$

$$\frac{1}{\theta_{21}} = n_o\left(\frac{m}{2\pi kT}\right)^3 \int_o^\infty v_c\ e^{-\frac{mv_c^2}{kT}} dv_c \left\{ \int_o^\infty v_r^3 \sigma_{21}(v_r) e^{-\frac{m^* v_r^2}{2kT}} dv_c \right\} \tag{21}$$

Notice that the right hand side of equations (20) and (21) differ only by the bracketed integrals. The principle of detailed balancing gives us the following relationship[9] between the cross sections $\sigma_{12}(v)$ and $\sigma_{21}(v)$

$$g_1 v^2 \sigma_{12}(v) = g_2 (v^2 - v'^2)\sigma_{21}([v^2 - v'^2]^{1/2}) \qquad (22)$$

where v is the relative velocity before the collision and $(v^2 - v'^2)^{1/2}$ is the relative velocity after the collision. Here $v'^2 = 2\Delta E/m^*$. Substituting for $\sigma_{12}(v_r)$ the value given by equation (22) into equation (20), we can write for the bracketed portion of the right hand side of equation (20)

$$\int_{v'}^{\infty} \frac{g_2}{g_1} (v_r^2 - v'^2)\sigma_{21}([v_r^2 - v'^2]^{1/2})\, e^{-\frac{m^* v_r^2}{2kT}} v_r dv_r \qquad (23)$$

Making a final change of variables,

$$v^2 = v_r^2 - v'^2$$

we can then rewrite equation (20) in the following manner

$$\frac{1}{\theta_{12}} = \frac{g_2}{g_1} \exp(-\frac{m^* v'^2}{2kT}) n_o (\frac{m}{2\pi kT})^3 \int_o^{\infty} v_c^2 e^{-\frac{mv_c^2}{kT}} dv_c \int_o^{\infty} v^3 \sigma_{21}(v) e^{-\frac{m^* v^2}{kT}} dv \qquad (24)$$

Dividing equation (21) by equation (24), we obtain for the ratio θ_{12}/θ_{21}

$$\frac{\theta_{12}}{\theta_{21}} = \frac{g_1}{g_2} \exp(+\frac{m^* v'^2}{2kT}) = \frac{g_1}{g_2} \exp(\Delta E/kT) \qquad (25)$$

Since the collision cross sections are velocity dependent and since we study the excitation transfer in a gas discharge where there is a distribution of velocities, we define an effective cross section in the following manner. The collision rate $1/\theta_{ij}$, due to collisions involving ground state atoms having a density n_o atoms per unit volume, may be written as

$$\frac{1}{\theta_{ij}} = n_o \, v_r \, \sigma_{ij} \tag{26}$$

where v_r is the relative thermal speed between colliding atoms, and σ_{ij} is the collision cross section. The product $v_r\sigma_{ij}$ in this equation is to be interpreted as an average over the velocity distribution of the colliding atoms. With an effective cross section defined in this manner, we obtain finally the ratio σ_{12}/σ_{21} as

$$\frac{\sigma_{12}}{\sigma_{21}} = \frac{g_2}{g_1} \exp(-\Delta E/kT) \tag{27}$$

It is of interest to consider the conditions under which the cross section for the type of excitation transfer discussed above might be expected to be sizeable. We can make an order of magnitude calculation in the following manner. The duration of an atomic collision can be approximated by the ratio of the atomic radius to the relative velocity of the colliding atoms. This is about 10^{-13} seconds for atoms under gas kinetic conditions. During this time the

energy of either atom is uncertain by an amount δE given by the uncertainty principle

$$\delta E \, \delta t \sim \hbar$$

From this, $\delta E/\hbar$ is approximately 10^{13} seconds^{-1}. Thus δE is about 300 cm^{-1}. If ΔE, the energy spacing between the two excited levels, is of this order of magnitude the cross section for excitation transfer may be expected to be large since the uncertainty widths of the two levels overlap each other during the collision. For $\Delta E/\hbar >> 10^{13}$ seconds^{-1} one expects, in general, a much smaller cross section. It is evident that the cross section for collision transfer of excitation will be velocity dependent.

This type of argument, while giving a feel for a limit on ΔE such that there is a finite cross section for excitation transfer, gives no indication of the size of the cross section to be expected. Several other generalizations about the cross section for this kind of event can be made.[10] The cross section for excitation transfer at a fixed initial relative velocity is a sharply peaked function of ΔE exhibiting a maximum at or near exact energy resonance. The maximum cross section will not greatly exceed the gas kinetic except for collisions in which a transfer of excitation occurs involving an optically allowed transition in each colliding atom. For a fixed ΔE and atomic radius r, the cross section increases rapidly with relative velocity until

$r\Delta E/h\nu$ is of order unity after which it decreases slowly. It is also to be expected that the cross section will be larger if total spin is conserved. For example, the cross section for an event such as

$$X(^3D_o) + X(^1S_o) \rightarrow X(^1S_o) + X(^3P_o)$$

will be larger than the cross section for an event such as

$$X(^3D_o) + X(^1S_o) \rightarrow X(^1S_o) + X(^1P_o).$$

REFERENCES

[1]Parts of this chapter are based on Ali Javan, "Gaseous Optical Masers," in C. DeWitt, A. Blandin, and C. Cohen-Tannaudji, eds., Quantum Optics and Electronics, (New York, 1965), pp. 393-396.

Joel H. Parks and Ali Javan, "Collision-Induced Transitions Within Excited Levels of Neon," The Physical Review, 139 (August, 1965), 1352-1355.

[2]Charlotte E. Moore, Atomic Energy Levels, Circular of the National Bureau of Standards, 467 (Washington D. C., 1949), I, 77.

[3]Paschen notation, although more convenient than the Racah notation for noble gas levels, suffers from the fact that it conveys little information about the level. However, the use of Paschen notation predominates in the laser literature and for that reason it will be used throughout this dissertation.

[4]Moore, op. cit., p. 77.

[5]Actually the resonance trapped lifetime.

[6]Harrie Massey and Eric Burhop, Electronic and Ionic Impact Phenomena, (Oxford University, 1952), pp. 68-72.

[7]James D. Cobine, Gaseous Conductors, (New York, 1941), pp. 233-234.

[8]Alan Mitchell and Mark Zemansky, Resonance Radiation and Excited Atoms, (London, 1934), p. 156.

[9]Massey and Burhop, op. cit., p. 417.

[10]Ibid., p. 450.

CHAPTER III

EXPERIMENTAL APPARATUS AND PROCEDURE

As shown in the preceding chapter, the ratio of the Einstein coefficients A_2/A_3 and the product $\tau_3\sigma_{23}$ can be found by measuring the ratio $\Delta I_2/\Delta I_3$ as a function of pressure. Experimentally this is accomplished by observing the changes in intensity ΔI_2 and ΔI_3 as the laser radiation field interacts with excited neon atoms in a small discharge tube in which the pressure can be varied. Figure 3 shows the experimental arrangement. In order to obtain the largest possible signal to noise ratio, the small discharge tube is placed within the laser cavity. The intensity of the laser radiation field within the cavity is at least two orders of magnitude greater than that obtainable outside of the cavity. To minimize loss, the small discharge tube is built with quartz Brewster angle windows.

The experimental arrangement allows a direct determination of ΔI_3 and ΔI_2. This is accomplished by switching the laser beam on and off, using a rotating chopper within the cavity, while monitoring the spontaneous emission from the side of the small discharge tube. The chopping frequency was either thirty or one hundred hertz. Hence the chopping rate is very slow compared to the relaxation times of the atomic processes occurring within the discharge. The side light from the small discharge cell was focused upon the entrance slit of a half meter grating spectrometer and

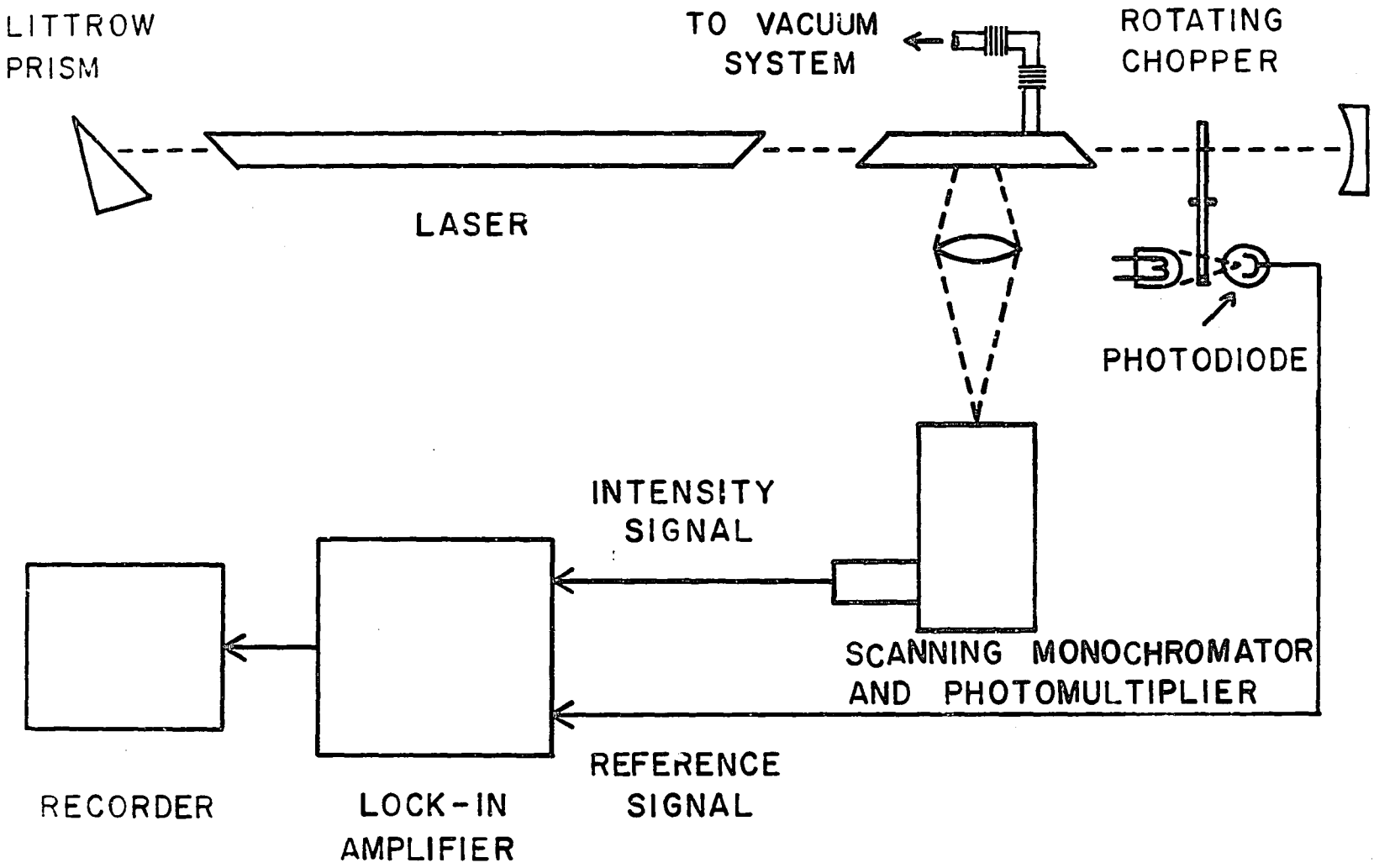

FIGURE 3. SCHEMATIC DIAGRAM OF THE EXPERIMENTAL APPARATUS

detected with a photomultiplier. The detected signal was then fed to a lock-in amplifier. The output of the lock-in amplifier is directly proportional to the change of the intensity of the detected signal as the laser is switched on and off. The ratio of the output of the lock-in amplifier when the spectrometer is focused for line I_3 and line I_2, respectively, gives directly the ratio $\Delta I_3/\Delta I_2$ at the particular pressure being used. The small discharge tube is connected through a metal bellows arrangement to a high vacuum system and a pure gas handling system in order to be able to vary the pressure within the tube.

Vacuum System

The vacuum system is shown in figure 4. The use of an ion pump enabled the attainment of very low pressures without the use of liquid nitrogen trapping and without the fear of contamination of the system with pump oil. In this experiment, however, large amounts of helium and neon had to be pumped. Ion pumps are notoriously slow pumps for noble gases, and this presented some problems. The pump used was a Varian Vac-Ion pump and had a rated air pumping speed of eight liters per second. The pumping speed for helium and neon is approximately ten percent of the air pumping speed. Only the relatively small volume to be evacuated allowed the use of such a slow pumping speed. Ion pumps pump noble gases by burying the gas atoms beneath a layer of sputtered titanium

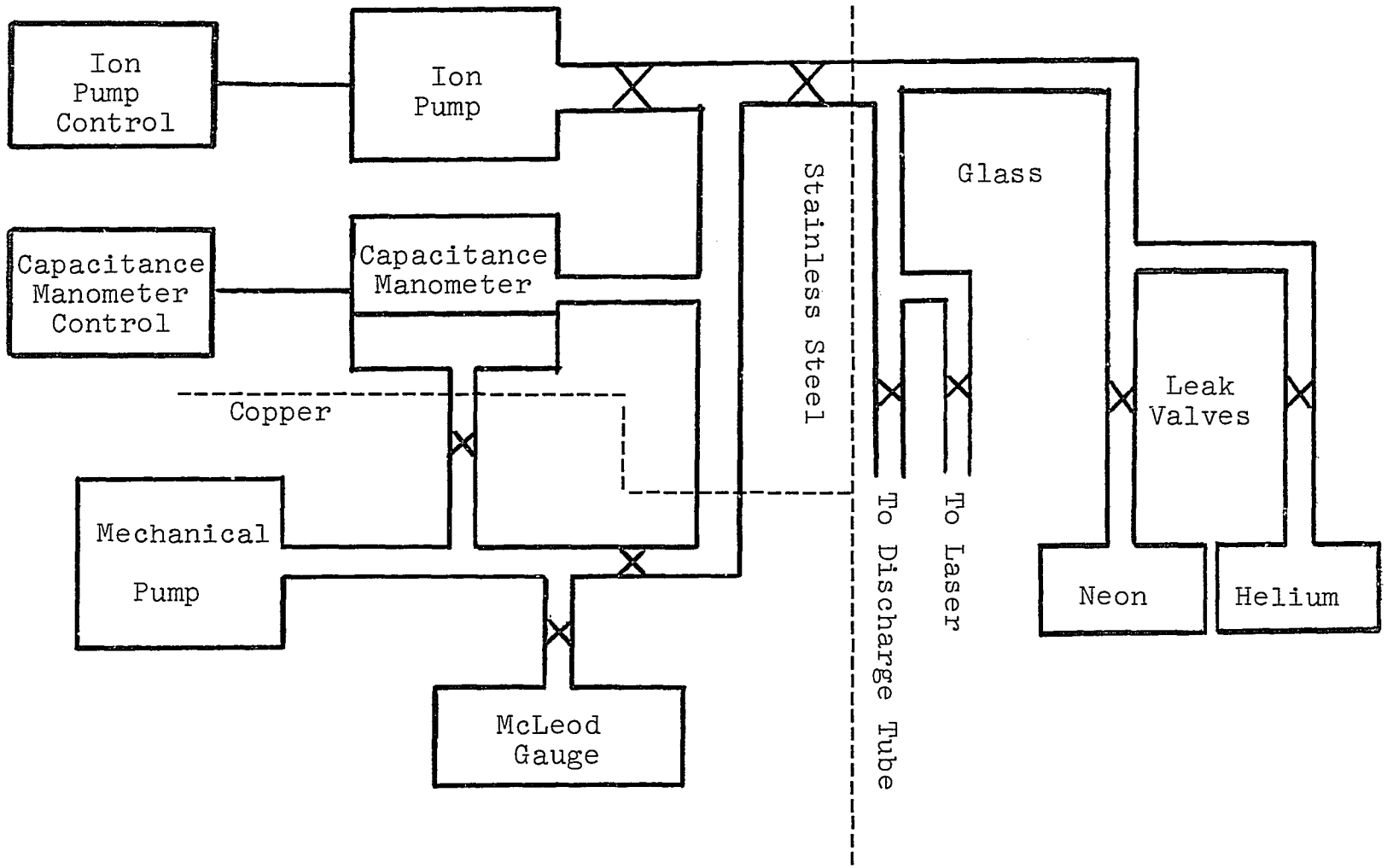

FIGURE 4. VACUUM SYSTEM

atoms. After pumping large amounts of noble gases some of these buried atoms begin to be re-admitted to the system, thus decreasing the net pumping speed even further.[1] Because of the large amounts of helium and neon that were pumped over long periods of time, an occasional bake out of the pump was undertaken. This was done by removing the magnet from the ion pump and wrapping the pump body with heating tape. The pump was then heated to approximately 200 to 300 degrees centigrade while pumping on the ion pump with a mechanical pump. This was done for a period of approximately one day. A great improvement in the pumping speed was obtained by this procedure. This was especially noticeable at higher pressures. Long periods of pumping at very high vacuums also contributed to maintaining the rated pumping speed.

In the stainless steel section of the vacuum system, it was possible to obtain pressures approaching 10^{-9} torr. After a thorough bake out of the laser tube and of the small discharge tube electrodes and the metal bellows system connecting the small discharge tube to the vacuum system, pressures below 5×10^{-8} torr. were obtained for the whole system. The electrodes of the laser tube were of the heated cathode variety and hence it was possible to bake these electrodes using the internal heaters. The electrodes of the small discharge tube were made of platinum and were

cleaned by running a low pressure neon discharge between them. When using this procedure it is necessary to use each electrode as the cathode for an equal amount of time. This is necessary since most of the power loss in a gas discharge takes place at the cathode. The bellows system connecting the vacuum system to the small discharge tube was made of copper and stainless steel and was baked out by using a hot air gun.

The pressure within the system was measured by reading the pump current of the ion pump. For filling the laser and also the small discharge tube, the pressure of the constituent gases was measured by using a capacitance manometer as a null reading instrument. Pressure on the other side of the capacitance manometer was measured by using a mercury McCleod gauge. This method assures that mercury does not enter the clean side of the vacuum system.

The gases used were research grade quality supplied in one liter Pyrex bulbs by the Matheson Corporation. These bulbs are constructed with a "break seal." They were opened after attachment to the vacuum system by dropping a small iron slug on the seal. To prevent impurities from entering the system, the iron slug was sealed in an evacuated glass capsule. The slug was dropped by raising it up the neck of the flask with a magnet and then removing the magnet suddenly. The gas was metered into the system through Granville-Phillips leak valves.

To fill the system to any desired pressure, the pressure on the mercury McCleod gauge side of the capacitance manometer was first adjusted to the desired pressure. Gas was then metered through the leak valve until the capacitance manometer was nulled. This system allows a rapid and precise method of filling the tube.

In filling the laser it is necessary to meter in both helium and neon. To obtain a particular total pressure and mixture ratio, the following procedure was used: knowing the total pressure and mixture ratio, the partial pressure of helium in the system was calculated. The system was then filled with this pressure of helium using the capacitance manometer. Neon was then leaked into the system until the desired total pressure was reached.

Stop-cocks C and D are the only valves within the system using grease. A high vacuum silicone stop-cock grease was used. No problems were encountered with excited atoms from the discharge reacting with this stop-cock grease.

Construction of the Laser

At the time this project was started the literature concerning construction details for gas lasers was very sparse. Even now the available literature lends little help, except for one excellent reference[2] which has just been published. Thus many hours of work were necessary before the proper methods of constructing a working helium-neon laser were developed.

Initial attempts at constructing a helium-neon laser were made with a tube which used commercial neon sign electrodes. These electrodes were made of iron. Iron absorbs large amounts of gas and is difficult to outgas.[3] The output of a helium-neon laser is adversely affected by small amounts of hydrogen or oxygen in the discharge. Attempts to clean out the iron electrodes were made using both rf induction heating and discharge cleansing. Even after long periods of heating the electrodes red hot using induction heating, while at vacuums of 10^{-5} torr., impurities from the electrodes could be seen when the tube was filled and the discharge started. The presence of the impurities could be noted as a change of color of the discharge with time.

The absolute pressure and the partial pressures of helium and neon are fairly critical in producing oscillation. Initially thermocouple gauge tubes were used to measure the pressure. These tubes were calibrated for air and proved to be too inaccurate for use with helium and neon. Also at this time there was some controversy in the literature concerning the proper total and partial pressures necessary for a particular tube diameter.

The problem of impurities evolving from the tube electrodes was solved by using commercial thyratron cathodes with internal heaters as the electrodes. Each electrode was heated

in vacuum until a pressure below 10^{-7} torr. could be reached with the heaters on. By following this procedure, no problems were encountered because of out gassing of the electrodes. A satisfactory means of measuring the pressure accurately was developed using a mercury McCleod gauge and a capacitance manometer as described in the section on the vacuum system. A relationship between the total pressure and the tube diameter which was found to produce satisfactory results for obtaining oscillation is given by Mielenz and Nefslen.[4]

Attempts to construct a laser oscillating on the 6328 A line of neon, even after the above problems were solved and proper laser alignment was obtained, were frustrated. The reason for failure to obtain oscillation at 6328 A was found to be due to the presence of oscillation at 3.39 microns. This result was unexpected because dielectric mirrors with greater than 99 percent reflectivity at 6328 A were being used.

The dielectric mirrors were on Borosilicate blanks which are not transparent beyond 3 microns. Hence oscillation at this wave length could not be detected in the normal manner. In fact, the first suspicion that oscillation was occurring at this wave length occurred when the Brewster angle windows were being cleaned with ethyl alcohol in the expectation that dust on the windows might be preventing oscillation at

6328 A. This cleaning was carried out while the laser was in alignment and the discharge running. As the film of alcohol dried, it formed a thin flat surface on the Brewster windows. Oscillation broke out at 6328 A and lasted for a few seconds. The oscillation quit as the film dried completely. The fact that oscillation would occur with the alcohol on the windows and not when it had dried off, indicated that the alcohol, by means of absorption, was probably preventing some other oscillation. Fortuitously it turns out that the CH stretching band's fundamental mode of vibration is at about 3.4 microns.[5] Thus the 3.39 micron oscillation was suppressed when the alcohol film was on the windows.

The reason that oscillation at 3.39 microns prevents oscillation at 6328 A is because these two transitions share the same upper level. The gain of the 3.39 micron transition is so much higher than that of 6328 A that oscillation on 3.39 depletes the upper level sufficiently to prevent oscillation at 6328 A. The gain is so great at 3.39 microns that in a tube whose length is slightly greater than one meter super-radiance occurs. This means that the gain per meter of this transition at the pressures and tube diameter used, is almost one. Thus even low reflectivity mirrors (that is a cavity with low Q) can produce oscillation on this transition.

As previously mentioned, the mirrors for 6328 A are opaque for 3.39 micron radiation. Consequently oscillation at this wave length had to be inferred indirectly. The method used was to monitor visible spontaneous emission from the side of the tube for transitions originating on the upper and lower laser levels.[6] A line sharing the same upper level as the laser will show a decrease in intensity when the laser is oscillating. A line originating on the lower laser level will show an increase in intensity when the laser is oscillating. In this manner it was determined that it was the 3.39 micron oscillation that was preventing oscillation at 6328 A. In fact with this experimental setup, it was possible to obtain oscillation at 6328 A only by replacing one of the mirrors with a Littrow prism.

Description of the Laser and Laser Cavity

The active length of the laser discharge is one meter. The end windows are made of Homosil quartz and set at Brewsters angle. Pyrex windows were not used, since for this experiment the windows must be transparent at 3.39 microns. It should be pointed out, however, that if one is interested only in operating a helium-neon laser in the visible, then Pyrex windows should be used. The use of Pyrex is preferred because it prevents oscillation at 3.39 microns. As previously explained this permits oscillation on the visible lines originating from the same upper level from which the 3.39 micron transition originates.

Although the electrodes have internal heaters, these were not used while running the discharge. Instead the discharge was run with cold cathodes. In cold cathode discharges, a process known as clean up occurs. Clean up reduces the pressure within the discharge by pumping the gas in a manner similar to that occurring in an ion pump. The clean up was rapid enough, that after about ten hours of operation, the pressure had decreased to a point at which oscillation ceased. To minimize the effect of clean up, a one liter Pyrex bulb was attached to the laser to act as a gas ballast. This increased the volume of gas in the laser system by more than an order of magnitude.

The laser and the small discharge tube are excited with separate dc power supplies. The laser was powered by a commercial 0 - 100 ma, 0 - 10 kv power supply. The usual excitation was 14 ma at 3.4 kv. Since the discharge has a small negative differential resistance it was necessary to use a ballast resistor in order to maintain a steady discharge. A ballast of 100 kohms was found to be satisfactory. The small discharge tube was powered by a half wave rectifier dc supply. This supply used a neon sign transformer and two high voltage solid-state rectifiers. A pi-section capacitor filter was used to smooth the output. It was also necessary to ballast this supply to provide a stable discharge through the tube. A current of 6 milliamperes was maintained in the

small discharge tube for these experiments. An rf discharge was originally considered for the laser but because of load matching difficulties and rf interference problems, this method was abandoned.

The small discharge tube was fifteen centimeters long and had quartz Brewster angle windows. The electrodes were made of platinum. However due to the peculiarities of gaseous discharges, a discharge could not be maintained between the two tube electrodes. The reason for this was because the connection of the small discharge tube to the vacuum system is made to the center of the small discharge tube, with a tube of larger diameter than that of the discharge tube itself. The discharge ran from one of the tube electrodes down through this connecting tube to the metal bellows system. Since it is not necessary to maintain a discharge in the total length of the tube but only in that part of the tube which is in front of the spectrometer entrance slit, it was decided to let the discharge take the easiest path. Thus the metal bellows system served as the grounded cathode for the discharge. Thorough baking and discharge cleansing was necessary to outgas the bellows completely. As a further precaution against contamination from this unorthodox electrode, the tube was pumped out every night and refilled in the morning. Using the bellows assembly as a cathode has one advantage however. The

majority of the heat generated in a dc discharge takes place at the cathode and the large area of the bellows assembly serves as a very good heat sink.

Subsequent tubes which were constructed used relatively large aluminum plugs as cathodes. The fill tube was connected at the cathode end. This prevented the discharge from running down the fill tube. Figure 5 shows the physical arrangement of the laser. The laser, the small discharge tube, and the mirrors are all mounted separately on a two meter triangular optical bench. Figure 5 also shows the mounting of the chopping motor. Note that the motor is not mounted on the optical bench. The mounts themselves will be discussed in detail in the section on laser alignment.

The choice of the radius of curvature of the cavity mirrors is not arbitrary. The Q of the cavity is dependent on the radius of curvature of both mirrors and the separation between the mirrors. Figure 6 is a Boyd-Kogelnik stability diagram,[7] which enables one to choose the proper radius of curvature mirrors for a given separation. Ordinarily one wishes to obtain the highest cavity Q, that is a cavity that has a low loss factor. The loss is due to diffraction. Thus one wishes to avoid having a combination of mirror radii and separation, the combination of which falls in the shaded portion of the stability diagram. In this stability diagram, L is the separation between the mirrors, and R' and R'' are the radii of curvature of the mirrors measured in the same units as L.

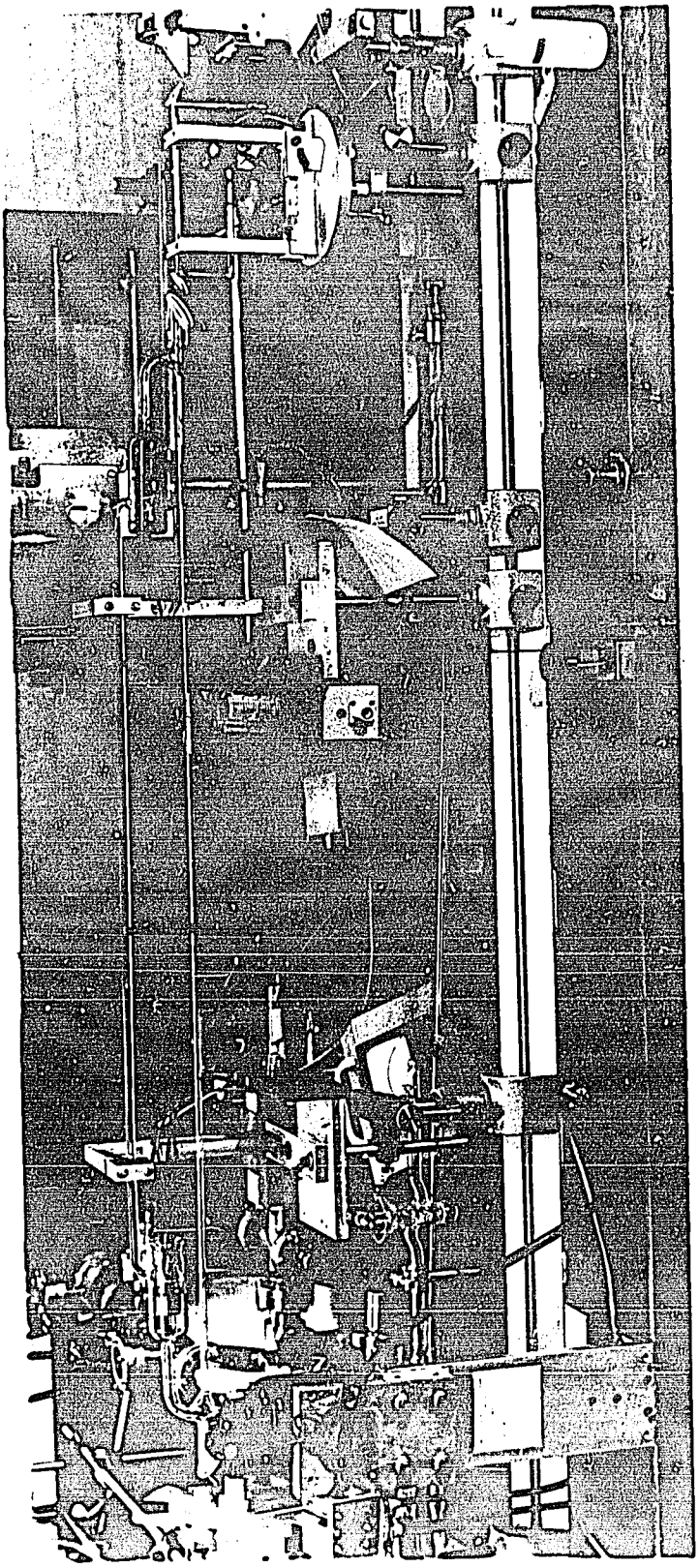

FIGURE 5. EXPERIMENTAL SETUP

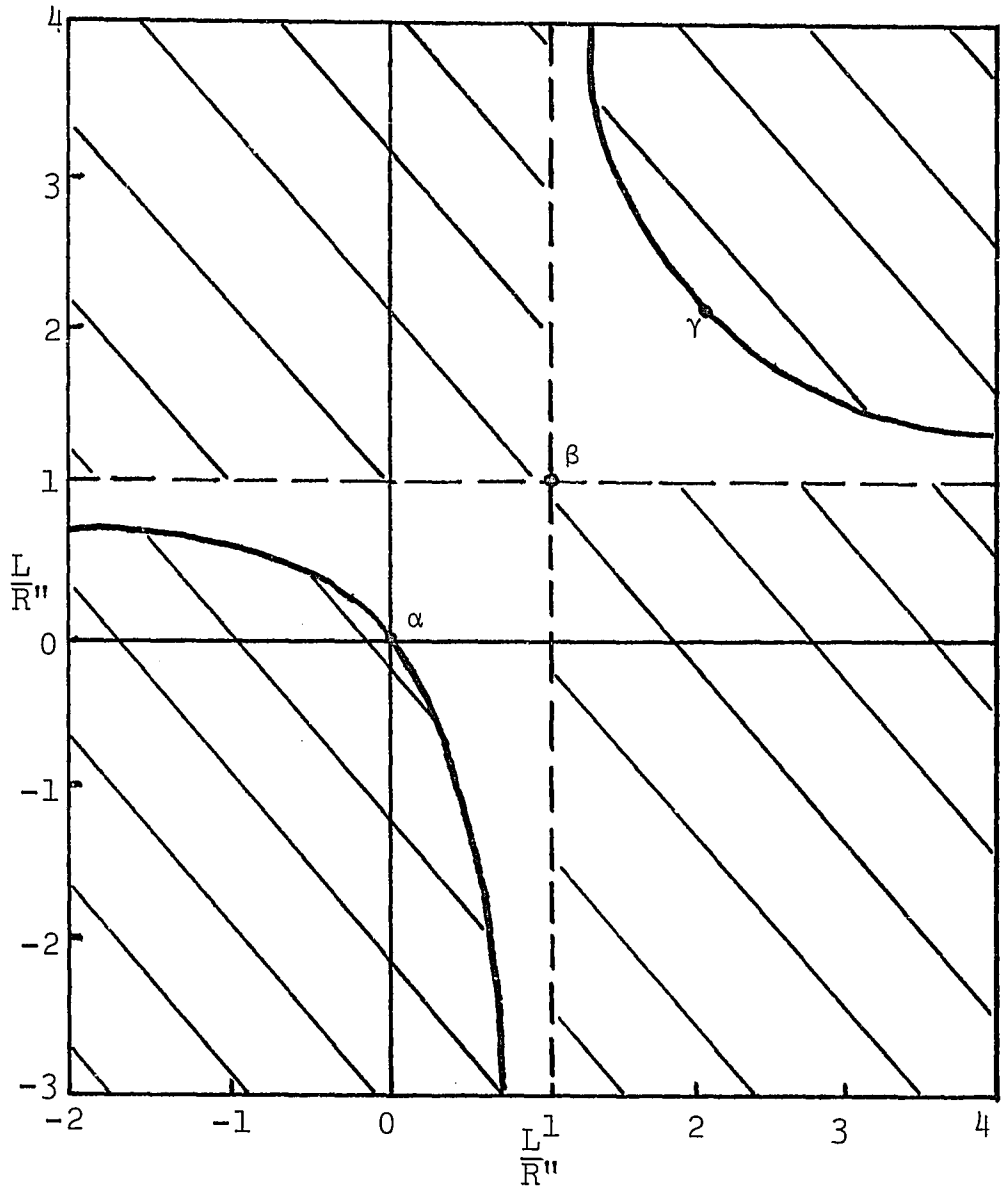

FIGURE 6. BOYD-KOGELNIK STABILITY DIAGRAM

Concave mirrors are taken to have a positive radius of curvature.

In this experiment, the cavity is closed at one end with a quartz Littrow prism. The prism makes it possible to select a particular wave length region to have a high Q. The other end of the cavity is closed with either a gold or multi-layered dielectric spherical mirror.

The Littrow prism is equivalent to a plane mirror. Hence its radius of curvature is infinite. Thus, as can be seen from figure 6, for a low loss cavity the radius of curvature of the mirror completing the cavity must be greater than the separation between the mirror and the Littrow prism. For this experimental arrangement it is therefore necessary to use a mirror whose radius of curvature is 1.8 meters or greater to have a low loss cavity.

For almost all laser transitions the gain is too low to permit oscillation in the high loss region. The 3.39 micron transition in neon is one of the exceptions to this rule.

The use of a Littrow prism as one of the cavity reflectors limits oscillation to a small wave length region about the wave length at which the prism is set for normal reflection. There are, however, several neon transitions which are known to oscillate at wave lengths which are too close to 3.39 microns for the prism to be able to suppress.[8] However, the gains of these transitions are much lower than that at 3.39 microns. In order to insure that oscillation

took place only at 3.39 microns, the laser cavity was deliberately set in a high loss region. This was done by using a one meter radius of curvature gold mirror along with the Littrow prism as the reflectors with the separation being approximately two meters. As can be seen from figure 6, this combination of reflectors is in the high loss region of the stability diagram.

As mentioned above, the gain at 3.39 microns is so high that oscillation takes place even though the cavity has a high loss. However, the other transitions will not be able to oscillate. In this manner the laser is set to oscillate only at 3.39 microns. Operating the laser in a high loss cavity does not result in any decrease in the radiation field within the cavity for the 3.39 micron transition. This is due to the tremendously high gain of the 3.39 micron transition. This very large gain causes the amplifying medium to saturate.[9] This means the loss within the cavity can be made quite high before the radiation density of the oscillation field decreases. This was experimentally verified for this experimental arrangement. In contrast, the 6328 A transition could not be made to oscillate even with a 99 percent reflecting dielectric mirror when the cavity was just inside the high loss region.

The stability diagram has several interesting features that are worth pointing out. Note that the points denoted by α, β and γ are all positions of marginal stability.

α represents the case of two plane parallel mirrors. β is the position of a confocal system; i.e. a system where the mirrors are separated by their radius of curvature. And γ is the case of the concentric system where the mirrors are separated by twice their radius of curvature. These points, particularly α and β, one might think without prior analysis to be desirable operating points thus turn out to be points which in general should be avoided. Spherical mirrors or the combination of a plane mirror and spherical mirror has another advantage over two plane mirrors. The degree of parallelism between two plane mirrors is an order of magnitude more strict than that between a spherical and a plane mirror to produce oscillation.[10]

Figure 7 shows a diagram of the Littrow prism. Bloom[11] was the first to use a prism in a laser cavity to obtain wave length selection. He used, however, a full prism and a separate mirror. For the purposes of this experiment, a system as complex as that was not necessary. The use of a Littrow mounting simplifies alignment greatly.

It is, of course, desirable to arrange the prism face so that it is inclined to the incident beam at Brewsters angle. A simple geometric construction and the use of Snells Law and Brewsters Law show that the prism angle α should be the complement of Brewsters angle for the particular wave length desired. Thus only for one particular wave length will the

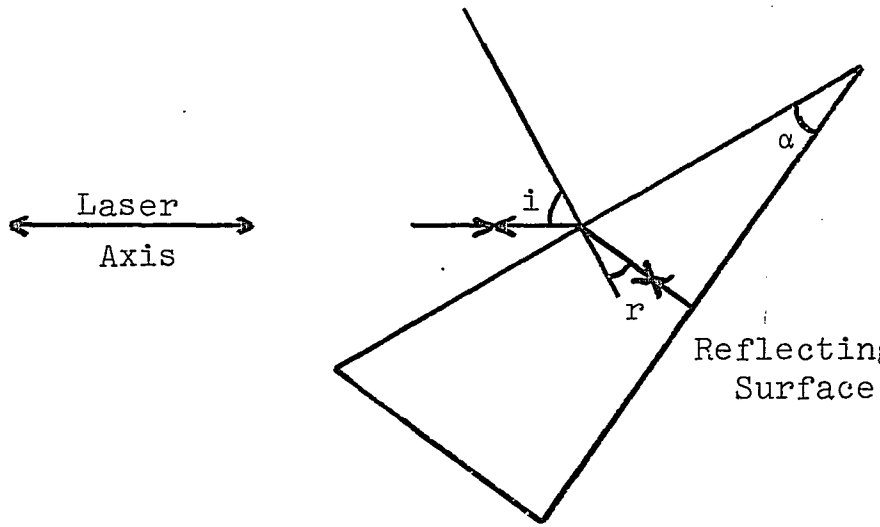

$$\tan i = n$$

$$\frac{\sin i}{\sin r} = n$$

$$\alpha = r$$

$$\therefore \cos i = \sin \alpha$$

$$\text{or } \alpha = i - \pi/2$$

FIGURE 7. LITTROW PRISM REFLECTOR

prism face actually be inclined at Brewsters angle. However, there is a relatively broad angular region about Brewsters angle where the reflectivity is very low. Thus changes in prism orientation in order to change the wave length of the cavity at which the cavity Q is high, does not introduce any large reflective losses.

Alignment of the Laser Cavity

The following procedure was used for the optical alignment of the laser cavity. Before attaching the laser tube to the vacuum system, the laser was aligned mechanically with the optical bench both in the vertical and horizontal planes. Figure 8 shows the mechanical mounting of the laser tube to the optical bench. The mounts are held in carriages which are fixed to the optical bench. These carriages have both vertical and horizontal travels. The use of these travels enables the laser tube to be set both parallel to and directly over the optical bench. After this is done, the travels are locked, the laser tube is tightened in its mounts, and then attached to the vacuum system.

A small commercial helium-neon laser oscillating on the 6328 A red line of neon was then used for the second step of the laser alignment. This laser was mounted at one end of the optical bench on a lab jack. It was then adjusted until its beam was parallel to the axis of the laser tube. This was done by adjusting the beam from the alignment laser so

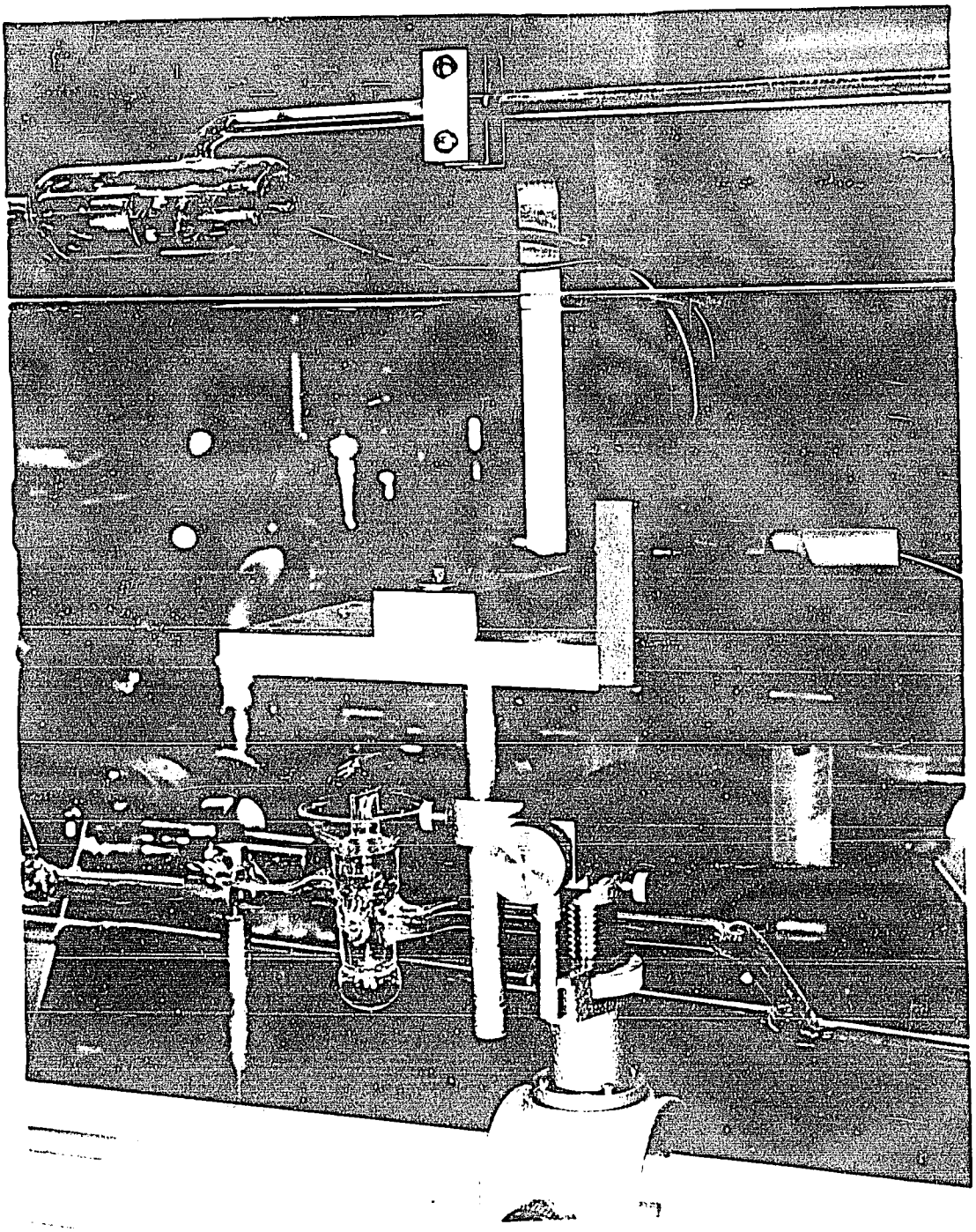

FIGURE 8. LASER MOUNTING

that it passed just below and parallel to the tube. The lab jack was then used to raise the alignment laser into a position such that its beam would pass through the laser tube. If sufficient care were taken in aligning the beam before raising it to this position, slight correction would then suffice to enable the beam to pass through the tube without striking the walls. The mirror mounts were then placed in position. These mounts were held in carriages which allowed both vertical and horizontal motion. In each mount was placed a disc which just fit the mount and which had a small hole at the center. The mirror mount at the near end of the tube (the alignment laser end) was then adjusted until the beam passed through the hole in the disc. The mount at the far end was then adjusted to obtain the same result. The laser tube and the two mirror mounts were thus set coaxially. A mirror was then placed in the mount at the far end of the tube and adjusted such that the beam striking it was reflected back though the tube without hitting the walls and passed back though the hole in the disc in the near mirror mount. When this is accomplished, the mirror at the far end of the tube was considered to be in alignment and was not disturbed until oscillation was obtained. The alignment laser was then turned off and the disc removed from the near mount and replaced with the mirror.

The mirrors used in this alignment procedure were multi-layer dielectric mirrors with a reflectivity of 99 percent at 6328 A. In the blue, however, they are quite transparent. This property is used in the third stage of alignment. Since the laser tube and the mirror centers are coaxial and since the mirror at the far end of the tube is also perpendicular to the tube axis, it remains only to set the mirror at the near end of the tube perpendicular to the tube axis to have the two mirrors and the laser tube in alignment. To set the near mirror perpendicular to the tube axis, an "eyeball" autocollimation method is used. This method consists of looking with one eye through the near mirror and down the axis of the laser tube. The mirror at the near end of the tube is then adjusted until the reflection seen of the eyeball from the back of the mirror is centered exactly with the tube axis. This procedure is precise enough if done with care, that usually with just a few minutes further work the desired optical alignment is completed. This is done by making small adjustments to the near mirror while looking for the well known "moon" to appear in the laser tube at the far end. When the "moon" appears, the laser will oscillate if the gas fill is correct. The final touch up to the adjustments is then made while the laser oscillates. Small corrections are made to both mirrors in order to maximize the output of the laser.

The mirror mounts are shown in figure 9. The mirror is held in a gimmal arrangement which allows independent motion about two mutually perpendicular axes. Only a very small amount of backlash is present in the micrometer drive system and thus repeatable settings are possible with this mounting arrangement. The mirror mounts and the carriages holding them are stable enough that the mirrors may be removed and then replaced without affecting the alignment of the system. The stability is so good that the carriage along with the attached mount and the mirror can be removed from the optical bench and then replaced without disturbing the alignment.

After oscillation has been obtained, the small discharge tube is placed within the cavity. This tube must be aligned coaxially with the laser tube. As previously mentioned the small discharge tube is connected to the vacuum system through a bellows arrangement. However, the bellows system is not connected rigidly to the vacuum system but is connected through a rotatable coupling. This allows the small discharge tube to be rotated into or out of the cavity without breaking the vacuum. The bellows system allows motion in three mutually perpendicular directions. The small discharge tube mount shown in figure 10 allows the discharge tube to be moved in both the vertical and horizontal planes. It also provides for rotation about a vertical axis and also about a horizontal axis passing though one end of the tube.

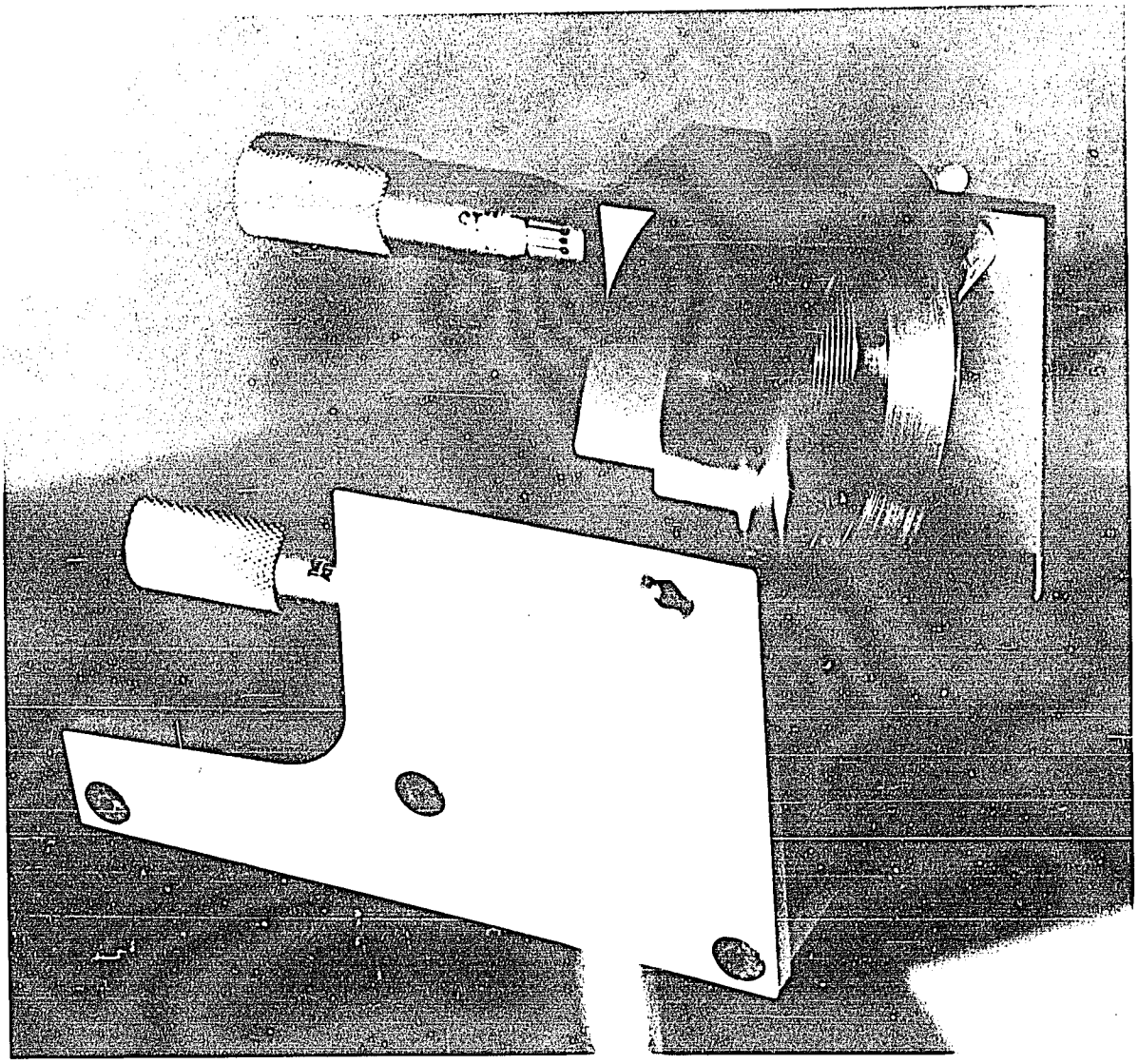

FIGURE 9. MIRROR MOUNT

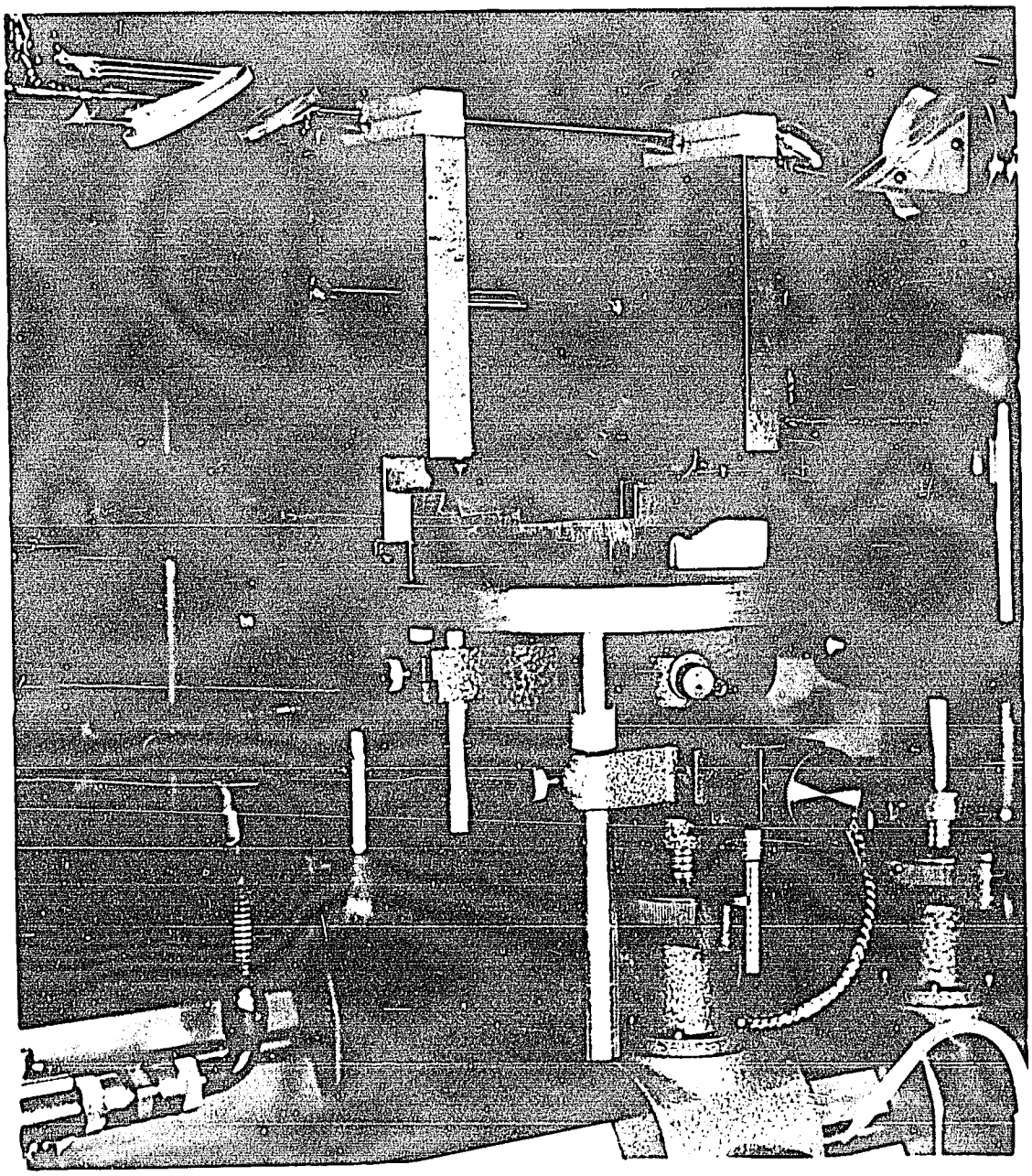

FIGURE 10. DISCHARGE TUBE MOUNT

The small discharge tube is aligned in the following manner. The near mirror is removed and the alignment laser turned back on. The small discharge tube is then adjusted such that the beam which passes down the axis of the laser tube also passes through the small discharge tube without striking the walls. The alignment of the small discharge tube in this manner is sufficient such that when the mirror is replaced, oscillation commences. Minor adjustments are then made in the positioning of the small discharge tube in order to maximize the output of the laser. This completes the cavity alignment.

An alternate method of aligning the small discharge tube was also developed. This method depends upon obtaining oscillation at 6328 A, i.e., in the visible. Oscillation at this wave length is obtained by placing the mirror between the laser tube and the small discharge tube. After oscillation is obtained the small discharge tube is adjusted by the means described above until the output beam of the laser passes through the discharge tube without striking the walls. The mirror is then placed at its normal position on the other side of the discharge tube and the cavity re-tuned to oscillate at 3.39 microns. As previously mentioned the large gain on this transition permits oscillation even with large cavity losses. Thus when the cavity is re-tuned to 3.39 microns there is some oscillation. Final adjustments to the

small discharge tube are then made in order to peak the oscillation at 3.39 microns.

To use the Littrow prism as one of the cavity reflectors, the following procedure was used. The laser was first aligned using the procedure described above. With the laser peaked on the 3.39 micron transition, one of the mirrors is removed and replaced with the Littrow prism. The prism is held in a fixture which fits directly into the mirror mount. This fixture is designed such that when it is placed within a mirror mount the prism is centered on the laser axis. This fixture is shown in figure 11. The prism fixture is rotated within the mirror mount until the face of the prism is approximately parallel to the nearest Brewster angle window. The prism is then rotated about the horizontal axis of the mirror mount until oscillation at 3.39 microns starts. The alignment of both the Littrow prism and the spherical mirror is then adjusted to maximize the output at 3.39 microns. To obtain oscillation at 6328 A, one then rotates the prism about the horizontal mirror axis until oscillation commences at 6328 A. The readings of the micrometer drives are recorded both for the prism-mirror cavity and the mirror-mirror cavity. This enables one to change from mirror-mirror to mirror-prism without any further alignment.

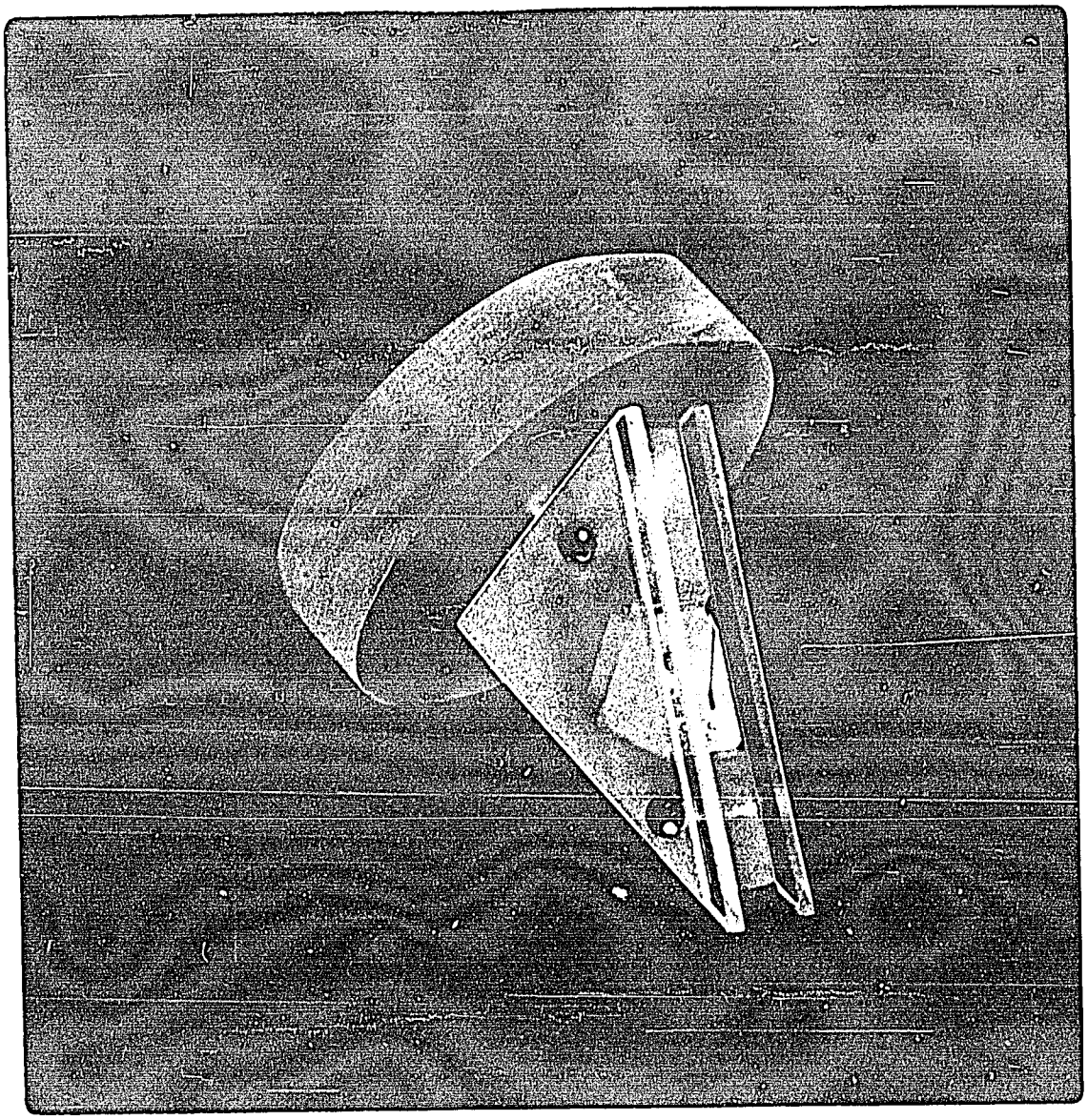

FIGURE 11. PRISM REFLECTOR MOUNT

Monochromator

The side light from the small discharge tube was focused on the entrance slit of a half meter Jarrell-Ash scanning monochromator. The monochromator is a grating instrument using an Ebert mounting. The grating used had 1180 grooves per millimeter and had a ruled area of 52 mm by 52 mm. The grating was blazed at 7000 A in the first order and had a high efficiency between 5000 and 9000 A. Great care must be taken with this instrument to minimize scattered light which might give spurious intensity measurements.

All grating spectrometers suffer from a defect known as Rowland ghosts.[12] These ghosts are due to periodic errors in spacing and are symmetrically spaced satellite lines at a spacing about the parent line given by

$$\Delta\lambda = n(\frac{a}{L})\lambda$$

Here a is the grating constant, L is the pitch of the grating ruling engine, and n is an integer either positive or negative. Figure 12 is a recorder tracing of a monochromator scan over the wave length region around the 5461 A line of mercury. Note that the tracing of the 5461 A line is attenuated by a factor of a thousand compared to those lines on either side of it. The mercury spectrum does not have any lines at these points. These are ghost lines due to the grating. From the figure one can see that this is actually a

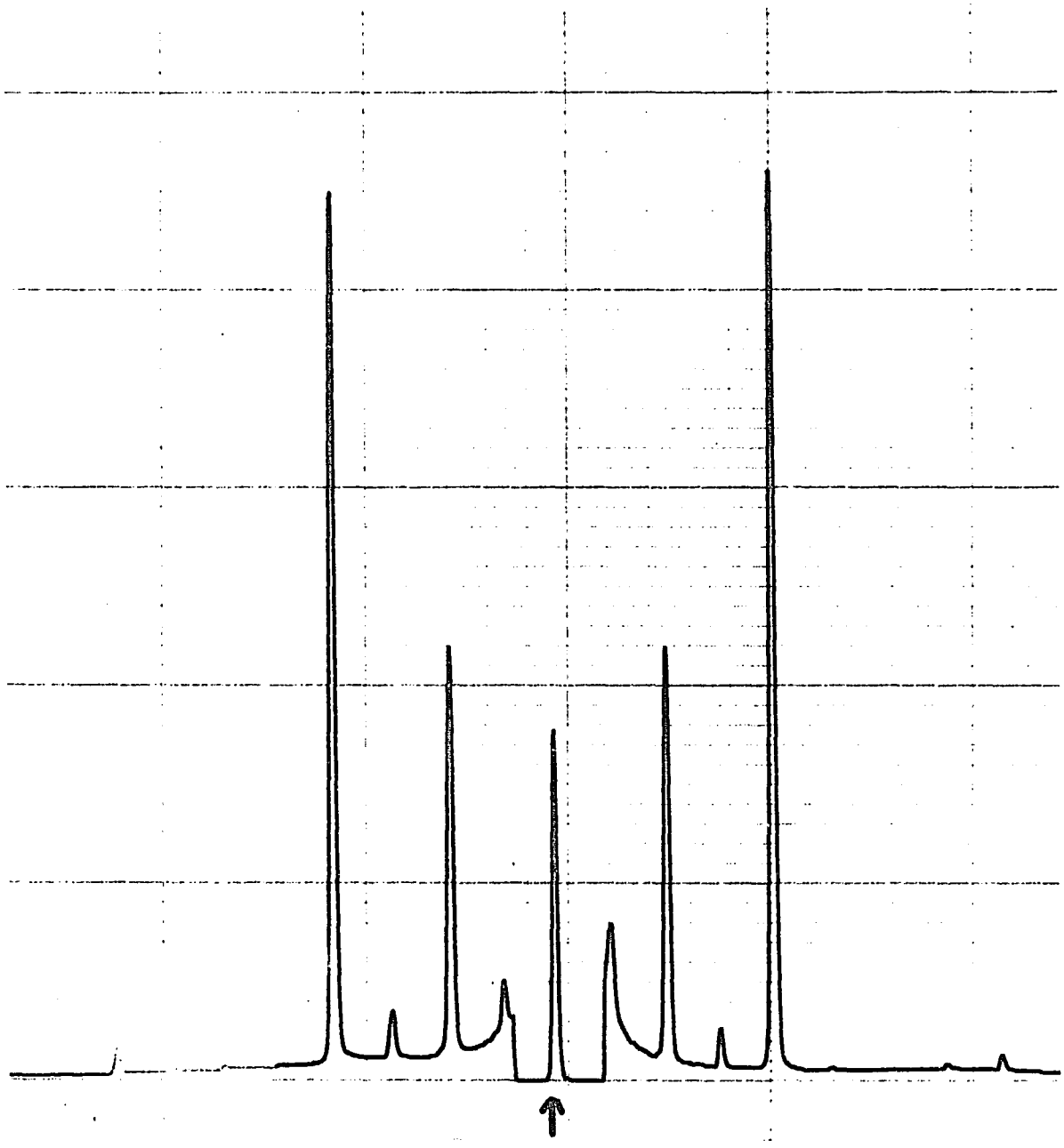

5461 A Hg Green Line Attenuated 10^3

With Respect to Ghosts

FIGURE 12. GRATING GHOST

good grating as the maximum intensity of the strongest ghost is only 3×10^{-3} that of the parent line. Note also that the strongest ghost line is not the first ghost but the fourth and that ghosts are detectable out to the seventh. From figure 12 $\Delta\lambda$ can be calculated and the result is

$$\Delta\lambda = n(5.5\ A) \qquad n = \pm 1, \pm 2, \ldots$$

This presents a problem in measuring relative intensities of some transitions in this experiment. The 6328 A line of neon, a very important transition in this experiment, lies only 5.5 A from 6334 A line which in normal neon discharges is approximately a factor of 1000 times more intense than 6328 A line. Thus the ghost from 6334 A will fall upon the 6328 A line and be of comparable intensity. Thus relative intensity measurements will be in error.

This problem was avoided by enhancing the intensity of the 6328 A line. This was accomplished by making the relative intensity measurements from a discharge which contained a mixture of helium and neon. Helium atoms in the 2^1S metastable level collide with neon atoms and selectively populate the 3s levels. This, of course, is the same mechanism responsible for the population inversion between the 3s and 2p levels of neon in a laser. This method is so effective that the intensities of the 6334 A and the 6328 A line become comparable in magnitude. Thus the ghost at 6328 A line adds only about 1/1000th to the intensity at this point and thus is negligible.

The ghost line falling upon 6328 A is not a problem when measuring the change ΔI of 6328 A line. This is because the lock-in amplifier's output is proportional to the change in the ac component of the signal being amplified. Since the 6334 A line does not originate on the upper or lower laser level, it is not modulated by the chopper and the ghost will have a constant intensity. Thus the ghost is merely a dc background and will not be measured by the lock-in amplifier. One could, of course, measure the relative intensities directly using the lock-in amplifier the same way the differential intensity is measured. However, since the signal to noise ratio is much larger for the direct measurements than for the differential measurement, direct measurement of the relative intensities was adopted.

Intensity Calibration

The detector at the exit slit was an Amperex XP1002 photomultiplier. This tube was found to be an excellent choice for the wave length region of interest. Although not having as large a gain as some tubes obtainable, it had a very low noise output. The peak wave length response is at 4200 A but with a long tail to the long wave length side. Sensitivity at 7000 A is still 20 percent of the maximum sensitivity.

Operating voltage for the photomultiplier tube was obtained from an electronically stabilized power supply, built into the photometer used to measure the anode current, and a

voltage divider mounted at the tube socket as shown in figure 13. In order for the photomultiplier anode current to be linear with intensity, the voltage divider current should be at least 100 times greater than the anode current. For the intensities encountered in this experiment, the voltage divider shown in figure 13 satisfied this requirement. For relative intensity measurements, the best signal to noise ratio was obtained with an operating voltage of about 1.25 kv. When measuring differential intensity, the best signal to noise ratio was found to be at a voltage of about 1.5 kv.

Since in this experiment only relative intensities are measured, an absolute calibration of the system's sensitivity is not necessary. The relative wave length response of the system was measured using an EOA quartz iodine standard lamp.[13] The calibration of this standard lamp is traceable to the National Bureau of Standards. The calibration curve provided by the manufacturer is accurate to five percent absolute.

The extreme intensity of the lamp makes calibration very easy. However, great care must be taken because of the high intensity to make sure scattered light does not give spurious results. It was found that the calibration was not repeatable if the lamp was focused on the spectrometer slit. This non-repeatability was found to be due to the high scattered light in the system. The measured response of the

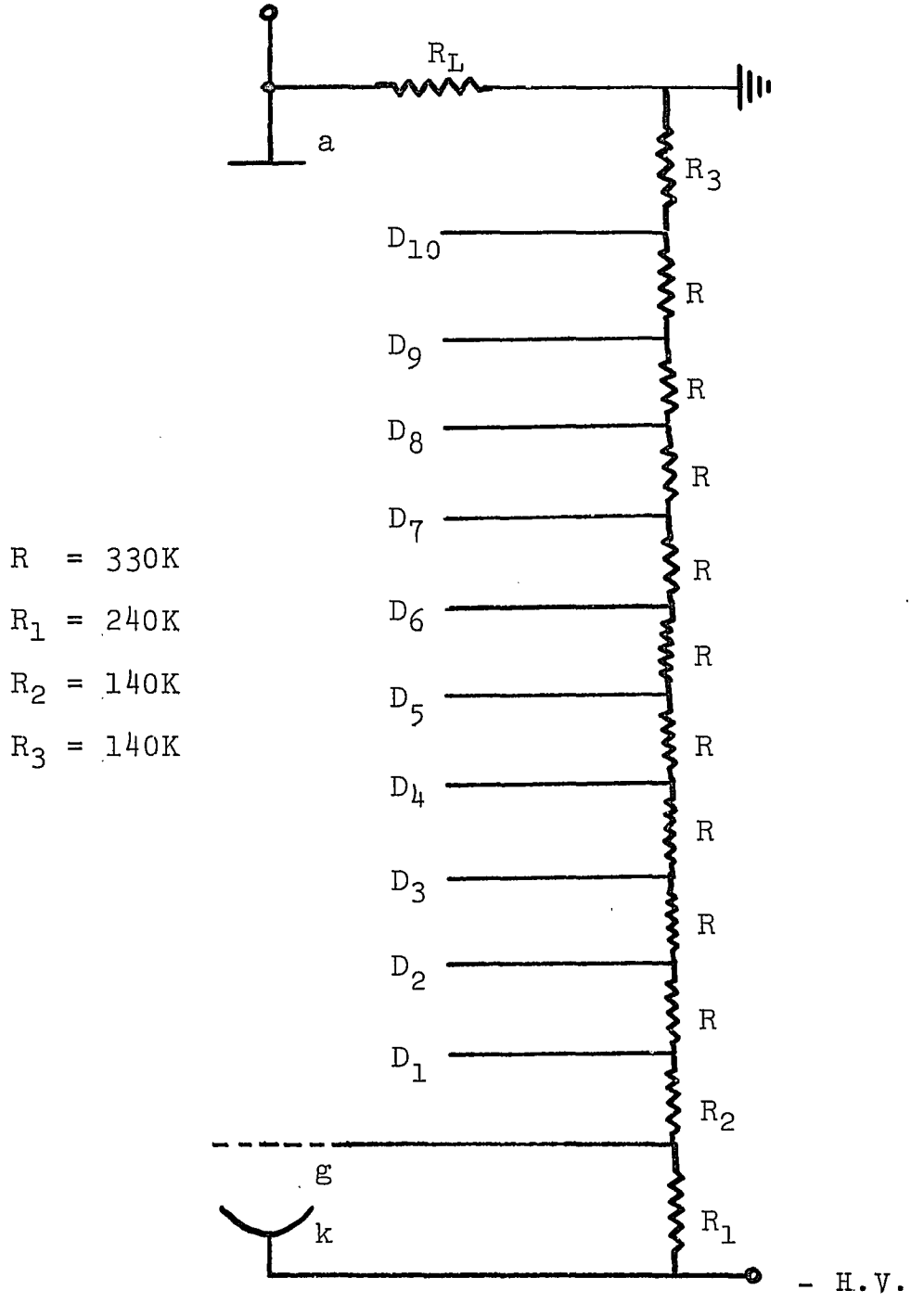

FIGURE 13. PHOTOMULTIPLIER VOLTAGE DIVIDER

system was found to be highly repeatable with the lamp at many different distances from the spectrometer when a condensing lense was not used. To make sure the lense used in the relative intensity measurements does not change the relative response of the system, calibration runs were made with the lense between the lamp and the spectrometer slit. However the lense was not used to focus the lamp upon the slit. No difference in response could be detected with or without the lense in the system.

At wave lengths longer than 7000 A, it is necessary to consider second order diffraction. In order to eliminate second order diffracted light at wave lengths above 7000 A, a long pass dielectric filter was used.[14] This filter had 91 percent transmission above 7000 A and essentially zero transmission below 4000 A. The use of this filter, however, introduces another factor into the relative wave length calibration. Hence the calibration curve for wave lengths above 7000 A cannot be considered as accurate as that for the region from 4000 to 7000 A.

For calibrating the relative spectral response of the system and for measuring relative intensities, the output of the photomultiplier was fed to an Oriel Optics photometer which measured the photomultiplier anode current. The technique used to measure the relative intensity between two different lines was as follows: The monochromator scanned

over one of the lines whose relative intensity was to be measured, first in one wave length direction and then in the other. The monochromator was then set to the other line to be measured and the same process repeated. This procedure was repeated ten times. The output of the photometer during each scan was recorded on a strip chart recorder. The average of the peak output for each direction of scan was calculated. Then the ratio between this average and the average for the other line on the next adjacent scan was calculated. This gave a total of nineteen ratios for the ten sets of data taken. An average ratio was then computed. The results of this method were repeatable with a high degree of precision.

Differential Intensity Measurement

In this experiment it is necessary to measure small changes in the intensity of spectral lines. The lines, themselves, are relatively weak and in a portion of the red part of the spectrum where photomultiplier sensitivity is considerably decreased.

The change in intensity of the spectral lines is due to the change in population of the upper levels of the lines. This population change is caused by the absorption of laser radiation. In detecting the change in intensity due to population changes induced by the laser radiation, one must discriminate against intensity changes which are due to other processes. The principal processes causing such intensity

changes are the following; amplitude modulation of the laser radiation field due to 120 hertz ripple in the laser discharge current, amplitude modulation of the laser radiation field due to fluctuations in the laser discharge current due to straiation and other processes occurring in gas discharges, and modulation of the excited state atom densities in the small discharge tube due to 60 hertz and 120 hertz ripple and fluctuations in the discharge current through the small discharge tube.

Since only ratios of intensity changes enter in the analysis of the experiment, the detection system only has to provide an output which is proportional to the change in intensity and which is linear with intensity. These requirements were met by the detection system shown in figure 3.

The laser beam is switched on and off at a fixed frequency by a rotating chopper within the cavity. The intensity of a spectral line originating from level two or level three is thus made up of the following components: a large dc signal, a small signal whose frequency is that of the rotating chopper, a signal occurring at 60 hertz and another at 120 hertz, and other components occurring at various frequencies due to fluctuations in the discharge. It is necessary to measure that portion of the signal occurring at the chopper frequency.

One method of measuring this signal would be to use a

tuned amplifier. However, a lock-in amplifier has a number of advantages over a tuned amplifier.[15] Some of the more important advantages are: the lock-in amplifier provides a dc output proportional to the component of the input signal which is at the same frequency and in phase with the reference signal. Lock-in detection is linear for even the weakest coherent input signals. The center frequency of the selective filter is locked to the reference frequency. No high - Q filters are needed because the band width of the system is actually set by the RC time constant after the synchronous detector. The lock-in averages any input signal not coherent with the reference frequency to zero. An incoherent detector will show some average reading proportional to the noise. In lock-in detection the noise shows up only as a fluctuation about the actual reading.

Basically a lock-in amplifier consists of the following: An amplifying stage which is loosely tuned to the input frequency ($Q \sim 20$). The output of this stage is fed to a synchronous rectifier. The rectifier output is then fed to an RC circuit and a dc voltage proportional to the input signal is developed across the capacitor. See figure 14 for a complete block diagram.

By varying the time constant of the RC circuit one can in theory make the band width of the amplifier as narrow as desired. The reference signal for the synchronous rectifier

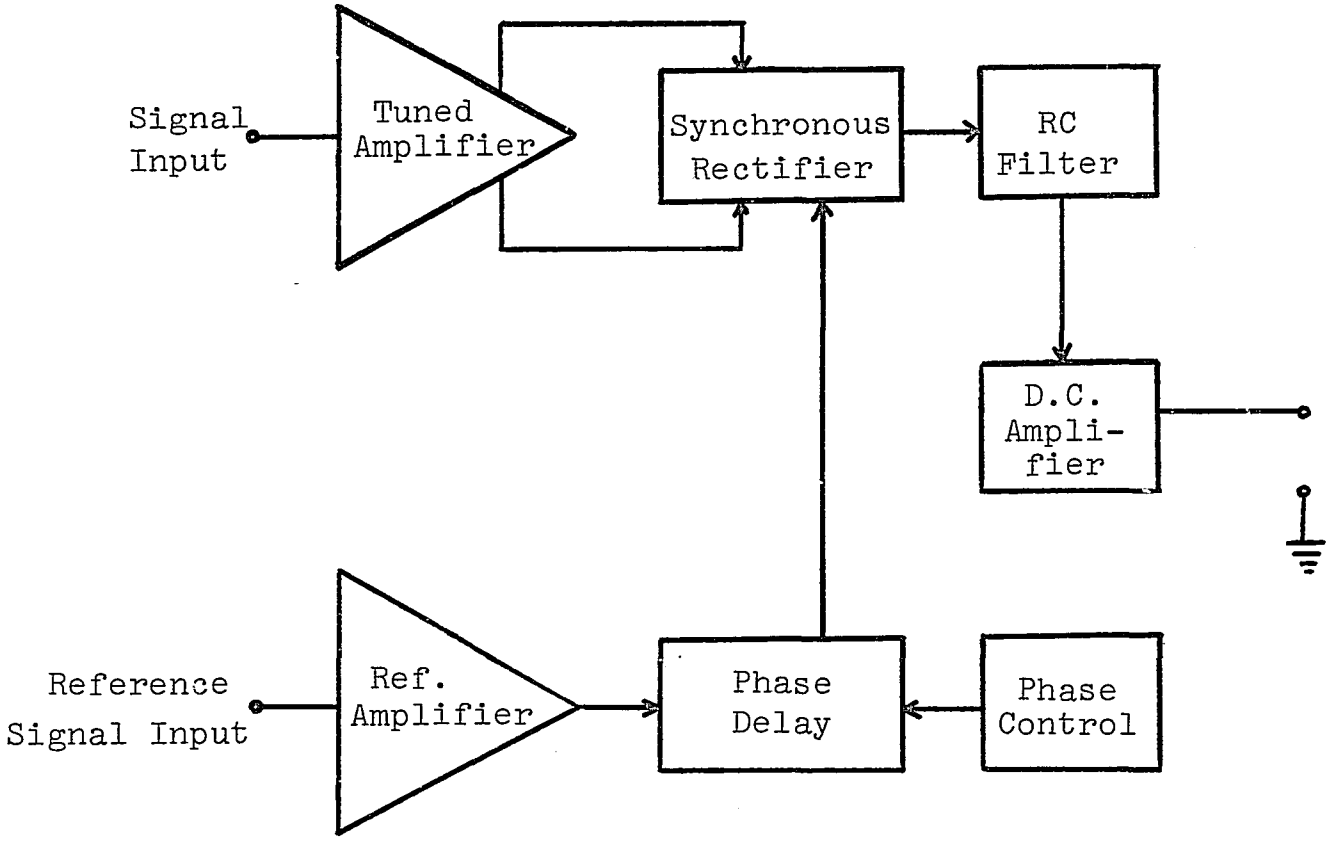

FIGURE 14. LOCK-IN AMPLIFIER BLOCK DIAGRAM

is provided by the same source which modulates the input signal.

The lock-in amplifier used was an EMC model RJB. A thirty microvolt rms signal coherent with the reference signal was sufficient to produce half scale deflections of the panel meter and associated recorder. Since the signal from level three, with the photomultiplier used, is quite a bit less than thirty microvolts, preamplification was necessary. This was accomplished by first feeding the photomultiplier signal to the Oriel Optics photometer. It was necessary to use the photometer on a low sensitivity range in order to have the necessary frequency response.

The reference signal is obtained from the rotating chopper using a small incandescent lamp and a photodiode. The circuit which produces the reference signal is shown in figure 15. Since a minimum of 200 millivolts rms of fundamental component is required for the reference signal, a large load resistor is necessary. This load resistor seriously degrades the rise time of the reference signal. However at the chopping frequency used, this does not seriously change the amplitude of the fundamental component of the reference signal. A twin - T filter is used in the reference channel input so that the synchronous rectifier is driven only at the fundamental chopping frequency. The chopper is driven by a Bodine 1800 rpm synchronous motor equipped with a

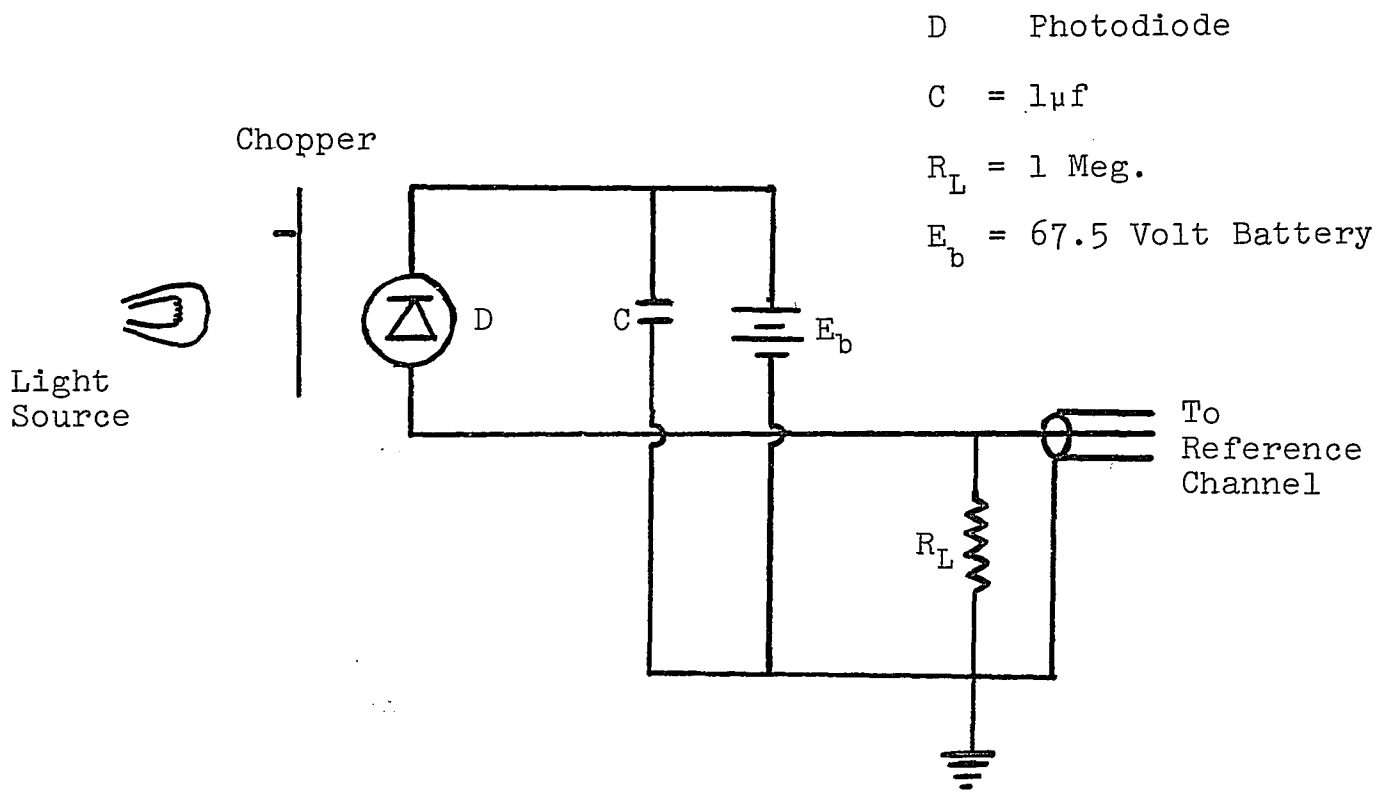

FIGURE 15. REFERENCE SIGNAL CIRCUIT

6:1 gear reducer. The chopping blade is cut such that the on and off times are equal. The phase of the reference signal is adjusted by means of a control in the reference channel of the lock-in amplifier to provide the maximum output signal.

The lock-in output is directly proportional to the change in spontaneous emission intensity. Since the important quantity in this experiment is the ratio ΔI_3 to ΔI_2, the proportionality factor is not important and the ratio of the lock-in amplifier output for two different lines I_3 and I_2 gives directly the ratio ΔI_3 to ΔI_2. The procedure used to obtain the average $\Delta I_3/\Delta I_2$ is the same as that described in measuring the relative intensities between two different lines.

As mentioned above, noise causes fluctuations of the output about the true signal. The RC filter is used to average out these fluctuations. The longer the time constant the smaller the fluctuation will be. However, the time constant is limited to times of about one tenth of that taken to scan through a spectral line. Since the slowest scan speed is two angstroms per minute, the time constant was limited to three seconds. A 60 hertz twin - T rejection filter was used in the input circuit of the lock-in amplifier to reduce noise in the output. However, at a chopping frequency of 100 hertz, the noise fluctuations were quite large

when measuring I_3. An intrinsic property of lock-in amplifiers is that they do not respond to even harmonics of the reference frequency.[16] For this reason the modulation frequency was changed to 30 cycles per second. This choice of chopping frequency gave a better signal to noise ratio than that at 100 cycles.

Although the reference frequency is locked to the modulation frequency of the signal, a drift in frequency will change the output of the lock-in amplifier because of the tuned amplifier stage in the lock-in. It was found that a drift of only a few percent in the modulation frequency was enough to give appreciable changes in the amplifier output. Therefore a synchronous motor was used to drive the chopper.

REFERENCES

[1]Richard W. Roberts and Thomas A. Vanderslice, Ultrahigh Vacuum and Its Applications, (New Jersey, 1963), pp. 22-23.

[2]C. G. B. Garrett, Gas Lasers, (New York, 1967).

[3]Roberts and Vanderslice, op. cit., p. 109.

[4]Klaus D. Mielenz and Karl F. Nefslen, "Gas Mixtures and Pressures For Optimum Power of rf-Excited Helium-Neon Gas Lasers at 632.8nm," Applied Optics, 4 (May, 1965), 565-567.

[5]Norman B. Colthup, Lawrence H. Daly, and Stephen B. Wiberly, Introduction to Infrared and Raman Spectroscopy, (New York, 1964), pp. 191-199.

[6]A. D. White and J. D. Rigden, "The Effect of Super-Radiance at 3.39 Microns on the Visible Transitions in the He-Ne Maser," Applied Physics Letters, 2 (June, 1963), 211-212.
R. J. Freiberg, L. A. Weaver and J. T. Werdeyen, "Infrared Laser Interferometry Utilizing Quantum Electronic Cross Modulation," Journal of Applied Physics, 36 (October, 1965), 3352.

[7]G. D. Boyd and H. Kogelnik, "Generalized Confocal Resonator Theory," Bell System Technical Journal, 41 (July, 1962), 1364.

[8]W. R. Bennett, Jr., "Inversion Mechanisms in Gas Lasers," Applied Optics Supplement on Chemical Lasers, (1965), p. 28.

[9]Ali Javan, "Gaseous Optical Masers," in C. DeWitt, A. Blandin, and C. Cohen-Tannoudji, (eds.), Quantum Optics and Electronics, (New York, 1965), pp. 385-393.

[10]Arnold L. Bloom, "Properties of Laser Resonators Giving Uniphase Wave Fronts," Spectra-Physics Laser Technical Bulletin, 2 (August, 1963), 6-7.

[11]Arnold L. Bloom, "Observations of New Visible Gas Lasers Transitions by Removal of Dominance," Applied Physics Letters, 2 (March, 1963), 101-102.

[12]Ralph A. Sawyer, Experimental Spectroscopy, (New York, 1963), pp. 181-182.

[13]Ralph Stair, William E. Schneider, and John K. Jackson, "A New Standard of Spectral Irradiance," Applied Optics, 2 (November 1963), 1151-1154.

[14]Optics Technology Inc., Filter Set No. 6320, Filter no. 700.

REFERENCES (cont.)

[15]Robert D. Moore, "Lock-in Amplifiers for Signals Buried in Noise," Electronics, 35 (June 8, 1962), 40-43.

[16]Ibid., p. 43.

CHAPTER IV

EXPERIMENTAL RESULTS

Preliminary Results

As described in the previous chapter, in order to obtain relative A values for transitions originating on the same upper level, it was necessary to calibrate the wave length response of the system. Figure 16 shows the relative intensity response of the entire optical system. The shape of the relative response curve is principally determined by the photomultiplier response curve and by the intensity versus wave length response of the monochromator. The monochromator response curve depends upon the blazed grating employed.

Table II gives the relative photon response of the system at the wave lengths of interest in this experiment. The relative photon response was calculated since the photomultiplier output is proportional to the number of photons and not to the incident energy. When the relative photon response of the system is used rather than the relative energy response, the νs in equations (3) and (5) of this chapter are eliminated.

As discussed in chapter III, care was taken to construct the laser cavity in such a way that oscillation took place only at 3.39 microns. It is, of course, essential to eliminate any oscillations which begin or end on level $|3\rangle$ or which might produce excessive cascade into level $|3\rangle$.

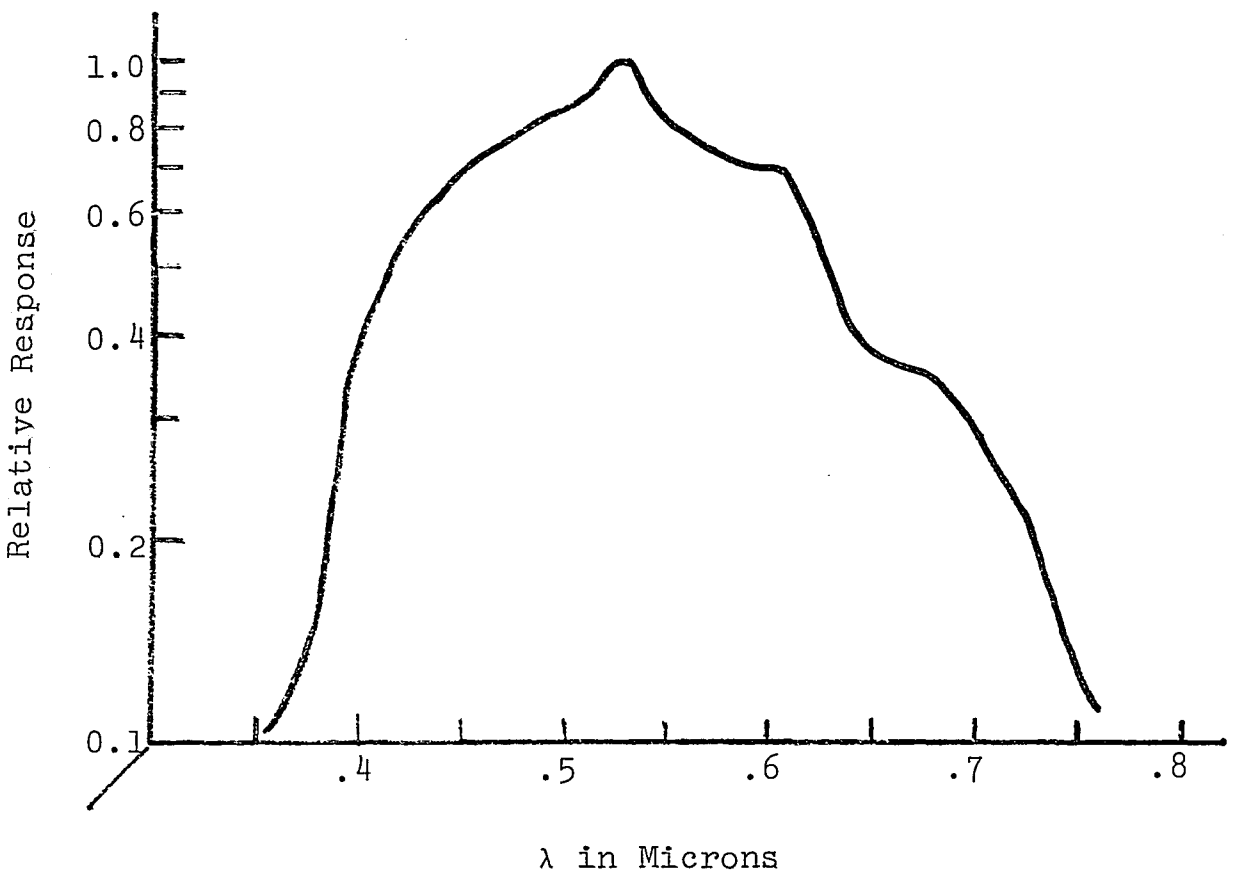

FIGURE 16. RELATIVE INTENSITY RESPONSE

TABLE II. RELATIVE PHOTON RESPONSE[a]

λ	Relative Response
7304.8	1.00
6421.7	3.36
6351.9	3.76
6328.2	4.00
6313.7	4.11
6293.8	4.29
6118.0	6.13
6064.6	6.61
6046.2	6.67
5939.3	6.40
5448.5	8.53
5433.7	8.83

[a]Relative photon response is used here in the sense that e.g. a photon of wavelength 6328.2 A produces a system response 4.00 times greater than a photon of wavelength 7304.8 A.

As a final indication that the change Δn_3 represents collision transfer, the ratio ΔI_3 to ΔI_2 was measured at a fixed pressure but as a function of the laser power. In order to avoid changing the discharge conditions, the power was varied by de-tuning the cavity from its optimum alignment. The intensity change ΔI_2 is a function of the change in the laser power since level $|2\rangle$ is the upper laser level. If level $|3\rangle$ is interacting with some other oscillation, ΔI_3 will not be proportional to ΔI_2.

This experiment was performed and the results are shown in figure 17. These results show that within experimental error, ΔI_3 depends linearly on ΔI_2 and therefore the ratio $\Delta n_3/\Delta n_2$ is independent of the laser power. As a result, the change in the population of level $|3\rangle$ can clearly be interpreted as the effect of collision transfer. Since the laser frequency varies with the laser power,[1] figure 17 also indicates that the ratio of ΔI_2 to ΔI_3 does not appear to depend on the frequency.

The Brewster angle laser used in this experiment produces a linearly polarized source of radiation. It has been pointed out that this will align the angular momentum of the laser levels even in the absence of a magnetic field.[2] This is a result of rapidly induced transitions for which ΔM_J is equal to zero. In this case the axis of quantization will be along the optical field axis.

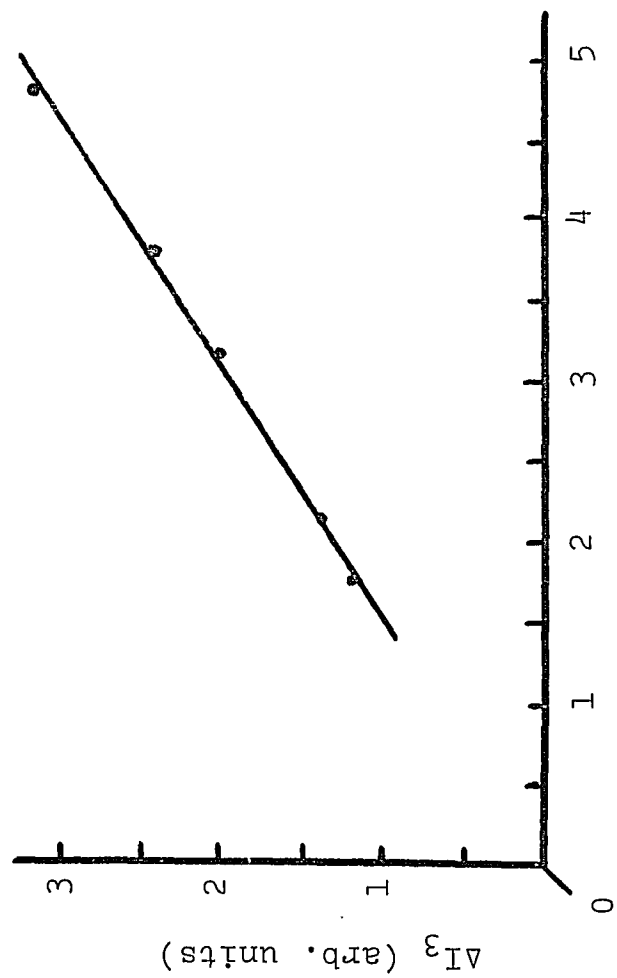

FIGURE 17. ΔI_3 vs. ΔI_2

The net effect of this alignment is to produce an anisotropy in the spontaneous emission originating from both of these levels. However, a nearby level coupled with one of these levels by atomic collision will not be aligned. As a result, spontaneous emission from the nearby level will be isotropic. From these considerations, it is evident that the measured ratio $\Delta I_3/\Delta I_2$ can be sensitive to this level alignment and consequently to the optical arrangement. Such an effect could be accounted for by taking a suitable average of the intensity measurements. However, there was no anisotropy detected for spontaneous emission from the upper level.

Figure 18 shows the energy level diagram of the laser transition. Here we have shown the M_J states split, although in this experiment no magnetic field is applied which could cause this splitting except the earth's. From Condon and Shortley,[3] the relative transition probabilities are as shown in the figure. These relative probabilities are independent of the coupling scheme. Thus taking the M_J states to be equally populated before the interaction with the laser beam, then because of the interaction, the $M_J = 0$ state of the upper level will become more populated than the $M_J = \pm 1$ states. The $M_J = \pm 2$ states of the lower level will also become more populated than the other M_J states of this level.

If the M_J states of the upper level are equally populated,

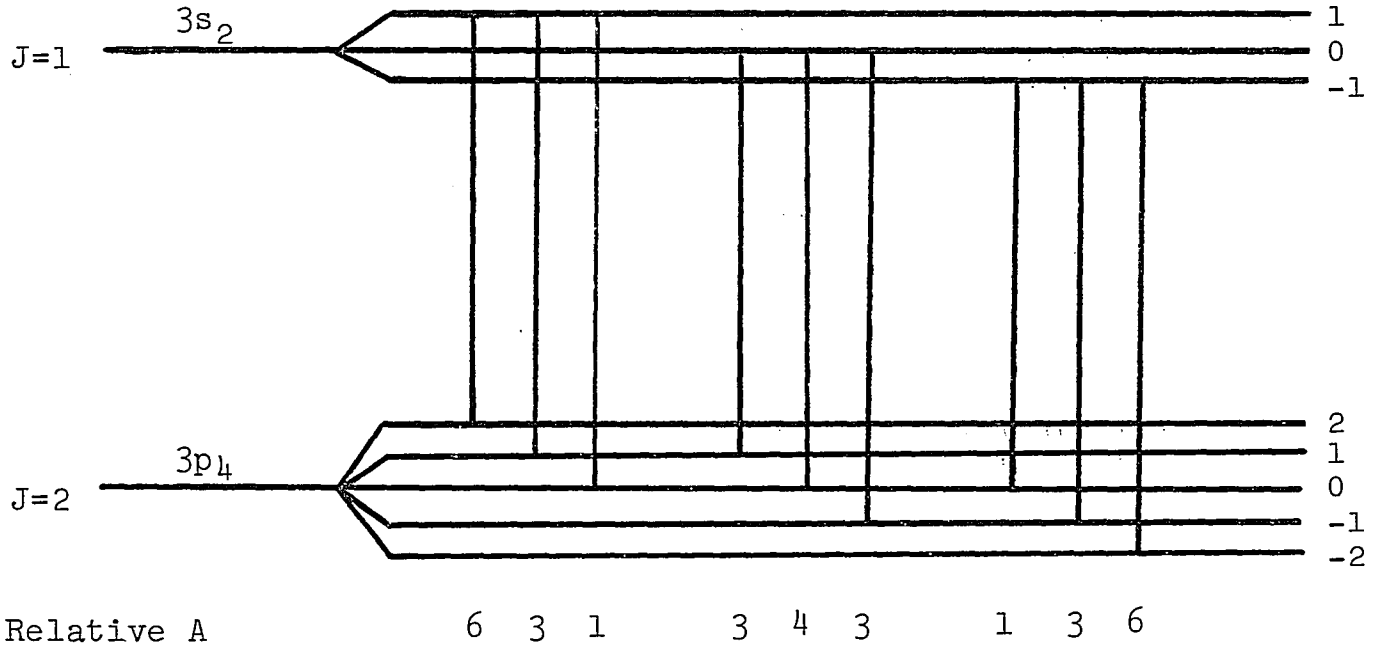

FIGURE 18. ZEEMAN TRANSITIONS BETWEEN LASER LEVELS

the radiation intensity for a transition to some lower level would be isotropic. Since the $M_J = 0$ state of the upper laser level has an excess population, an anisotropy arises in the following manner. Consider the 6328 A transition $3s_2 - 2p_4$. We consider only those transitions taking place from the excess population of the $M_J = 0$ state of the $3s_2$ level. There are three possible transitions ($\Delta M_J = 0$ and $\Delta M_J = \pm 1$). The total intensity in any direction θ (see figure 19) is proportional to[3,4]

$$6 + \sin^2\theta \qquad (1)$$

Thus the differential intensity from level $|2\rangle$ should be anisotropic and have a minimum in the $\theta = 0$ direction.[5]

Absence of anisotropy was noted by Parks and Javan[6] as occurring also for the $2s_2$ levels of neon. They suggest that this may be because of collision excitation transfer within the M_J states of the $2s_2$ level. However, the magnetic field of the earth could cause a destruction of the alignment of the M_J states, if the lifetime of the $3s_2$ level is long enough.

Destruction of the M_J alignment was studied first by Wood[7] using resonance radiation. From Korff and Breit[8] we obtain the following formula for calculating the magnetic field necessary to destroy the alignment for a given lifetime.

$$B \sim \frac{2 \times 10^{-7}}{g\tau} \text{ (gauss)} \qquad (2)$$

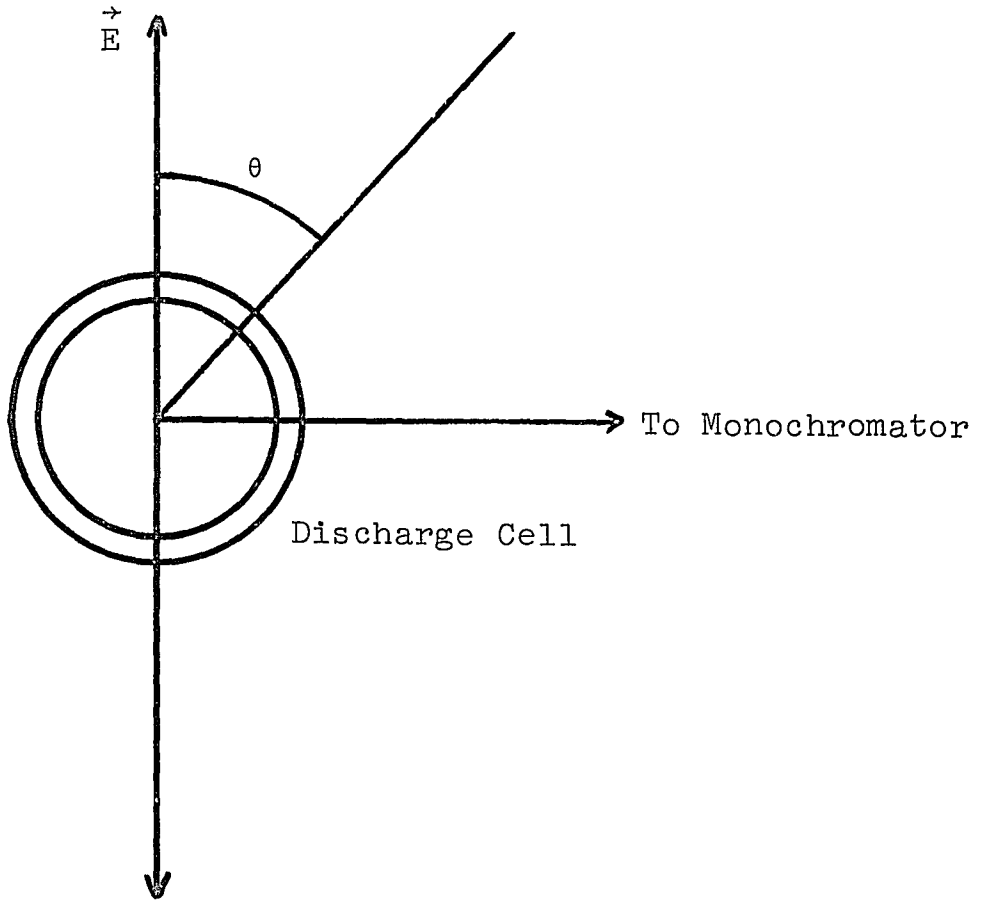

FIGURE 19. OPTICAL ARRANGEMENT

Using the resonance trapped lifetime (51 x 10^{-9} s) measured by Klose[9] for the $3s_2$ level, we see that the earth's magnetic field could account for the destruction of the alignment. We note also that this effect could be used to measure the lifetime of the upper or lower laser level.

Relative Intensities

Table III gives the results of the relative A measurements. The indicated error is .6745 times the standard deviation for the ratios. The results are presented in this manner since relative intensities were measured between nearest spectral neighbors only.

Table IV presents the transition probabilities for the visible transitions from the $3s_2$ level relative to most intense transition from this level, the $3s_2$ - $2p_4$ transition at 6328 A. Table IV also presents transition probabilities for the visible transitions from the $3s_3$ level relative to the $3s_3$ - $2p_5$ transition at 6313 A.

Differential Intensity

Experimentally, we observe changes in intensity in the spontaneously emitted light when the applied laser field is periodically interrupted. The intensity change in the spontaneous emission from level $|3\rangle$ and level $|2\rangle$ is related to the change in population by

$$\frac{\Delta I_3}{\Delta I_2} = \frac{A_3}{A_2}\frac{\nu_3}{\nu_2}\frac{\Delta n_3}{\Delta n_2} \qquad (3)$$

TABLE III. RELATIVE TRANSITION PROBABILITIES

λ_1/λ_2	$A_{\lambda_1}/A_{\lambda_2}$
7304/6351	0.807 ± .034
6351/6293	0.538 ± .016
6293/6328	0.184 ± .006
6293/6118	1.050 ± .030
6046/6118	0.374 ± .011
5939/6046	0.854 ± .025
5939/5433	0.740 ± .023
6421/6313	0.630 ± .019
6064/6313	0.489 ± .014
5448/6064	0.282 ± .008

TABLE IV. RELATIVE TRANSITION PROBABILITIES

λ	Transition	Relative Transition Probability
6328.2	$3s_2 - 2p_4$	1.000
7304.8	$3s_2 - 2p_1$	0.080 ± .005
6351.9	$3s_2 - 2p_3$	0.099 ± .005
6293.8	$3s_2 - 2p_5$	0.184 ± .006
6118.0	$3s_2 - 2p_6$	0.175 ± .008
6046.2	$3s_2 - 2p_7$	0.065 ± .003
5939.3	$3s_2 - 2p_8$	0.056 ± .003
5433.7	$3s_2 - 2p_{10}$	0.076 ± .005
6313.7	$3s_3 - 2p_5$	1.000
6421.7	$3s_3 - 2p_2$	0.630 ± .019
6064.6	$3s_3 - 2p_7$	0.489 ± .014
5448.5	$3s_3 - 2p_{10}$	0.138 ± .006

Here A_3/A_2 is the ratio of Einstein coefficients for spontaneous emission from levels $|3\rangle$ and $|2\rangle$ to lower levels at frequency ν_3 and ν_2 respectively. This ratio may be measured directly by applying equation (3) at the high pressure limit where $\Delta n_3/\Delta n_2$ is thermalized according to equation (7) of chapter II. Once A_3/A_2 is determined, it can then be used to obtain $\Delta n_3/\Delta n_2$ in the low pressure region from equation (3).

Equation (6) of chapter II describes the linear region of the plot of the experimentally determined values of $\Delta n_3/\Delta n_2$ versus pressure. The slope is the product $v_r\sigma_{23}\tau_3$. In this experiment τ_3 is not known, so that only the product of τ_3 and the cross section can be measured. Using equations (4), (5) and (8) of chapter II, we can write

$$\frac{\Delta n_2}{\Delta n_3} = \frac{1}{n_o v_r \sigma_{23} \tau_3} + \frac{g_2}{g_3} \exp\ (-\Delta E/kT) \qquad (4)$$

By defining

$$y = \frac{\Delta I_2}{\Delta I_3} \qquad x = 1/p$$

and noting the gas pressure is given by $p = n_o kT$, equation (4) becomes

$$y = \left\{\frac{A_2}{A_3}\frac{\nu_2}{\nu_3}\frac{kT}{v_r\sigma_{23}\tau_3}\right\}\frac{1}{p} + \frac{A_2}{A_3}\frac{\nu_2}{\nu_3}\frac{g_2}{g_3}\exp\ (-\Delta E/kT) \qquad (5)$$

$$= b\ x + a$$

If the gas temperature is known, the constants a and b determine the Einstein ratio A_3/A_2 and the quantity $\tau_3\sigma_{23}$. The

question of the temperature will be discussed later. We determine the parameters a and b by fitting the experimental data (y_i, x_i) to equation (5) by the method of least squares, that is, by minimizing

$$\sum_i (\delta y_i)^2 = \sum_i (y_i - a - bx_i)^2 \qquad (6)$$

with respect to a and b.[10]

Figure 20 is a plot of the experimentally determined ratio $\Delta I_2/\Delta I_3$ versus the reciprocal of the neon pressure in the small discharge tube measured in torr. I_2 and I_3 are the transitions noted in figure 1. The solid curve is a least squares fit to the data. The current in the small discharge tube was maintained at six milliamperes for all data points shown in figure 20. Figure 21, like figure 20, is a plot of $\Delta I_2/\Delta I_3$ versus the reciprocal of the pressure in torr. However, here I_2 was the $3s_2 - 2p_3$ transition at 6351 A. I_3 is the same transition as used in figure 20. These datum points were obtained with a discharge current of six milliamperes. The data presented in figure 22 were obtained with a discharge current of eight milliamperes. Here I_3 and I_2 are the same transitions as those used in figure 20.

Figures 23, 24, and 25 show the same data, respectively, as that in figures 20, 21, and 22. However in figures 23, 24 and 25 we have plotted $\Delta I_3/\Delta I_2$ versus the pressure in torr. An examination of figures 23, 24, and 25 shows that the linear

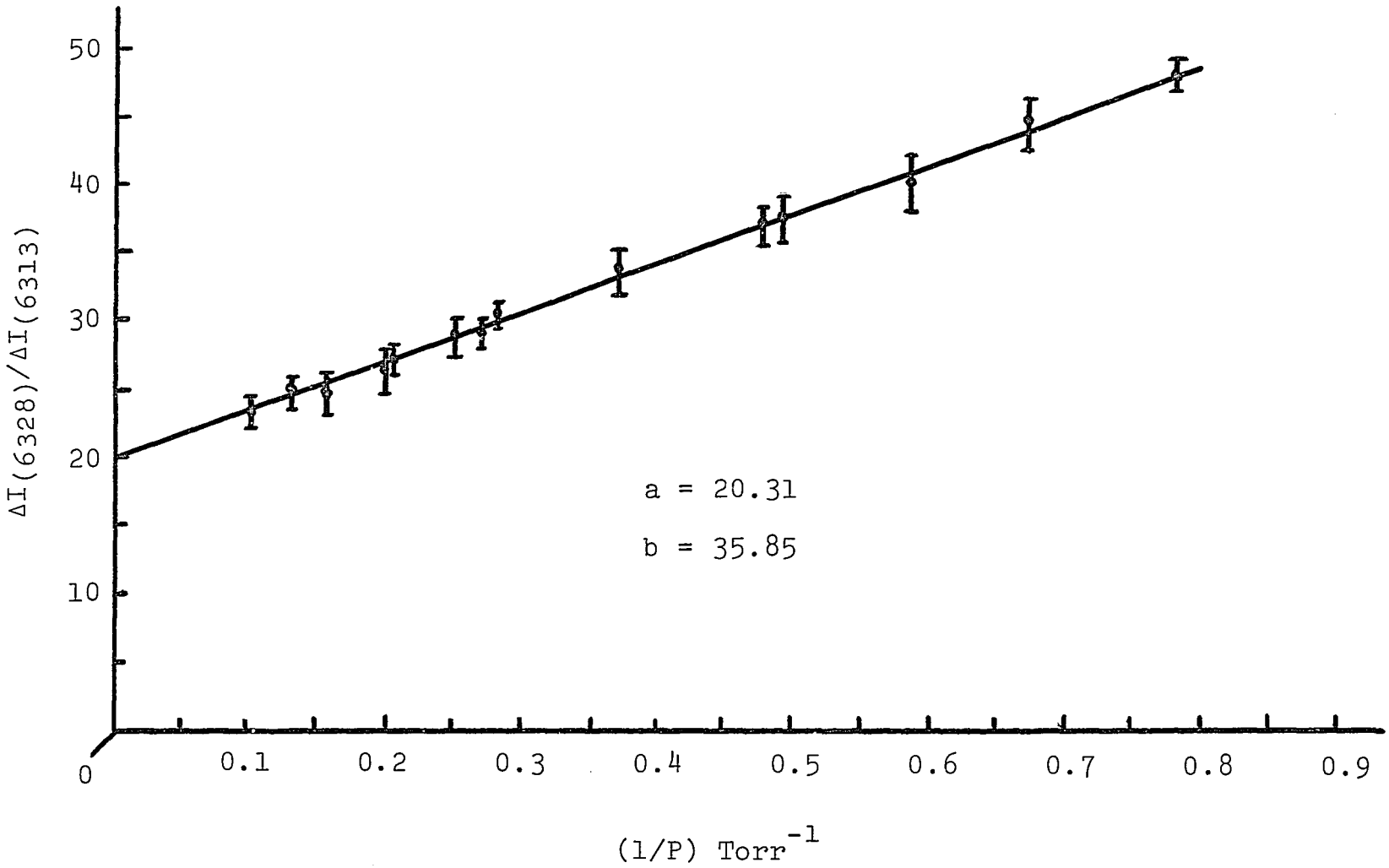

FIGURE 20. $\Delta I_{(6328)}/\Delta I_{(6313)}$ vs. THE RECIPROCAL OF THE PRESSURE

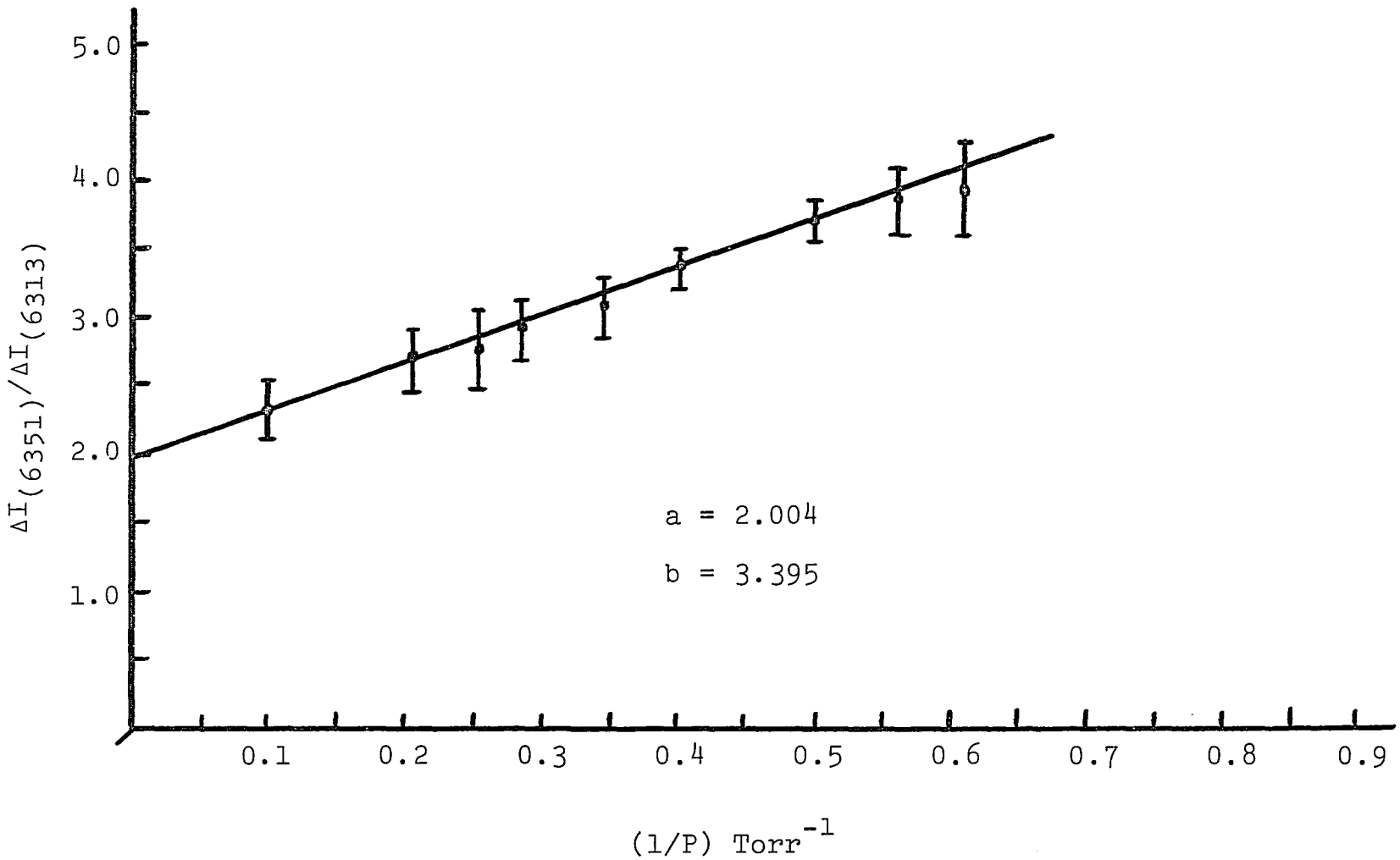

FIGURE 21. $\Delta I_{(6351)}/\Delta I_{(6313)}$ vs. THE RECIPROCAL OF THE PRESSURE

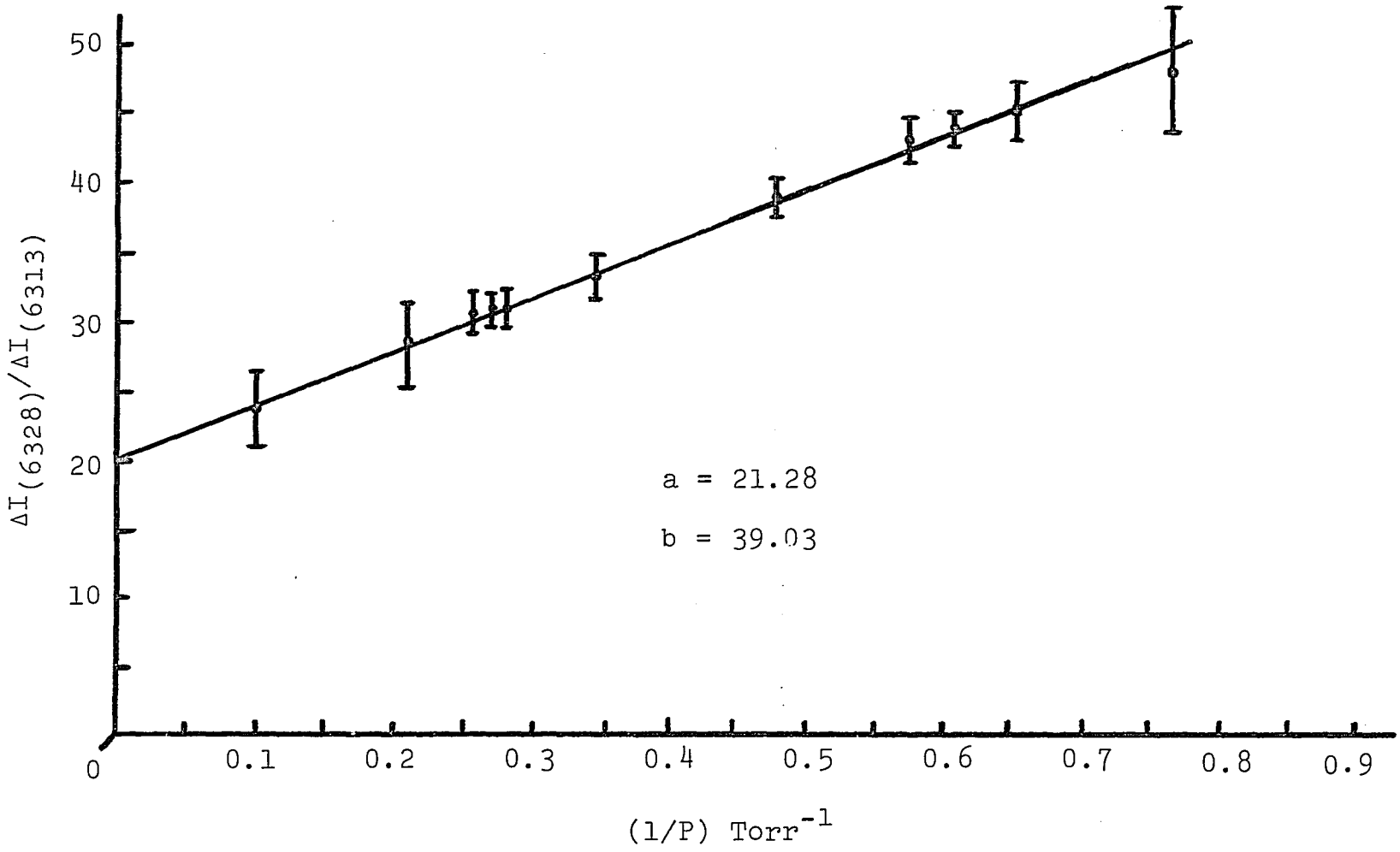

FIGURE 22. $\Delta I_{(6328)}/\Delta I_{(6313)}$ vs. THE RECIPROCAL OF THE PRESSURE

DISCHARGE CURRENT 8 MA

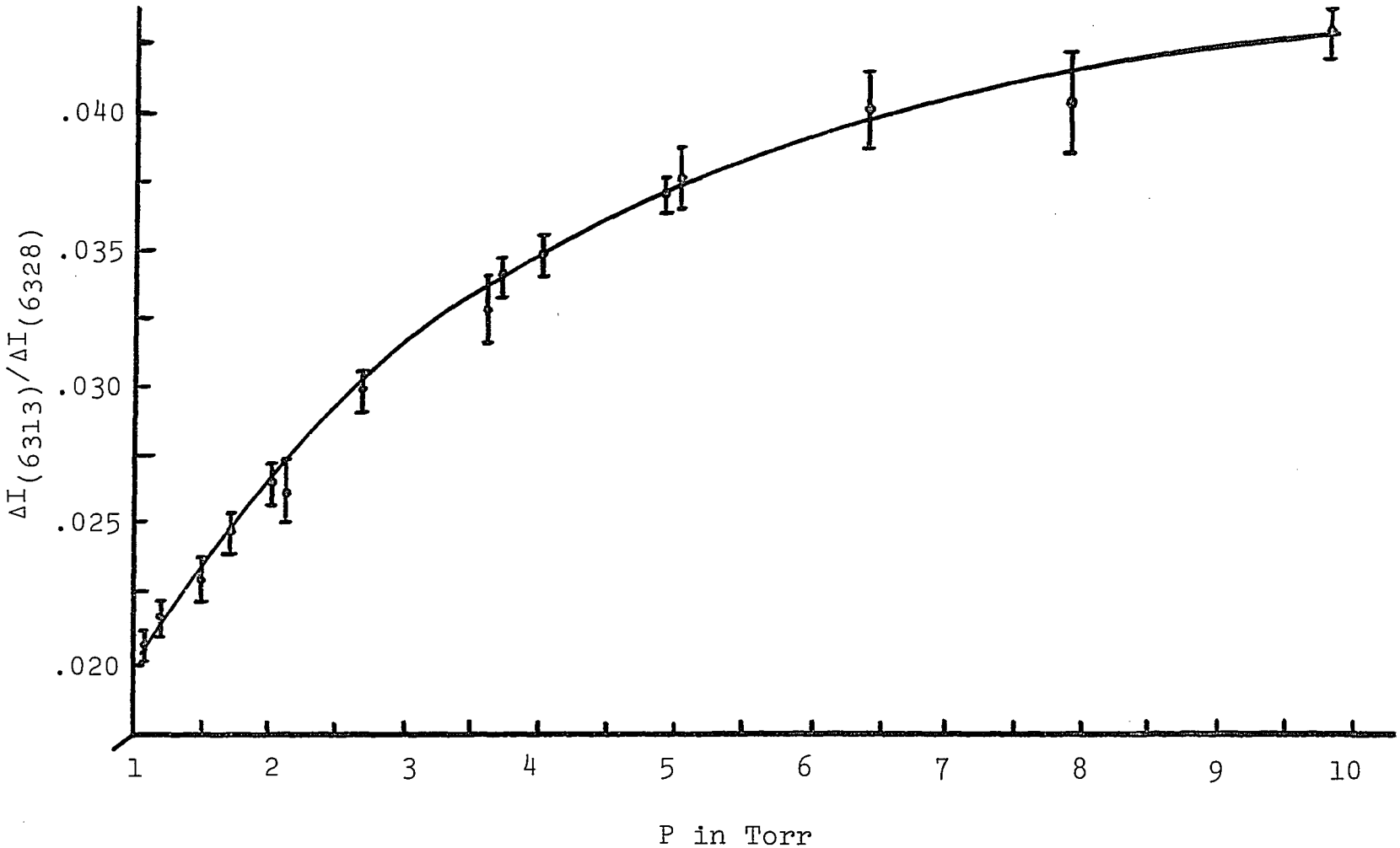

FIGURE 23. $\Delta I_{(6313)}/\Delta I_{(6328)}$ vs. THE PRESSURE

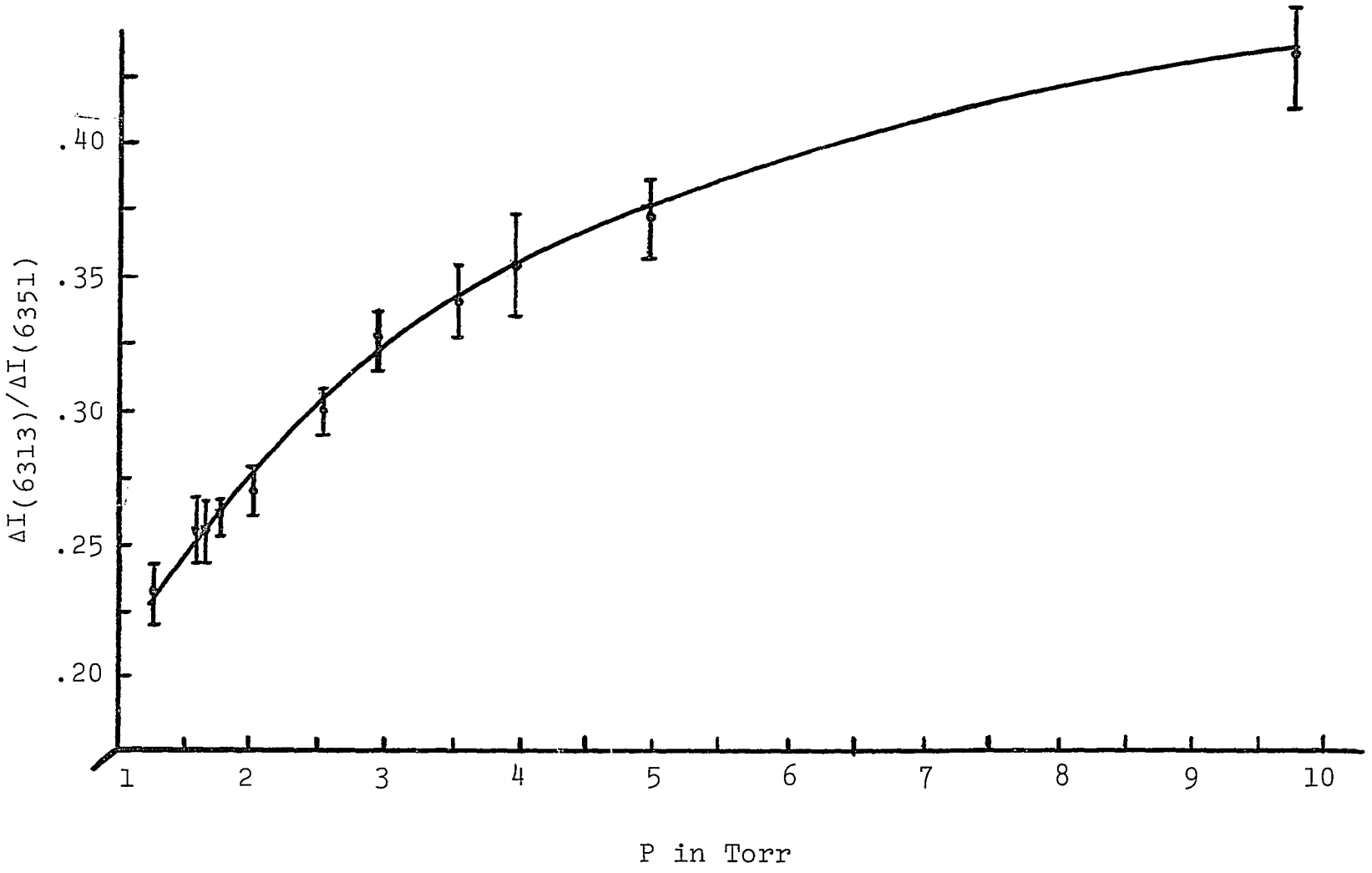

FIGURE 24. $\Delta I_{(6313)}/\Delta I_{(6351)}$ vs. THE PRESSURE

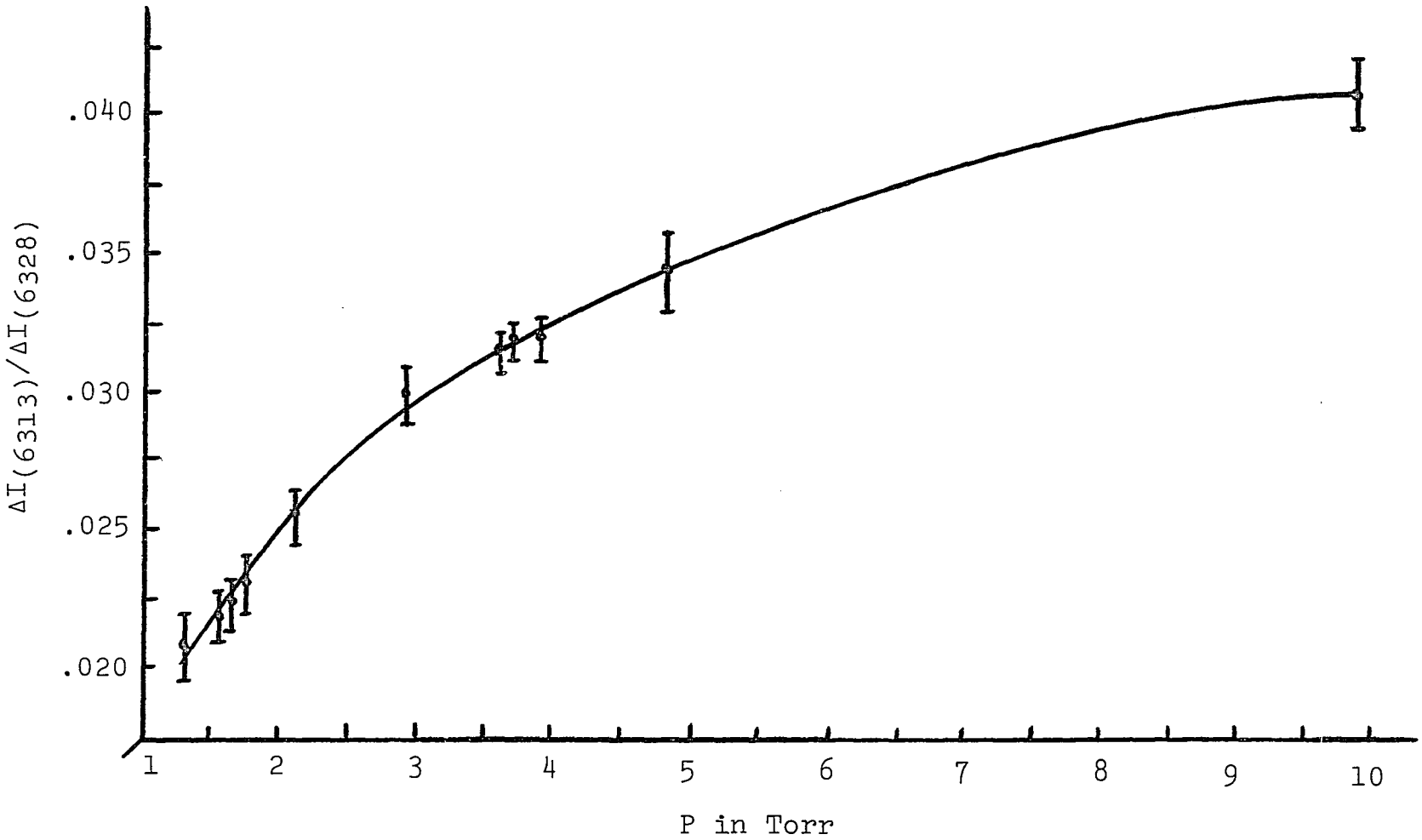

FIGURE 25. $\Delta I_{(6313)}/\Delta I_{(6328)}$ vs. THE PRESSURE

DISCHARGE CURRENT 8 MA

region described by equation (6) of chapter II extends to about three torr. At pressures above ten torr., the ratio $\Delta n_3/\Delta n_2$ appears to be completely thermalized.

Errors

Since we are measuring the quantities A_2/A_3 and $\tau_3\sigma_{23}$ indirectly, we have two sources of error to investigate. The first is the usual experimental error. The second is the error caused by the assumptions used in obtaining equation (3) of chapter II. One of these assumptions (the assumption that the $3s_2$ and the $3s_3$ levels are isolated) was discussed in chapter II. Another assumption which was not discussed in chapter II is that R_3 was taken to be the same with the laser on as it was with the laser off.

The net rate R_3 is dominated by electron-atom collisions. These collisions may be with atoms in the ground state or in excited states. It is possible that a significant contribution to R_3 results from electron collisions with atoms in excited levels whose population is a function of the population of the upper and/or lower laser level.[11] If this is the case, then R_3 will not be the same with the laser on as with the laser off. The effect of this on the ratio $\Delta n_3/\Delta n_2$ can be seen by re-writing equation (1) and (2) of chapter II in the following manner.

$$\frac{dn_3}{d\tau} = -\frac{n3}{\tau_3} + \frac{n2}{\theta_{23}} - \frac{n3}{\theta_{32}} + R_3 + Kf(n_2,n_1)i = 0 \qquad (7)$$

$$\frac{dn_3'}{d\tau} = -\frac{n_3'}{\tau_3} + \frac{n_2'}{\theta_{23}} - \frac{n_3'}{\theta_{32}} + R_3 + Kf(n_2',n_1')i = 0 \quad (8)$$

Here the product Kfi represents a net rate of an electron-atom collision process which populates the level $|3>$ and $f(n_2,n_1)$ is the population of some lower level(s) which depends in some manner on the population of the upper laser level (n_2) and/or the population of the lower laser level (n_1). K is a proportionality constant and i is the current in milliamperes. The other symbols retain the same meanings given them in chapter II.

Subtracting equation (8) from equation (7) and rearranging terms, we obtain

$$\frac{\Delta n_3}{\Delta n_2} = \left(\frac{1}{\tau_3} + \frac{1}{\theta_{32}}\right)^{-1} \frac{1}{\theta_{23}} + \left(\frac{1}{\tau_3} + \frac{1}{\theta_{32}}\right)^{-1} \frac{\Delta f}{\Delta n_2} Ki \quad (9)$$

$$\Delta f = f(n_2',n_1') - f(n_2,n_1)$$

Thus the ratio $\Delta n_3/\Delta n_2$ would be proportional to the current.

In order to investigate the effect of the discharge current on the measured ratio $\Delta I_3/\Delta I_2$, this ratio was measured at a constant pressure for three different currents. Figure 26 shows a plot of $\Delta I_3/\Delta I_2$ versus discharge current for pressures of 2.1 and 3.7 torr.

We see from equation (5) that the ratio $\Delta I_3/\Delta I_2$ is a function of the temperature. In the high pressure region, the

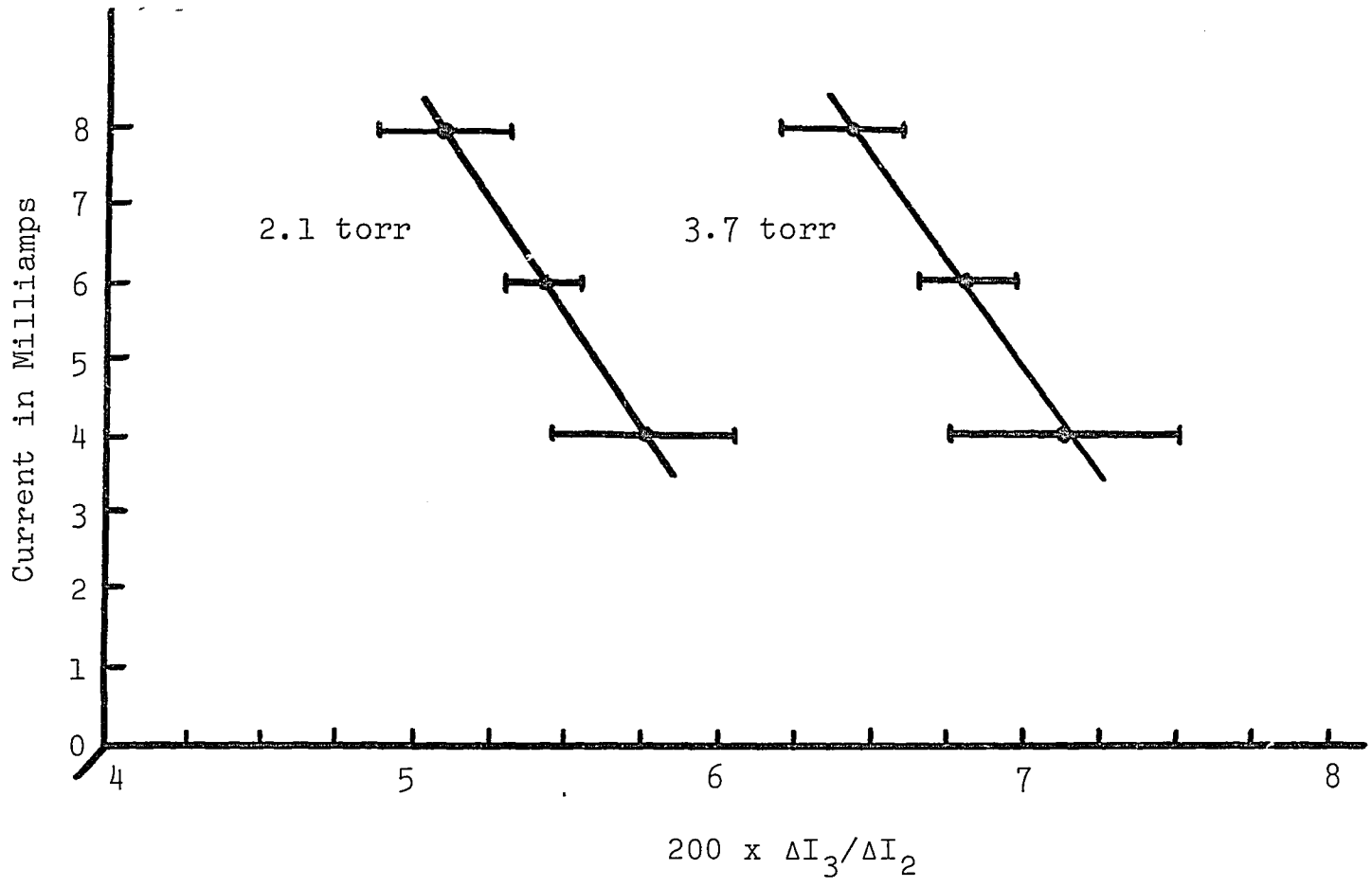

FIGURE 26. $\Delta I_3/\Delta I_2$ AS A FUNCTION OF CURRENT

relationship is particularly simple. From equation (7) of chapter II and equation (3) of this chapter (dropping the νs), we can write

$$\frac{\Delta I_3}{\Delta I_2} = \frac{A_3}{A_2}\frac{g_3}{g_2}\exp(\Delta E/kT) \qquad (10)$$

To determine whether the observed change in $\Delta I_3/\Delta I_2$ with current might be a temperature effect, we take the differential of both sides of equation (10).

$$\Delta(\Delta I_3/\Delta I_2) = -\frac{A_3}{A_2}\frac{g_3}{g_2}\frac{\Delta E}{kT^2}\exp(\Delta E/kT)\ \Delta T \qquad (11)$$

Assuming a temperature of 400 degrees K and using the value of 1/7 for A_3/A_2, we obtain[12]

$$\frac{\Delta(\Delta I_3/\Delta I_2)}{\Delta T} = -2.7 \times 10^{-5}(\text{degrees K})^{-1} \qquad (12)$$

The 3.7 torr. curve of figure 26 is closer to the pressure region where equation (11) is applicable. The slope of the 3.7 torr. curve is

$$\frac{\Delta(\Delta I_3/\Delta I_2)}{\Delta i} = -9.5 \times 10^{-4}(\text{ma})^{-1} \qquad (13)$$

If the change of the ratio $\Delta I_3/\Delta I_2$ with current is because of a temperature change, then from equation (12) and (13), we obtain

$$\frac{\Delta T}{\Delta I} = 35.2^{\circ}\ \text{K/ma} \qquad (14)$$

However, such a temperature rise with current is not consistent with the type of glow discharge maintained in the tube. According to Cobine[13] the temperature within the discharge should be about 400 degrees K and sensibly independent of the current, for currents on the order of 1 to 10 milliamperes.

We conclude, therefore, that the change in the ratio $\Delta I_3/\Delta I_2$ with current is probably because R_3 does not subtract completely out of equation (3) of chapter II. Lending credence to this conclusion is the following. Although not shown in figures 20, 21, and 22 at pressures below 1.5 torr., the data tended to fall along a horizontal line. Unfortunately, the signal to noise ratio deteriorates rather rapidly when one goes below 1.5 torr. For this reason these points were not included. However the possibility that the ratio $\Delta I_3/\Delta I_2$ approaches a constant at low pressures is consistent with equation (9). Physically one can understand this in the following way. At very low pressures, there will be little collision excitation transfer between levels $|2\rangle$ and $|3\rangle$. However, if R_3 contains a term which is a function of the population of the upper and/or lower laser level, then the population of level $|3\rangle$ will continue to be modulated as the laser is switched on and off, no matter how low the pressure.

To obtain a value for the constant a at zero current, we proceed as follows. We note from equation (9) that the ratio $\Delta I_3/\Delta I_2$ should be linear with the current. This appears to

be experimentally verified by the data presented in figure (26). If this is true, then we see from equation (5) that 1/a should be linear with the current. Thus to obtain the value of a at zero current, we plot 1/a versus the current and then extrapolate to zero current.

It is of interest to note that Parks and Javan[14] did not note any dependence of $\Delta I_3/\Delta I_2$ on the current. Their signal to noise ratio would not have let them detect changes with current as small as detected with this experiment, however.

In determining the relative A values for transitions originating on the same upper level, a number of errors must be taken into account. These are the precision with which the intensity ratios for these two transitions were measured, the precision with which the relative response of the system was able to be determined, and the precision of the calibration of the standard lamp used in the calibration of the system. The manufacturer of the standard lamp states that the calibration curve is within ±5% absolute. For purposes of calculating the standard deviation of the relative A values, a standard deviation of 3% of the value given by the calibration curve was assumed. The various standard deviations were combined in the usual manner[15] to obtain the standard deviation of the ratio of the relative A values of the transitions originating on the same upper level.

As described previously in this chapter, to obtain the ratio A_2/A_3 and the product $\tau_3\sigma_{23}$, we plot the experimentally determined values of $\Delta I_2/\Delta I_3$ versus the reciprocal of the pressure. A straight line is fitted to the experimental data by the method of least squares. The intercept of this line determines the ratio A_2/A_3.

The least squares fit was made assuming the values of the reciprocal of the pressure were known better than the value $\Delta I_2/\Delta I_3$ at the corresponding pressure. The latter statement is true in so far as the precision of the pressure measurements was much better than that of the measurement of the ratio $\Delta I_2/\Delta I_3$. However, it should be pointed out that although the pressure measurements were very repeatable, the absolute accuracy in the knowledge of the pressure was probably no better than ±5%.

The relative variances of the experimentally determined values $\Delta I_2/\Delta I_3$ were approximately the same for each point. The variance was about 5% for the measured points. Therefore in making the least squares fit, each point was equally weighted. As can be seen by figures 20, 21, and 22, the experimental data fits a straight line extremely well.

We can calculate the standard deviation of the constants a and b of the straight line using the following formulas[16]

$$S_b = \left(\frac{\Sigma x_i^2}{n\Sigma x_i^2 - (\Sigma x_i)^2}\right)^{\frac{1}{2}} S_y \qquad (15)$$

$$S_a = \left(\frac{n}{n\Sigma x_i^2 - (\Sigma x_i)^2}\right)^{\frac{1}{2}} S_y \qquad (16)$$

From an examination of equation (5), it is seen that an accurate knowledge of the temperature is not necessary. Calculations show that a temperature variation of ±70 degrees about 400 degrees K would produce an error of only ±5% in the derived values of a and b. From the foregoing considerations, it can be seen that the precision of this experiment is fairly good. The final experimental results (after extrapolation to zero current) are presented in table V.

TABLE V. FINAL RESULTS

$A_{(6328)}/A_{(6313)} = 7.10 \pm 0.57$

$\tau_3\sigma_{23} = (9.93 \pm 0.80) \times 10^{-23} cm^2\text{-sec}$

λ	Transition	Relative Transition Probability
6328.2	$3s_2 - 2p_4$	10.00
7304.8	$3s_2 - 2p_1$	0.80 ± .05
6421.7	$3s_3 - 2p_2$	0.89 ± .08
6351.9	$3s_2 - 2p_3$	0.99 ± .05
6313.7	$3s_3 - 2p_5$	1.41 ± .11
6293.8	$3s_2 - 2p_5$	1.84 ± .05
6118.0	$3s_2 - 2p_6$	1.75 ± .08
6064.6	$3s_3 - 2p_7$	0.69 ± .06
6046.2	$3s_2 - 2p_7$	0.65 ± .03
5939.3	$3s_2 - 2p_8$	0.56 ± .03
5448.5	$3s_3 - 2p_{10}$	0.19 ± .02
5433.7	$3s_2 - 2p_{10}$	0.76 ± .05

REFERENCES

[1]Willis E. Lamb, Jr., "Theory of an Optical Maser," The Physical Review, 134 (June, 1964), A1437.

[2]Ali Javan, "Alignment of the Angular Momenta of the Maser Levels," Bulletin of the American Physical Society, 9 (April, 1964), 489.

[3]E. U. Condon and G. H. Shortley, The Theory of Atomic Spectra (Cambridge University, 1963), p. 387.

[4]Ibid., pp. 90-91.

[5]The direction in which the minimum occurs depends upon the J of the lower level.

[6]Joel H. Parks and Ali Javan, "Collision-Induced Transitions Within Excited Levels of Neon," The Physical Review, 139 (August, 1965), A1354.

[7]R. W. Wood, "Polarized Resonance Radiation of Mercury Vapour," Philosophical Magazine and Journal of Science, 44 (December, 1922), 1107-1111.

[8]S. A. Korff and G. Breit, "Optical Dispersion," Reviews of Modern Physics, 4 (July, 1932), 488.

[9]Jules Z. Klose, Private Communication.

[10]Lyman G. Parratt, Probability and Experimental Errors in Science (New York, 1961), pp. 127-128.

[11]L. A. Weaver and R. J. Freiberg, "Laser-Induced Perturbations of Excited-State Populations in a He:Ne Discharge," Journal of Applied Physics, 37 (March, 1966), 1528-1535.

[12]James D. Cobine, Gaseous Conductors (New York, 1941), p. 233.

[13]Ibid.

[14]Parks and Javan, op. cit., p. A1355.

[15]Parratt, op. cit., p. 115.

[16]Ibid., p. 131

CHAPTER V

DISCUSSION OF RESULTS

Comparison With Previous Experimental Work

Relative transition probabilities for transitions between the $3s_2$ and 2p levels of neon have previously been reported by Hänsch and Toschek[1] and by Bychkova et. al.[2] Their results are compared with the results obtained in this experiment in table VI. An examination of this table shows that our results tend to agree more closely with those of Hänsch and Toschek than with those of Bychkova et. al.

An absolute value of the transition probability for the $3s_2 - 2p_4$ transition is given by both reference 1 and reference 2. This absolute value depends upon the value of the transition probability for the $2p_4 - 1s_4$ transition measured by Ladenburg.[3] The uncertainty in the absolute value of this transition probability is on the order of 20 to 30%. Thus the uncertainty in the measured absolute value of the $3s_2 - 2p_4$ transition probability is of at least this value.

Table VII presents absolute transition probabilities for the transitions studied in this experiment based on the value given by reference 1. The probable error indicated in table VII does not include the error in the absolute value of the $3s_2 - 2p_4$ transition probability.

TABLE VI. RELATIVE TRANSITION PROBABILITIES FOR $3s_2$ - 2p TRANSITIONS

Transition	λ	Relative Transition Probabilities: Bychkova et. al.[a]	Hänsch and Toschek[b]	This Work
$3s_2 - 2p_4$	6328.2	10.00	10.00	10.00
$3s_2 - 2p_1$	7304.8	-	0.73	0.80 ± .05
$3s_2 - 2p_3$	6351.7	1.06 ± .26	1.02	0.99 ± .05
$3s_2 - 2p_5$	6293.8	2.05 ± .46	-	1.84 ± .05
$3s_2 - 2p_6$	6118.0	1.95 ± .34	1.8	1.75 ± .08
$3s_2 - 2p_7$	6046.2	1.03 ± .19	0.76	0.69 ± .06
$3s_2 - 2p_8$	5939.3	0.85 ± .15	-	0.56 ± .03
$3s_2 - 2p_{10}$	5433.7	0.89 ± .16	1.0	0.76 ± .05

[a]Errors quoted are what the authors call "mean error."

[b]No errors are quoted for these values as there is some ambiguity as to what the authors quoted errors mean.

TABLE VII. ABSOLUTE TRANSITION PROBABILITIES

Transition	λ	A x 10^{-6} sec.
$3s_2 - 2p_1$	7304.8	.41 ± .06
$3s_3 - 2p_2$	6421.7	.45 ± .07
$3s_2 - 2p_3$	6351.7	.50 ± .07
$3s_2 - 2p_4$	6328.2	5.1 ± .7
$3s_3 - 2p_5$	6313.7	.72 ± .11
$3s_2 - 2p_5$	6293.8	.94 ± .13
$3s_2 - 2p_6$	6118.0	.89 ± .13
$3s_3 - 2p_7$	6064.6	.35 ± .06
$3s_2 - 2p_7$	6046.2	.33 ± .05
$3s_2 - 2p_8$	5739.3	.29 ± .04
$3s_3 - 2p_{10}$	5448.5	.10 ± .02
$3s_2 - 2p_{10}$	5433.7	.39 ± .06

Comparison With Theory

In the past few years, several papers have appeared giving the results of theoretical calculations of line strengths for the transitions studied in this experiment.[4,5,6] These calculations are based on a j-ℓ coupling model for the neon atomic configuration. j-ℓ coupling is an intermediate coupling scheme between L-S coupling and j-j coupling.

j-ℓ coupling in neon comes about in the following manner. In the parent ion of neon the electro-static repulsion and the exchange correlation forces are much larger than the spin orbit interaction. Thus the parent ion of neon forms an inverted doublet whose splitting is due to spin orbit interaction. However, because of the considerably weaker electro-static interaction between the running electron and the core electrons, the angular momentum of this electron couples with the total angular momentum (j) of the core forming a resultant angular momentum (K). Then the total angular momentum is given by

$$J = K \pm \tfrac{1}{2}$$

Notice that the degree of j-ℓ coupling will depend both on the energy of the level (the higher the level lies, the more apt it is to be j-ℓ coupled) and the angular momentum of the running electron (a s state is not as likely to be j-ℓ coupled as a d state, for instance).

Table VIII presents theoretical relative transition probabilities for the levels of interest in this experiment.

TABLE VIII. COMPARISON OF THEORETICAL TRANSITION PROBABILITIES WITH EXPERIMENTALLY DETERMINED TRANSITION PROBABILITIES

Transition	λ	Relative Transition Probabilities		
		L - S	j - ℓ	Experimental
$3s_2 - 2p_1$	7304.8	2.13	6.40	4.35
$3s_3 - 2p_2$	6421.7	0	9.41	4.82
$3s_2 - 2p_3$	6351.9	0	0	5.38
$3s_2 - 2p_4$	6328.2	0	49.19	54.35
$3s_3 - 2p_5$	6313.7	0	59.43	7.65
$3s_2 - 2p_5$	6293.8	10.00	10.00	10.00
$3s_2 - 2p_6$	6118.0	18.15	0	9.51
$3s_3 - 2p_7$	6064.6	18.63	0	3.74
$3s_2 - 2p_7$	6046.2	0	0	3.53
$3s_2 - 2p_8$	5939.3	0	0	3.04
$3s_3 - 2p_{10}$	5448.5	2.05	0	1.06
$3s_2 - 2p_{10}$	5433.7	0	0	4.13

Transition probabilities are given for both L-S coupling[7] and j-ℓ coupling. The results obtained in this experiment are listed for comparison. It is clear that j-ℓ coupling is a closer description of the actual coupling scheme in neon than is L-S coupling. It is also clear, however, that j-ℓ coupling is not an adequate model for calculating transition probabilities for these levels.

Summary

The goals described in the first chapter of this thesis have been met. However, the developed system can be further improved. The great advantage of this system lies in its ability to investigate excited levels of atoms. To do this, however, it is necessary to detect small signals in the presence of a large noise background. For high precision, therefore, it is necessary that the detection system have a signal to noise ratio as large as possible. Steps to improve the signal to noise ratio of the detection system have already been started. As mentioned in chapter III, a photometer was used as a preamplifier for the lock-in amplifier. By no means could this photometer be described as a low noise pre-amplifier. A low noise preamplifier, made especially to be used in conjunction with lock-in amplifiers, has been obtained and has already demonstrated that it will improve the signal to noise ratio of the system. The signal to noise ratio may also be improved by cooling the photomultiplier cathode. The

signal is proportional to the laser power (before saturation). Thus an investigation into the optimum conditions for laser output should prove fruitful. This will be particularly necessary if one wishes to use weaker laser transitions such as the 6328 A transition ($3s_2 - 2p_4$).

Of course the experiment described in this dissertation is not the only one to which the developed system can be applied. The system could be modified to measure lifetimes by the phase-shift technique. Another problem of interest is electron-atom collision cross sections. It has been noted that levels lying higher than the laser levels by many thousands of wave numbers also have their populations modulated when a modulated radiation laser field passes through a discharge.[8] The interpretation of this phenomenon is that the population of the higher lying levels is dependent in part on electron collision with atoms in either the upper or lower laser level. By studying this phenomenon, it should be possible to obtain information on electron-atom collision cross sections.

It would certainly be of interest to use the same technique as described in this dissertation with the laser oscillating on a transition originating from the $3s_3$ level. Such an experiment would yield the product $\tau_2\sigma_{32}$. Since σ_{32} is related in a simple way to σ_{23} and τ_2 is known, σ_{32} could be found. If τ_3 could be determined by some other method, then

the experiment described above could serve as a critical check on the experimental technique.

Finally we point out that finding two levels conveniently spaced such as the $3s_2$ and $3s_3$ levels of neon is not an unusual occurrence in the noble gases (with the exception of helium). This is the result of the j-ℓ coupling tendency of the neon configurations and the configurations of the heavier noble gases.

REFERENCES

[1]Th. Hänsch and P. Toschek, "Measurement of Neon Atomic Level Parameters by Laser Differential Spectrometry," Physics Letters, 20 (February 15, 1966), 273-275.

[2]T. V. Bychkova, V. G. Kirpilenko, S. G. Rautian, and A. S. Khaikin, "Measurement of Probabilities of the Spontaneous $3s_2$ - 2p Transitions in Neon," Optics and Spectroscopy, 22 (April, 1967), 371-372.

[3]Rudolf Ladenburg, "Dispersion in Electrically Excited Gases," Reviews of Modern Physics, 5 (October, 1933), 248.

[4]G. F. Koster and H. Statz, "Probabilities of Neon Laser Transitions," Journal of Applied Physics, 32 (October, 1961), 2054-2055.

[5]H. Statz, C. L. Tang and G. F. Koster, "Approximate Electromagnetic Transition Probabilities and Relative Electron Excitation Cross Sections for Rare Gas Masers," Journal of Applied Physics, 34 (September, 1963), 2625-2632.

[6]W. L. Faust and R. McFarlane, "Line Strengths for Noble Gas Maser Transitions; Calculations of Gain/Inversion at Various Wavelengths," Journal of Applied Physics, 35 (July, 1964), 2010-2015.

[7]E. U. Condon and G. H. Shortley, The Theory of Atomic Spectra, (Cambridge University, 1963), p. 247.

[8]L. A. Weaver and R. J. Freiberg, "Laser-Induced Perturbations in a He:Ne Discharge," Journal of Applied Physics, 37 (March, 1966), 1528-1535.

BIBLIOGRAPHY

A. Periodical Articles.

Bloom, Arnold L. "Observations of New Visible Gas Lasers Transitions By Removal of Dominance," Applied Physics Letters, 2 (March, 1963), 101-102.

Boyd, G. D. and H. Kogelnik. "Generalized Confocal Resonator Theory," Bell System Technical Journal, 41 (July, 1962), 1364.

Bychkova, T. V., V. G. Kirpilenko, S. G. Rautian, and A. S. Khaikin. "Measurement of Probabilities of the Spontaneous $3s_2$-2p Transitions in Neon," Optics and Spectroscopy, 22 (April, 1967), 371-372.

Einstein, Albert. Physikalische Zeitschrift, 18 (1917), 121.

Faust, W. L. and R. McFarlane. "Line Strengths for Noble Gas Maser Transitions; Calculations of Gain/Inversion at Various Wavelengths," Journal of Applied Physics, 35 (July, 1964) 2010-2015.

Foster, E. W. "The Measurement of Oscillator Strengths in Atomic Spectra," Reports on Progress in Physics, 27 (1964), 470-551.

Freiberg, R. J., L. A. Weaver and J. T. Werdeyen. "Infrared Laser Interferometry Utilizing Quantum Electronic Cross Modulation," Journal of Applied Physics, 36 (October, 1965), 3352.

Hänsch, Th. and P. Toschek. "Measurement of Neon Atomic Level Parameters by Laser Differential Spectrometry," Physics Letters, 20 (February 15, 1966), 273-275.

Javan, Ali. "Alignment of the Angular Momenta of the Maser Levels," Bulletin of the American Physical Society, 9 (April, 1964), 489.

_____, William R. Bennett, Jr. and Donald R. Herriot. "Population Inversion and Continuous Optical Maser Oscillation in a Gas Discharge Containing a He-Ne Mixture," Physical Review Letters, 6 (1961), 106.

Koopman, David W. "Line Strengths for Neutral and Singly Ionized Gases," Journal of the Optical Society of America, 54 (1964), 1354.

Korf, S. A. and G. Breit. "Optical Dispersion," Reviews of Modern Physics, 5 (1933), 471-503.

Koster, G. F. and H. Statz, "Probabilities of Neon Laser Transitions," Journal of Applied Physics, 32 (October, 1961), 2054-2055.

Ladenburg, Rudolf. "Dispersion in Electrically Excited Gases," Reviews of Modern Physics, 5 (1933), 243-256.

Lamb, Jr., Willis E. "Theory of an Optical Maser," The Physical Review, 134 (1964), A1429, A1437.

Mainman, Theodore H. "Stimulated Radiation in Ruby," Nature, 187 (1960), 493.

Mielenz, Klaus D. and Karl F. Nefslen. "Gas Mixtures and Pressures For Optimum Power of rf-excited Helium-Neon Gas Lasers at 632.8nm," Applied Optics, 4 (May, 1965), 565-567.

Moore, Robert D. "Lock-in Amplifiers for Signals Buried in Noise," Electronics, 35 (June 8, 1962), 40-43.

Parks, Joel H. and Ali Javan, "Collision-Induced Transitions Within Excited Levels of Neon," The Physical Review, 139 (August, 1965), A1352-1355.

Rigrod, W. W., H. Kogelnik, D. Brangaccio, and D. R. Herriot. "Gaseous Optical Maser With External Concave Mirrors," Journal of Applied Physics, 33 (1962), 743.

Stair, Ralph, William E. Schneider, and John K. Jackson. "A New Standard of Spectral Irradiance," Applied Optics, 2 (November, 1963), 1151-1154.

Statz, H., C. L. Tang and G. F. Koster, "Approximate Electromagnetic Transition Probabilities and Relative Electron Excitation Cross Sections for Rare Gas Masers," Journal of Applied Physics, 34 (September, 1963), 2625-2632.

Weaver, L. A. and R. J. Freiberg, "Laser-Induced Perturbations in a He:Ne Discharge," Journal of Applied Physics, 37 (March, 1966), 1528-1535.

White, A. D. and J. D. Rigden. "The Effect of Super-Radiance at 3.39 Microns on the Visible Transitions in the He-Ne Maser," Applied Physics Letters, 2 (June, 1963), 211-212.

Wood, R. W. "Polarized Resonance Radiation of Mercury Vapour," Philosophical Magazine and Journal of Science, 44 (December, 1922), 1107-1111.

_____ Physikalische Zeitschrift, 13 (1912), 353.

B. Books

Birnbaum, George. Optical Masers, (New York, 1964), pp. 6 et seq.

Cobine, James D. Gaseous Conductors, (New York, 1941), pp. 233-234.

Colthup, Norman B., Lawrence H. Daly, and Stephen B. Wiberly. Introduction to Infrared and Raman Spectroscopy, (New York, 1964), pp. 191-199.

Condon, E. U. and G. H. Shortley. The Theory of Atomic Spectra (Cambridge University, 1963), pp. 90-91, 247, 387.

Garbuny, Max. Optical Physics, (New York, 1965), pp. 327, et seq.

Garrett, C. G. B. Gas Lasers, (New York, 1967).

Heavens, O. S. Optical Masers, (London, 1964), p. 76.

Massey, Harrie and Eric Burhop. Electronic and Ionic Impact Phenomena, (Oxford University, 1952), pp. 68-72, 417, 450.

Mitchell, Alan and Mark Zemansky. Resonance Radiation and Excited Atoms, (London, 1934), p. 156.

Optical Transition Probabilities, Israel Program for Scientific Translation, (Jerusalem, 1962).

Parratt, Lyman G. Probability and Experimental Errors in Science (New York, 1961), pp. 115-131.

Roberts, Richard W. and Thomas A. Vanderslice. Ultrahigh Vacuum and Its Applications, (New Jersey, 1963), pp. 22-23, 109.

Sawyer, Ralph A. Experimental Spectroscopy, (New York, 1963), pp. 181-182.

C. Compilations

Bennett, Jr., W. R. "Inversion Mechanisms in Gas Lasers," Applied Optics Supplement on Chemical Lasers, (1965), p. 28.

Javan, Ali. "Gaseous Optical Masers," in C. DeWitt, A. Blandin, and C. Cohen-Tannoudji, (eds.), Quantum Optics and Electronics, (New York, 1965), pp. 385-396.

D. Government Documents

Glennon, B. M. and W. L. Wiese. "Bibliography on Atomic Transition Probabilities," National Bureau of Standards Miscellaneous Publications 278, (Washington D. C., 1964), pp. 64-65.

Moore, Charlotte E. Atomic Energy Levels, Circular of the National Bureau of Standards, 467 (Washington D. C., 1949), I, 77.

E. Unpublished Material

Klose, Jules Z. Private Communication.

F. Special Studies

Bloom, Arnold L. "Properties of Laser Resonators Giving Uniphase Wave Fronts," Spectra-Physics Laser Technical Bulletin, 2 (August, 1963), 6-7.